THE UNIVERSITY OF QUEENSLAND

AUSTRALIA

Theory of Delocalised Charge Transfer

Natasha Brianne Taylor

B.Sc. (Hons)

A thesis submitted for the degree of Doctor of Philosophy at

The University of Queensland in 2019

School of Mathematics and Physics

Abstract

Charge transfer in molecular systems occurs between molecules, atoms, or ions, collectively called *sites*. Theories of charge transfer are fundamental to understanding both natural molecular systems, such as photosynthesis, and artificial molecular systems, such as organic semiconductors or inorganic coordination complexes. Charge transfer in many of these systems is, however, complicated by the existence of delocalisation, where the coupling between sites causes the charge's wavefunction to extend over multiple sites, to the point where it becomes meaningless to describe the charge as occupying any particular site.

While quantum-chemical computational techniques exist to calculate charge transfer rates between these delocalised states, they can be computationally expensive (scaling up to exponentially with system size), are inflexible (that is, any change to the system requires a complete recalculation), and offer limited qualitative insight as to how the rate of charge transfer will change with various system properties.

To overcome these limitations, this thesis presents a general theory of charge transfer between delocalised molecular states, *generalised Marcus theory*. Generalised Marcus theory is computationally cheap, flexible, and expressed in closed form. The closed-form nature of generalised Marcus theory allows for qualitative understanding of how charge transfer between delocalised molecular states is affected by changing the charge-transfer properties of the constituent molecules.

Importantly, generalised Marcus theory leads to a number of predictions: supertransfer, or the enhancement of charge transfer through the constructive interference of delocalised charge transfer pathways; reorganisation energy suppression, where the environmental impact on charge transfer is somewhat mitigated by delocalisation; and the possibility of energetic tuning, where tuning energy offsets or reorganisation energies can allow significant enhancement to the charge transfer rate.

This thesis applies generalised Marcus theory to a system in which delocalised charge transfer occurs, the *photosynthetic reaction centre*, a dimeric pigment-protein complex consisting of two monomeric branches. The reaction centre in photosynthetic organisms accepts excitons from an antenna system and outputs electrons, serving to convert solar energy into chemical energy. Importantly, excitons are transferred to a delocalised state where the two monomeric branches meet, a pair of molecules called the *special pair*, and charge separation occurs from this delocalised state. Many organisms only use a single monomeric branch for charge transfer, which raises an open question in biology: why is the reaction centre dimeric?

This thesis compares the modern dimeric reaction centre, with delocalised exciton and charge transfer occurring at the special pair, to a model of the ancestral monomeric reaction centre, which lacks one half of the special pair and consequently does not experience exciton or charge delocalisation. By using Sumi's generalised Förster theory to describe exciton transfer, and generalised Marcus theory to describe charge transfer, this thesis answers the question by showing that the evolution of the reaction centre from a monomer to a dimer likely improved the overall reaction centre efficiency.

Declaration by Author

This thesis is composed of my original work, and contains no material previously published or written by another person except where due reference has been made in the text. I have clearly stated the contribution by others to jointly-authored works that I have included in my thesis.

I have clearly stated the contribution of others to my thesis as a whole, including statistical assistance, survey design, data analysis, significant technical procedures, professional editorial advice, financial support and any other original research work used or reported in my thesis. The content of my thesis is the result of work I have carried out since the commencement of my higher degree by research candidature and does not include a substantial part of work that has been submitted to qualify for the award of any other degree or diploma in any university or other tertiary institution. I have clearly stated which parts of my thesis, if any, have been submitted to qualify for another award.

I acknowledge that an electronic copy of my thesis must be lodged with the University Library and, subject to the policy and procedures of The University of Queensland, the thesis be made available for research and study in accordance with the Copyright Act 1968 unless a period of embargo has been approved by the Dean of the Graduate School.

I acknowledge that copyright of all material contained in my thesis resides with the copyright holder(s) of that material. Where appropriate I have obtained copyright permission from the copyright holder to reproduce material in this thesis and have sought permission from co-authors for any jointly authored works included in the thesis.

Publications During Candidature

Peer-Reviewed Papers

N. B. Taylor, and I. Kassal, Generalised Marcus theory for multi-molecular delocalised charge transfer, *Chem. Sci.*, **9**, 2942, 2018, DOI: 10.1039/C8SC00053K.

N. B. Taylor, and I. Kassal, Why are photosynthetic reaction centres dimeric?, *Chem. Sci.*, **10**, 9576, 2019, DOI: 10.1039/C9SC03712H.

Publications Included in this Thesis

N. B. Taylor, and I. Kassal, Generalised Marcus theory for multi-molecular delocalised charge transfer, *Chem. Sci.*, **9**, 2942, 2018, DOI: 10.1039/C8SC00053K – included as as Chapter 2.

Contributor	Statement of Contribution	%
NB Taylor	Concept and Design	60
	Analysis and Interpretation	95
	Drafting and Production	80
I Kassal	Concept and Design	40
	Analysis and Interpretation	05
	Drafting and Production	20

N. B. Taylor, and I. Kassal, Why are photosynthetic reaction centres dimeric?, *Chem. Sci.*, **10**, 9576, 2019, DOI: 10.1039/C9SC03712H – included as as Chapter 3.

Contributor	Statement of Contribution	%
NB Taylor	Concept and Design	50
	Analysis and Interpretation	90
	Drafting and Production	80
I Kassal	Concept and Design	50
	Analysis and Interpretation	10
	Drafting and Production	20

Submitted Manuscripts Included in this Thesis

No other publications.

Other Publications During Candidature

No other publications.

Contributions by Others to the Thesis

No contributions by others

Statement of Parts of the Thesis Submitted to Qualify for the Award of Another Degree

No works submitted towards another degree have been included in this thesis.

Research Involving Human or Animal Subjects

No animal or human subjects were involved in this research.

Acknowledgements

I would like to thank my supervisors, Dr Ivan Kassal and Prof. Ben Powell, for the support and encouragement they have shown me throughout my PhD. In particular, thank you Ivan for your mentorship, patience, knowledge, humour, and your constant pushing me to do my best—you are not only my supervisor and mentor, but a source of inspiration.

Thank you to the Australian Research Council Centre of Excellence for Engineered Quantum Systems (EQUS), in particular the University of Queensland Node and my EQUS mentor, Dr Wei-Wei Zhang. EQUS has given me many opportunities to present my work, network with fellow researchers, and grow as a scientist since I commenced my PhD; the opportunity to meet researchers from across Australia and the world has been invaluable.

My parents, Marie and Michael, instilled in me the love of learning, the importance of education, and every opportunity within their power. Thank you, with all my heart, for everything you have done.

Finally, I would like to thank Teagan and Kirt, who have been a constant source of support on the hard days, joy on the good days, and unwavering confidence in me always.

Financial Support

This research was supported by an Australian Government Research Training Program Scholarship.

Keywords

charge transfer, photosynthesis, marcus theory, quantum biology, reaction centre, delocalisation, evolution

Australian and New Zealand Standard Research Classifications (ANZSRC)

ANZSRC code: 020699 Quantum Physics not elsewhere classified, 30%
ANZSRC code: 030703 Reaction Kinetics and Dynamics 30%
ANZSRC code: 029901 Biological Physics 40%

Fields of Research (FoR) Classification

FoR code: 0206 Quantum Physics, 30%
FoR code: 0307 Theoretical and Computational Chemistry, 30%
FoR code: 0299 Other Physical Sciences, 40%

To my family,
who taught me the importance
of education.

Contents

List of Figures

List of Tables

List of Abbreviations

Abbreviations	
2DES	two-dimensional electronic spectroscopy
BChl	bacteriochlorophyll
BIF	banded iron formation
BPhe	bacteriophaeophytin
Chl	chlorophyll
CT	charge transfer
EET	excitation energy transfer
ENAQT	environment-assisted quantum transport
FAP	filamentous anoxygenic phototrophs
FGR	Fermi's golden rule
FMO	Fenna-Matthews-Olson complex
FRET	Förster resonance energy transfer
gFRET	generalised FRET
gMT	generalised Marcus theory
HID	homogeneous, isotropic continuum dielectric
LH	light-harvesting complex (bacteria)
LHC	light-harvesting complex (cyanobacteria & eukaryotes)
MC-FRET	multi-chromophoric FRET
MOF	metal-organic framework
MT	Marcus theory
PES	potential energy surface
Phe	phaeophytin
PS	photosystem
Q	quinone
RC	reaction centre
SP	special pair (bacterio)chlorophylls

Chapter 1

Introduction

Charge transfer (CT) is ubiquitous in the world around us, with CT reactions responsible for the functioning of batteries, the rusting of iron, the metabolism of sugars, and much more. These reactions are known as *redox* reactions, a portmanteau of *reduction*, the gain of electrons, and *oxidation*, the loss of electrons.

While many reactions involve the making or breaking of chemical bonds, such as the combustion of glucose ($C_6H_{12}O_6 + 6O_2 \longrightarrow 6H_2O + 6CO_2$), there are many CT reactions where bonds are neither formed nor broken, such as the ionisation of sodium in ammonia ($Na \longrightarrow Na^+ + e^-$), or the self-exchange reaction between iron cations ($Fe^{2+} + Fe^{3+} \longrightarrow Fe^{3+} + Fe^{2+}$). This thesis discusses CT in molecular systems, where charge is transferred from an atomic, molecular, or ionic donor, D, to a charge acceptor, A without the formation or breaking of a chemical bond: $D^- + A \rightarrow D + A^-$.

This is complicated in molecular systems where there are multiple donors that are more strongly coupled with each other than their environment, which we call an *aggregate*, transferring a charge to an acceptor aggregate. A charge present on one donor or acceptor site will have its wavefunction spread throughout the entire aggregate, at which point describing the charge as being on an individual site is meaningless, since its wavefunction is—to some degree or another—spread across every site. We call the transfer of charge from one aggregate to another *delocalised charge transfer*, as the charge cannot be associated with a single site: $(D_1D_2\ldots D_N)^- + (A_1A_2\ldots A_M) \rightarrow (D_1D_2\ldots D_N) + (A_1A_2\ldots A_M)^-$.

There are many systems where delocalisation of charge occurs, such as conductive metal-organic frameworks, organic semiconductors, and inorganic coordination complexes. One such system that we choose to examine is the *photosynthetic reaction centre* (RC). The RC is at the core of all light-harvesting systems in photosynthetic organisms, converting energy absorbed from the sun into chemical energy by initiating charge separation. It is a dimeric structure, but in most organisms CT is restricted to one monomeric branch of the dimer. This raises the question: why is the RC a dimer at all?

The dimeric RC experiences both delocalised charge and exciton transfer, but a monomeric RC would not, so understanding how dimerisation affects the RC requires both localised and delocalised charge and exciton transfer theories.

As such, Section 1.1 provides an introduction to charge and exciton transfer in molecular systems.

Context for understanding RC dimerisation is presented in Section 1.2, where the field of quantum biology and the structure of light-harvesting systems are introduced and discussed.

1.1 Charge and Energy Transport

1.1.1 Charge transfer

Early charge transfer theories

The physics of charge transfer can be traced back to the late 19th century, following the systematic study of kinetics in chemical reactions[1,2]. James Clerk Maxwell[3] and Ludwig Boltzmann[4] proposed the principle of detailed balance, which states that, at equilibrium, the reaction $i \to j$ must occur at the same rate as the reverse reaction, $j \to i$; if this were untrue, the population of i or j must change, and hence the two populations would not be at equilibrium (a contradiction). At equilibrium, the populations, P_i and P_j, and rate of transfer between them, $k_{i\to j}$ and $k_{j\to i}$, are related by

$$P_i k_{i\to j} = P_j k_{j\to i}. \tag{1.1}$$

The population of each state can be described as a Boltzmann distribution, Equation 1.1 becomes the equilibrium equation

$$\frac{k_{i\to j}}{k_{j\to i}} = \exp\left(\frac{-\Delta E_{ji}}{k_\mathrm{B} T}\right), \tag{1.2}$$

where k_B is the Boltzmann constant, T the temperature, and $\Delta E_{ji} = E_j - E_i$, the energies of states i and j. Importantly, this predicts that for any kinetic reaction, including CT, the rate of transfer between two states should increase with the energy difference between them, $-\Delta E_{ji}$. Conversely, the rate should decrease as the energy difference does. A differential form of this temperature-dependent equilibrium reaction was described by the van't Hoff equation[5],

$$\frac{d}{dT}\ln K = \frac{\Delta H}{k_\mathrm{B} T^2}, \tag{1.3}$$

where the rate-constant $K = k_{i\to j}/k_{j\to i}$, and ΔH is the change in enthalpy.

By analogy to equilibrium equations, in 1884 Jacobus van't Hoff proposed that rate equations may be written

$$\frac{d}{dT}\ln k_{i\to j} = \frac{C}{k_\mathrm{B} T^2} + D, \tag{1.4}$$

for some reaction-specific constants C and D. However, with the data available, he was unable to demonstrate that C was non-zero or that D was zero[1]. Building on this work, in 1889 Svante Arrhenius assigned physical meaning to the constant C by arguing chemical reactions took place via an 'activated' species, which required some activation energy E_A. As such, he proposed the rate equation[6]

$$k_{i\to j} = c \cdot \exp\left(\frac{-E_A}{k_\mathrm{B} T}\right), \tag{1.5}$$

where c is a constant depending on the particular reaction. Equation 1.5 is known as the Arrhenius rate equation, and was used as the basis to derive subsequent CT rate equations.

One example of such a rate equation is the Miller-Abrahams equation. In the early 1950's, experimentation with semiconductors indicated that, at high impurity concentrations, conduction of charge did not take place in a delocalised band but via electron hopping[7,8]. In order to understand this phenomenon, Miller and Abrahams derived an expression for the hopping rate[9],

$$k_{i\to j} = \begin{cases} \nu_0 \exp(-\gamma r_{ij}) \exp(-\Delta E_{ji}/k_\mathrm{B}T) & \Delta E_{ji} \geq 0, \\ \nu_0 \exp(-\gamma r_{ij}) & \Delta E_{ji} < 0, \end{cases} \tag{1.6}$$

which can be broken into three terms:

1. the hopping attempt frequency, ν_0;
2. the tunneling term, $\exp(-\gamma r_{ij})$, where r_{ij} is the distance between sites i and j, and γ is the inverse localisation radius; and
3. the Boltzmann term, which is 1 for downhill transfer and $\exp(-\Delta E_{ji}/k_\mathrm{B}T)$ for uphill.

Note that this is very similar to the Arrhenius rate, Equation 1.5, with the activation energy the difference in site energies as per Equation 1.2, and the rate constant $c = \nu_0 \exp(-\gamma r_{ij})$, although only the uphill rate is temperature-dependent (*i.e.* for downhill transfer $E_A = 0$), consistent with an electron needing thermal energy from the environment to move uphill, but freely moving downhill.

Marcus theory

In 1956, Rudolph Marcus developed a theory to describe charge transfer in a dielectric medium[10], where a charge would be transferred from an atomic, molecular, or ionic donor, D, to an electron acceptor, A, without the formation of a chemical bond: $D^- + A \to D + A^-$. If the solvent is initially relaxed about the reactant state, charge transfer would result in the environment being out of equilibrium with the product state, due to separation of timescales between nuclear and electronic motion. Since the energy required to transfer the charge without solvent reorganisation is typically 0.1 eV to 1 eV, significantly larger than $k_\mathrm{B}T$, the direct reaction cannot happen with the available thermal energy.

In order to resolve this issue, Marcus proposed that instead of transferring from a relaxed state, thermal environmental fluctuations perturb the solvent from relaxation about the reactant state. At some point, the solvent would reach a configuration where the reactant and product state are isoenergetic, at which point charge transfer would occur (Figure 1.1). This theory is known as Marcus theory (MT), and for its predictions Marcus received the 1992 Nobel Prize in Chemistry.

Derivation of energy surfaces

In MT, the solvent is taken to be a homogeneous, isotropic continuum dielectric (HID), allowing us to write the identity $\mathbf{D} = \varepsilon_0 \mathbf{E} + \mathbf{P}$, where $\mathbf{D}$ is the displacement field in an HID, $\mathbf{E}$ the electric field, $\mathbf{P}$ the polarisation density, and ε_0 the permittivity of free space.

Using $\mathbf{E} = \varepsilon^{-1}\mathbf{D}$, we write $\mathbf{P} = (1 - \varepsilon_0/\varepsilon)\mathbf{D}$. Characterising the HID on two timescales—a fast timescale for electronic behaviour and slow timescale for nuclear behaviour—we write $\mathbf{P} = \mathbf{P}_s - \mathbf{P}_\infty$,

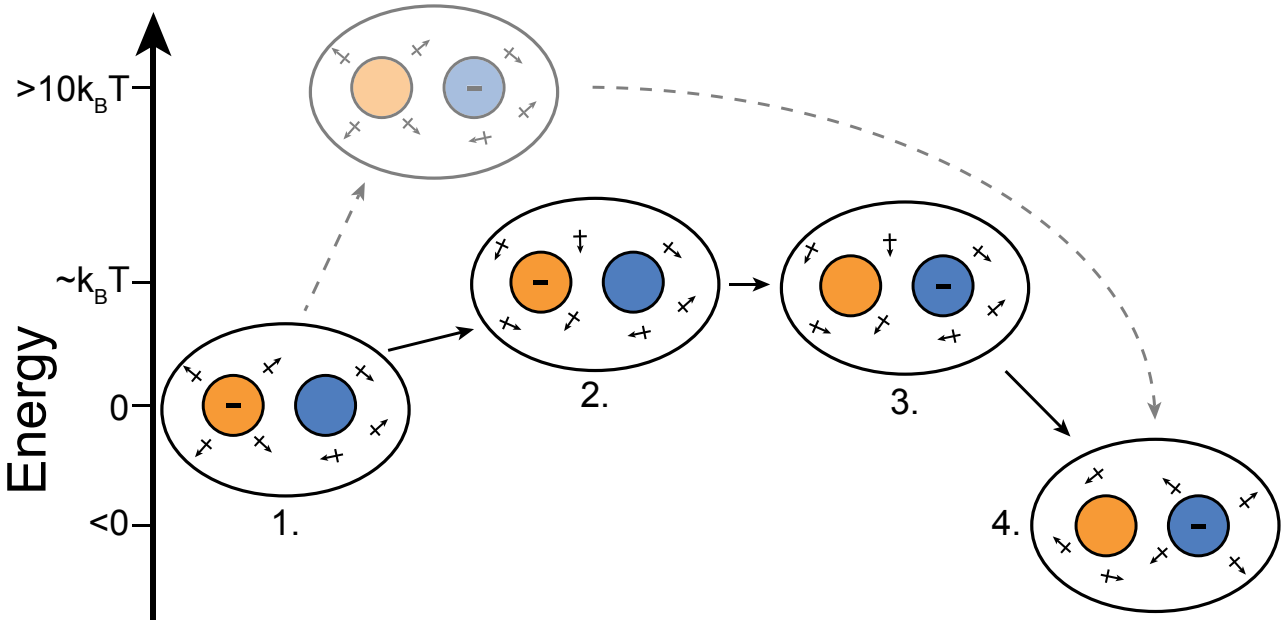

Figure 1.1: Charge transfer in a polar solvent between a charge donor site (orange) and a charge acceptor site (blue): 1) The charge is initially on the donor, and the solvent is arranged in equilibrium about this charge state; 2) Thermal energy in the environment rearranges the solvent configuration; 3) Once the solvent has reached a configuration such that it is isoenergetic for the charge to be on either the donor or acceptor, charge transfer occurs; 4) Solvent relaxes about the new charge configuration. The transparent pathway shows direct charge transfer without solvent reorganisation, but doesn't occur due to the high energy cost.

where $\mathbf{P}_s$ is the polarisation due to the (slow) nuclear modes, and $\mathbf{P}_\infty$ the polarisation due to the (fast) electronic modes. This lets us write

$$\mathbf{P} = \mathbf{P}_s - \mathbf{P}_\infty \tag{1.7}$$

$$= \varepsilon_0 \left(\frac{1}{\varepsilon_\infty} - \frac{1}{\varepsilon_s} \right) \mathbf{D}, \tag{1.8}$$

and by using the equilibrium energy expression for the solvent[11],

$$E_{\text{eq}} = \frac{1}{\varepsilon_0} \int d^3\mathbf{x}' \, \mathbf{D} \cdot \mathbf{P}. \tag{1.9}$$

If we assume that our charge distribution consists of a donor and acceptor, described by spheres of radius R_D and R_A respectively, separated by a distance $R_\text{DA} \gg R_\text{D}, R_\text{A}$, we can consider a small change in the solvent polarisation, parametrised by x such that $\mathbf{P}_x = \mathbf{P}_\text{D} + x(\mathbf{P}_\text{A} - \mathbf{P}_\text{D})$, where $\mathbf{P}_\text{D}$ and $\mathbf{P}_\text{A}$ are the polarisations of the solvent being relaxed about the reactant and product state respectively. Evaluating Equation 1.9 with this displacement, we can write the reactant and product potential energy surfaces (PES) as:

$$W_\text{R}(x) = E_\text{R} + q^2 \left(\frac{1}{\varepsilon_\infty} - \frac{1}{\varepsilon_s} \right) \left(\frac{1}{2R_\text{D}} + \frac{1}{2R_\text{A}} - \frac{1}{R_\text{DA}} \right) x^2, \tag{1.10}$$

$$W_\text{P}(x) = E_\text{P} + q^2 \left(\frac{1}{\varepsilon_\infty} - \frac{1}{\varepsilon_s} \right) \left(\frac{1}{2R_\text{D}} + \frac{1}{2R_\text{A}} - \frac{1}{R_\text{DA}} \right) (1-x)^2, \tag{1.11}$$

where we have used $\mathbf{D} = q\hat{\mathbf{x}}'/|\mathbf{x}'|^2$ for the charge distribution over a sphere, and q is the amount of charge transferred. By substituting Equation 1.8 into Equation 1.9, we also have

$$E_{\text{eq}} = \left(\frac{1}{\varepsilon_\infty} - \frac{1}{\varepsilon_s} \right) \int d^3\mathbf{x}' \, \mathbf{D}^2, \tag{1.12}$$

allowing us to write the energy required to transfer from solvent equilibrium in the reactant state to solvent equilibrium in the product state without changing electronic state, λ_{DA}, as

$$\lambda_{\mathrm{DA}} = \left(\frac{1}{\varepsilon_\infty} - \frac{1}{\varepsilon_s}\right) \int d^3\mathbf{x}' \, (\mathbf{D}_{\mathrm{A}} - \mathbf{D}_{\mathrm{D}})^2 \tag{1.13}$$

$$= q^2 \left(\frac{1}{\varepsilon_\infty} - \frac{1}{\varepsilon_s}\right) \left(\frac{1}{2R_{\mathrm{D}}} + \frac{1}{2R_{\mathrm{A}}} - \frac{1}{R_{\mathrm{DA}}}\right). \tag{1.14}$$

This gives an important qualitative result that will help in our understanding of charge transfer: the PES for charge transfer in an HID can be approximated as harmonic potentials in nuclear displacement with the same curvature. This allows us to consider a simple model of charge transfer involving two intersecting harmonic PES.

Classical picture of Marcus theory

Using the potential energy surfaces (PES) from Equations 1.10 and 1.11, we can draw a configurational diagram, plotting the nuclear co-ordinate x against energy (Figure 1.2). This allows us to treat charge transfer classically, as a ball rolling in a potential, with charge transfer occurring when it reaches the cross-over in the two potentials. To be general, we write[12]

$$W_{\mathrm{R}}(x) = \frac{1}{2}kx^2 + \frac{1}{2}Ax + \varepsilon_{\mathrm{R}}, \tag{1.15}$$

and

$$W_{\mathrm{P}}(x) = \frac{1}{2}kx^2 - \frac{1}{2}Ax + \varepsilon_{\mathrm{P}}. \tag{1.16}$$

Here k is the harmonic force constant, A the relative displacement of the two PES in the nuclear coordinate, and ε the PES energy displacement.

The minimum of the reactant PES is located at $x_{\mathrm{R}} = \frac{-A}{2k}$, with

$$W_{\mathrm{R}}(x_{\mathrm{R}}) = -\frac{3A^2}{8k} + \varepsilon_{\mathrm{R}}$$

$$\equiv E_{\mathrm{R}}, \tag{1.17}$$

and the product PES minimum at $x_{\mathrm{P}} = \frac{A}{2k}$, with

$$W_{\mathrm{P}}(x_{\mathrm{P}}) = -\frac{3A^2}{8k} + \varepsilon_{\mathrm{P}}$$

$$\equiv E_{\mathrm{P}}. \tag{1.18}$$

The difference in energy between these two points is $\Delta E_{\mathrm{PR}} = E_{\mathrm{P}} - E_{\mathrm{R}} = \varepsilon_{\mathrm{P}} - \varepsilon_{\mathrm{R}}$.

The reorganisation energy, λ, is the energy required to move from x_{R} to x_{P}, or *vice versa*, while remaining on the same PES,

$$\lambda = W_{\mathrm{R}}(x_{\mathrm{P}}) - W_{\mathrm{R}}(x_{\mathrm{R}})$$

$$= \frac{A^2}{2k}. \tag{1.19}$$

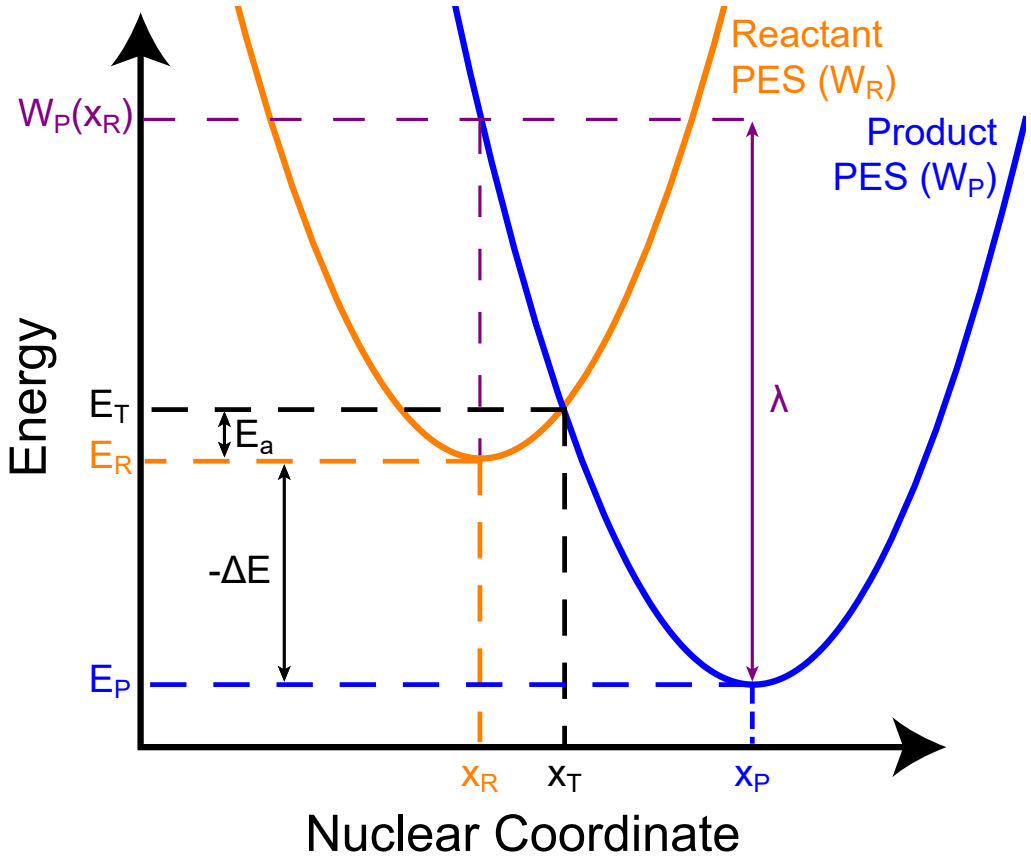

Figure 1.2: Configurational diagram of the reactant (orange) and product (blue) potential energy surface (W_R and W_P respectively) along the reaction nuclear coordinates. Labelled are the reactant minimum, (x_R, E_R), the product minimum, (x_P, E_P), and the transition state (x_T, E_T), as well as the activation energy (E_a), the energy difference (ΔE), and the reorganisation energy (λ).

The intersection of the PES occurs at x_T, where $W_\mathrm{R}(x_\mathrm{T}) = W_\mathrm{P}(x_\mathrm{T})$. The energy required to move from x_R to x_T along W_R is called the activation energy, $E_a = W_\mathrm{R}(x_\mathrm{T}) - W_\mathrm{R}(x_\mathrm{R})$. Using Equations 1.17 to 1.19, we can write

$$E_a = \frac{(\Delta E_\mathrm{PR} + \lambda)^2}{4\lambda}. \tag{1.20}$$

This allows us to calculate the expected rate of charge transfer from the reactants to the products, using the Arrhenius rate equation (Equation 1.5)

$$k = c \cdot \exp\left(\frac{-E_a}{k_\mathrm{B} T}\right) \tag{1.21}$$

$$= c \cdot \exp\left(\frac{-(\Delta E_\mathrm{PR} + \lambda)^2}{4 k_\mathrm{B} T \lambda}\right). \tag{1.22}$$

This is the form presented in the original MT paper, with c the collision rate in solution[10].

Initially, λ only included the behaviour of the solvent *cf.* Equation 1.14, known as outer-sphere transfer, with

$$\lambda_\mathrm{O} = q^2 \left(\frac{1}{\varepsilon_\infty} - \frac{1}{\varepsilon_s}\right)\left(\frac{1}{2R_\mathrm{D}} + \frac{1}{2R_\mathrm{A}} - \frac{1}{R_\mathrm{DA}}\right). \tag{1.23}$$

Later approaches included intra-molecular vibrations. This inner-sphere transfer, proposed and developed by Hush[13], λ_I, is added to the outer-sphere reorganisation energy of the initial MT to find the total reorganisation energy, $\lambda = \lambda_\mathrm{O} + \lambda_\mathrm{I}$. Because of this major development, and other

contributions to the underlying quantum mechanical theory, MT is sometimes known as Marcus-Hush theory.

Regimes of Marcus theory

Equation 1.22 predicts three regimes of charge transfer (Figure 1.3): the *activationless* regime, where $\Delta E = -\lambda$ and the rate is maximised; the *normal* regime, where $\Delta E > -\lambda$ and the rate increases as the energy difference between product and reactant state increases; and the *inverted* regime, where $\Delta E < -\lambda$, and increasing the difference between product and reactant results in a decreased transfer rate.

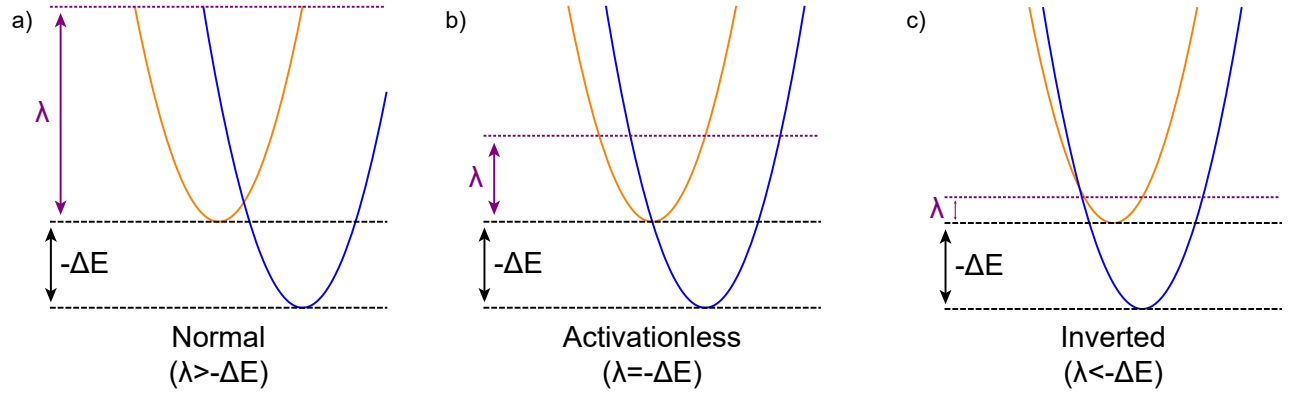

Figure 1.3: The three regimes of Marcus theory. a) Normal regime: $\lambda > -\Delta E$. In this regime, increasing the energy gap between the reactant state (orange) and product state (blue) will increase the rate of charge transfer. b) Activationless regime: $\lambda = -\Delta E$. Due to the product state PES crossing the reactant state minimum, $E_A = 0$, which allows electron transfer to occur down to cryogenic temperatures. c) Inverted regime: $\lambda < -\Delta E$. In this regime, increasing the energy gap between states decreases the rate of charge transfer, an 'inversion' of the normal regime.

Notably, the prediction of the inverted regime is an important prediction of MT, and it differentiated MT from other theories such as Miller-Abrahms, which predicted a constant downhill rate. It was the experimental detection of this regime that lead to the widespread acceptance of MT.

A fully quantum approach

Levich and Dogondaze calculated the collision rate in Equation 1.22 using Landau-Zener theory, a semi-classical approach derived in 1932 independently by Landau, Zener, Stückelberg, and Majorana[14–17]. By defining the Hamiltonian

$$H_{ab}(x) = W_R(x)\,|\phi_R\rangle\langle\phi_R| + W_P(x)\,|\phi_P\rangle\langle\phi_P| + V_{RP}\,|\phi_R\rangle\langle\phi_P| + V_{PR}\,|\phi_P\rangle\langle\phi_R|, \tag{1.24}$$

with V_{RP} the electronic coupling between the reactant and product states, they were able to show that[18]

$$c = \frac{2\pi}{\hbar}\frac{|V_{ab}|^2}{\sqrt{4\pi k_B T \lambda}}. \tag{1.25}$$

Details of this derivation may be found in the appendix, Section 1.4.1.

While Landau-Zener theory was sufficient to describe charge transfer in harmonic potentials, the Fermi golden rule (FGR) offers a more general approach. The FGR describes the transition rate between two quantum states that are coupled by a weak perturbation, to second order in the perturbative

coupling, and as is used frequently in describing charge and energy transfer. To understand FGR, we must consider the microscopic behaviour of electrons and atoms.

The behaviour of a system of nuclei and electrons can be described using the Hamiltonian

$$H = (T_{\text{el}} + V_{\text{el}}(\mathbf{r})) + (T_{\text{nuc}} + V_{\text{nuc}}(\mathbf{R})) + V_{\text{el,nuc}}(\mathbf{r},\mathbf{R}), \tag{1.26}$$

where $(T_{\text{el}} + V_{\text{el}}(\mathbf{r}))$ is the Hamiltonian of the electrons with co-ordinates $\mathbf{r}$, $(T_{\text{nuc}} + V_{\text{nuc}}(\mathbf{R}))$ the Hamiltonian of the nuclei with co-ordinates $\mathbf{R}$, and $V_{\text{el,nuc}}(\mathbf{r},\mathbf{R})$ their interaction. To solve this Hamiltonian, we recognise that the difference in mass between electrons and nuclei leads to a separation of timescales for motion, with electronic motion significantly faster than nuclear. Taking the electronic states to be independent of $\dot{\mathbf{R}}$ allows us to separate nuclear and electronic states, an approximation known as the Born-Oppenheimer approximation[19]. This allows us to write the eigenstates of H as

$$\psi(\mathbf{r},\mathbf{R}) = \phi(\mathbf{r},\mathbf{R})\chi(\mathbf{R}), \tag{1.27}$$

with separate electronic, $\phi(\mathbf{r},\mathbf{R})$, and nuclear, $\chi(\mathbf{R})$, solutions.

An additional approximation is the Franck-Condon principle. Initially developed to describe the absorption and emission of light, but extended to charge transfer, the Franck-Condon principle describes transitions between electronic states at fixed nuclear coordinates, known as the Condon approximation (Figure 1.4). The Franck-Condon principle can be illustrated by considering the absorption cross-section of a photon, A,

$$A \propto \langle \psi | \, \mu \, | \psi' \rangle , \tag{1.28}$$

where μ is the transition dipole moment operator coupling the two states $|\psi\rangle$ and $|\psi'\rangle$. Using the Born-Oppenheimer approximation, $|\psi\rangle = |\chi\rangle\,|\phi\rangle$, we write

$$A \propto \langle \phi | \langle \chi | \, \mu \, | \chi' \rangle \, | \phi' \rangle , \tag{1.29}$$

with $|\phi\rangle$ and $|\chi\rangle$ the electronic and nuclear modes respectively. With the Condon approximation, μ only couples electronic states, not nuclear ones, meaning

$$A \propto \langle \chi | \chi' \rangle \, \langle \phi | \, \mu \, | \phi' \rangle . \tag{1.30}$$

The term $\langle \phi | \, \mu \, | \phi' \rangle$ is the transition dipole moment between the two electronic states, while $\langle \chi | \chi' \rangle$ is the nuclear wavefunction overlap. For the absorption of a photon, the nuclear wavefunction overlap is determined by vertically displacing the ground state potential energy surface (PES) by the energy of the photon, known as the vertical Franck-Condon principle (Figure 1.4a). Charge transfer occurs between isoenergetic states and so the PES are not displaced; this is known as the horizontal Franck-Condon principle (Figure 1.4b).

To find the FGR rate, we consider the Hamiltonian $H = H_{\text{S}} + H'$, consisting of a system term, H_{S}, and a perturbative coupling term, H', connecting reactant states $|\psi_{\text{R}}\rangle = \sum_i |\chi_{\text{R}i}\rangle\,|\phi_{\text{R}}\rangle$ to the product states $|\psi_{\text{P}}\rangle = \sum_f |\chi_{\text{P}f}\rangle\,|\phi_{\text{P}}\rangle$. The system term $H_{\text{S}} = H_{\text{R}} + H_{\text{P}}$ consists of a reactant state Hamiltonian,

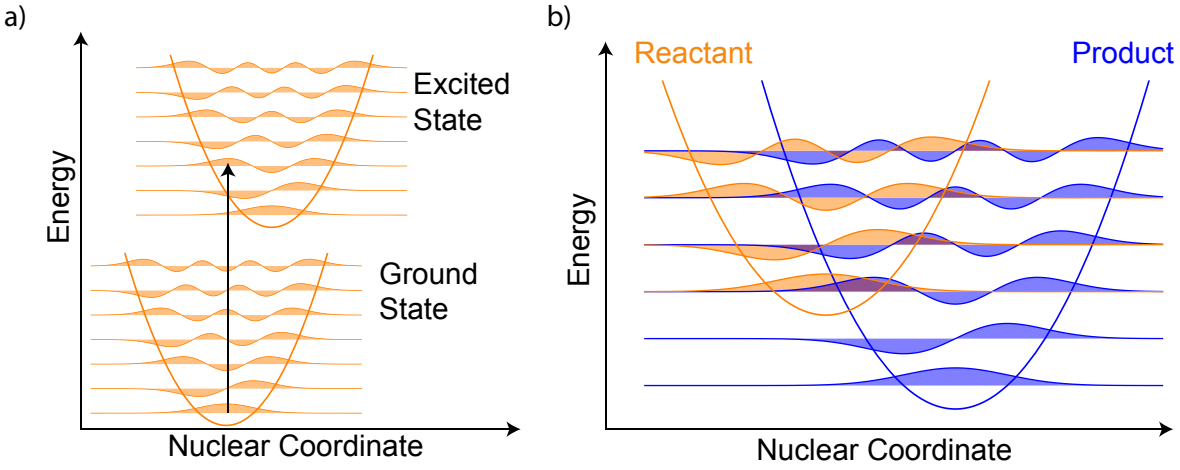

Figure 1.4: Franck-Condon principle. Since electronic states move faster than nuclear, any transition between electronic states takes place at a fixed nuclear coordinate. **(a)** For transfer between states of different energies (*e.g.* due to photon absorption), this is known as vertical transfer (black arrow). **(b)** In the case of states at the same energy, the transition rate is determined through overlap of the reactant and product wavefunctions (plum), known as horizontal transfer.

H_R, and a product state Hamiltonian, H_P. While these Hamiltonians can be general, for the sake of illustration we consider the case where there are no internal dynamics *i.e.* H_R and H_P are diagonal. As such, we write

$$H_\mathrm{R} = E_\mathrm{R} \left|\phi_\mathrm{R}\right\rangle \left\langle\phi_\mathrm{R}\right| + \sum_i E_{\mathrm{R}i} \left|\chi_{\mathrm{R}i}\right\rangle \left\langle\chi_{\mathrm{R}i}\right|, \tag{1.31}$$

$$H_\mathrm{P} = E_\mathrm{P} \left|\phi_\mathrm{P}\right\rangle \left\langle\phi_\mathrm{P}\right| + \sum_f E_{\mathrm{P}f} \left|\chi_{\mathrm{P}f}\right\rangle \left\langle\chi_{\mathrm{P}f}\right|, \tag{1.32}$$

where $E_{\mathrm{R}i}$ and $E_{\mathrm{P}f}$ are the energy of the ith vibrational mode on the reactant PES and the fth vibrational mode on the product PES, respectively. The perturbative coupling is given by

$$H' = V_\mathrm{RP} \left|\phi_\mathrm{R}\right\rangle \left\langle\phi_\mathrm{P}\right| + V_\mathrm{PR} \left|\phi_\mathrm{P}\right\rangle \left\langle\phi_\mathrm{R}\right|. \tag{1.33}$$

With the Hamiltonian defined, we can write the FGR rate

$$k_{\mathrm{R}\to\mathrm{P}} = \frac{2\pi}{\hbar} \left|\left\langle\psi_\mathrm{R}\right| H' \left|\psi_\mathrm{P}\right\rangle\right|^2 \rho \tag{1.34}$$

$$= \frac{2\pi}{\hbar} \left|V_\mathrm{RP}\right|^2 \mathscr{F}; \tag{1.35}$$

$$\mathscr{F} = \sum_{i,f} \rho_{\mathrm{R}i} \left|\left\langle\chi_{\mathrm{R}i}|\chi_{\mathrm{P}f}\right\rangle\right|^2 \delta\left(-\Delta E_\mathrm{PR} + E_{\mathrm{R}i} - E_{\mathrm{P}f}\right), \tag{1.36}$$

where we have used the Condon approximation $\left\langle\psi_\mathrm{R}\right| H' \left|\psi_\mathrm{P}\right\rangle = \left\langle\phi_\mathrm{R}\right| H' \left|\phi_\mathrm{P}\right\rangle \left\langle\chi_\mathrm{R}|\chi_\mathrm{P}\right\rangle$. Here $\mathscr{F}$ is known as the Franck-Condon weighted density of states, which includes the density of states ρ along with the overlap of nuclear wavefunctions. The density of states ensures energy is conserved with the delta function. $\Delta E_\mathrm{PR} = E_\mathrm{P} - E_\mathrm{R}$ is the difference in energy between the two PES. The initial distribution of states on the reactant, $\rho_{\mathrm{R}i}$, is usually taken to be thermal.

By using the Fourier definition of the delta function, $\delta(x) = \int_{-\infty}^{\infty} dt \exp(ixt)/2\pi$, we can write

$$\mathscr{F} = \frac{1}{2\pi\hbar} \sum_{i,f} \int_{-\infty}^{\infty} dt e^{-i\Delta E_\mathrm{PR} t/\hbar} \rho_{\mathrm{R}i} \left|\left\langle\chi_{\mathrm{R}i}|\chi_{\mathrm{P}f}\right\rangle\right|^2 e^{i\left(E_{\mathrm{R}i} - E_{\mathrm{P}f}\right)t/\hbar}, \tag{1.37}$$

and using the completeness relation $\sum_f |\chi_{Pf}\rangle \langle \chi_{Pf}| = \hat{1}$, we write

$$\mathscr{F} = \frac{1}{2\pi\hbar} \int_{-\infty}^{\infty} dt e^{-i\Delta E_{PR} t/\hbar} \sum_i \langle \chi_{Ri}| \rho_R e^{iH_R t/\hbar} e^{-iH_P t/\hbar} |\chi_{Ri}\rangle . \tag{1.38}$$

Equation 1.38 is exactly solvable in the case where H_R and H_P describe normal mode vibrations and ρ_R is a thermal distribution. The Hamiltonians are displaced harmonic oscillators,

$$H_R = E_R + D_R^\dagger H_{vib} D_R \tag{1.39}$$

$$D_R^\dagger = \exp\left(\sum_\xi g_R(\xi)(c_\xi - c_\xi^\dagger) \right) \tag{1.40}$$

$$H_{vib} = \sum_\xi \hbar\omega_\xi \left(c_\xi^\dagger c + 1/2 \right), \tag{1.41}$$

Where E_R is the ground-state energy for the reactant PES, $g_R(\xi)$ the coupling between the reactant state and the ξth vibrational mode, $c_\xi^\dagger$ and c_ξ are the creation and annihilation operators for the ξth vibrational mode respectively, and ω_ξ the frequency of the ξth vibrational mode. The product Hamiltonian is analogously defined by replacing the subscript R with P.

It can be shown that[11]

$$\mathscr{F} = \frac{1}{2\pi\hbar} e^{-G(0)} \int_{-\infty}^{\infty} dt e^{-i\Delta E_{PR} t/\hbar + G(t)}, \tag{1.42}$$

where

$$G(t) = \sum_\xi (g_R(\xi) - g_P(\xi))^2 \left(e^{-i\omega_\xi t}(1 + n(\omega_\xi)) + e^{i\omega_\xi t} n(\omega_\xi) \right), \tag{1.43}$$

with $n(\omega_\xi)$ the Bose-Einstein distribution

$$n(\omega_\xi) = \left(e^{\hbar\omega_\xi / k_B T} - 1 \right)^{-1}. \tag{1.44}$$

By recognising $\lambda = \sum_\xi \hbar\omega_\xi (g_R(\xi) - g_P(\xi))^2$, we can evaluate Equation 1.42 in the high-temperature limit (a detailed solution is available in Chapter 2 from Equation 2.16). We assume 1) that the spectral density goes to zero beyond some cut-off frequency ω_c and $k_B T \gg \hbar\omega_c$; and 2) that the vibrational modes are faster than changes in the electronic energy gap due to nuclear motion, allowing us to consider only the leading terms in the exponents of $G(t)$. This enables us to approximate Equation 1.42 as

$$\mathscr{F} = \frac{1}{\sqrt{4\pi k_B T \lambda}} \exp\left(\frac{-(\Delta E_{PR} + \lambda)^2}{4 k_B T \lambda} \right). \tag{1.45}$$

Substituting Equation 1.45 into Equation 1.35, we arrive at the expression for the rate of charge transfer

$$k_{R\to P} = \frac{2\pi}{\hbar} \frac{|V_{RP}|^2}{\sqrt{4\pi k_B T \lambda}} \exp\left(\frac{-(\Delta E_{PR} + \lambda)^2}{4 k_B T \lambda} \right). \tag{1.46}$$

Note this expression is identical to Equation 1.22 with the coefficient defined in Equation 1.25.

Bridge-mediated charge transfer

While we have so far considered two-state charge transfer, we can also consider the case where transfer does not occur directly between the donor and acceptor but via an intermediary bridge of states. There are two mechanisms by which bridge-mediated charge transfer may occur: sequential hopping, involving charge hopping between sites, $D^-BA \rightarrow DB^-A \rightarrow DBA^-$; and superexchange, where the coupling between the donor and acceptor is extended by a delocalised bridge state, $D^-BA \rightarrow DBA^-$. These are shown in Figure 1.5.

In both cases, we consider a bridge with N elements and nearest-neighbour coupling only, with only the first bridge element coupling directly to the donor, and the Nth coupling to the acceptor. We take the bridge to be energetically distinct, where the energy of the bridge sites, E_n is greater than that of the donor E_D or the acceptor E_A, and the energy difference between elements of the bridge is small compared to the average energy of the bridge E_b, i.e. $|E_n - E_b| \ll E_n - E_D, E_n - E_A$.

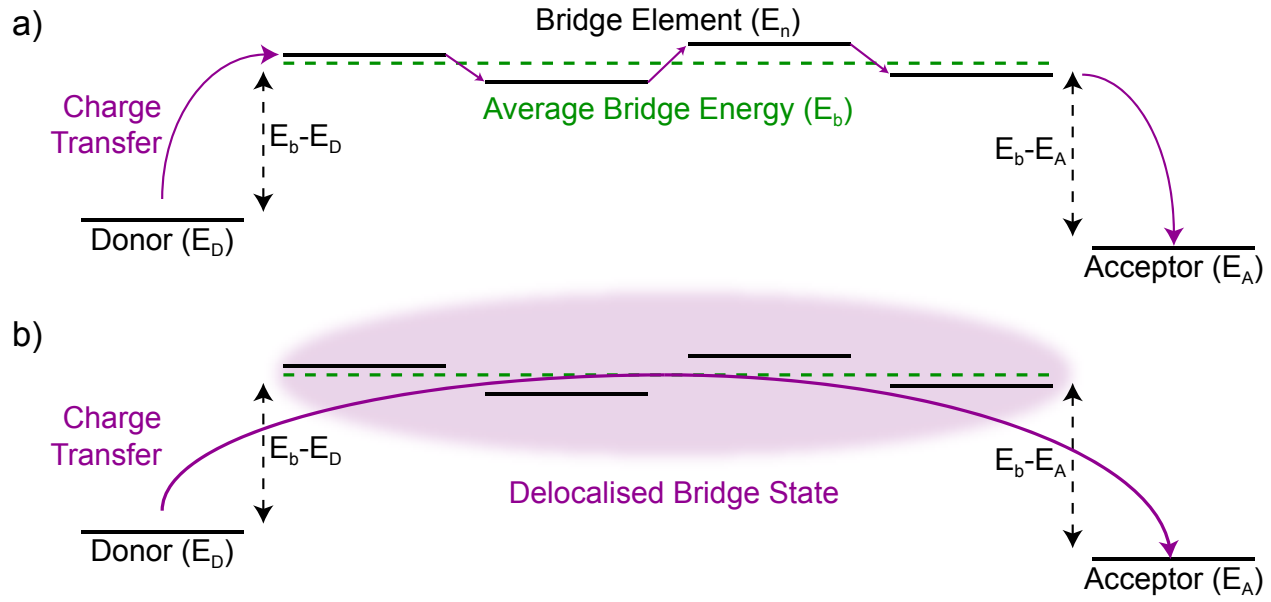

Figure 1.5: Bridge-mediated charge transfer. a) In sequential hopping transfer, the charge engages in a series of hops from the donor to each bridge element, before being transferred to the acceptor. b) In superexchange transfer, the charge wavefunction is extended from the donor through a delocalised bridge state, and subsequently transferred to the acceptor.

In the case of sequential hopping bridge-mediated transfer, the process is a series of thermally-activated charge transfers, with $E_1 - E_D, E_N - E_A \gtrsim k_B T$, whose rates are calculated using Marcus theory. The rate can be calculated by examining the rate of change of charge population on each site:

$$\dot{P}_D = -k_{D,1}P_D + k_{1,D}P_1 \tag{1.47}$$

$$\dot{P}_n = -(k_{n,n+1} + k_{n,n-1})P_n + k_{n+1,n}P_{n+1} + k_{n-1,n}P_{n-1} \tag{1.48}$$

$$\dot{P}_A = -k_{A,N}P_A + k_{N,A}P_N. \tag{1.49}$$

The population of the donor, acceptor, and nth bridge element are P_D, P_A, and P_n respectively, and $\dot{P}$ their rate of change, with $k_{m,n}$ the rate of charge transfer from site m to site n. Following Boltzmann

statistics[20], we also have $k_{n,n+1}/k_{n+1,n} = \exp(E_{n+1,n}/k_{\mathrm{B}}T)$, where $E_{n+1,n} = E_{n+1} - E_n$ is the difference in the site energies of the $n+1$th and nth site.

We can find the charge transfer rate $k_{\mathrm{D,A}}$ by considering that at steady state, $\dot{\mathbf{P}} = 0$, and that the flux into A must be equal to the rate at which charge is transferred from the donor to the acceptor *i.e.* $k_{N,A}P_N = k_{\mathrm{D,A}}P_D$. By taking k_b to be the characteristic rate of charge transfer between bridge elements, and treating A as a sink where $P_A = 0$, we can write the simultaneous equation

$$0 = -k_{1,D}P_1 + k_{D,1}P_D - k_{N,A}P_N \tag{1.50}$$

$$0 = k_bP_1 - k_bP_N - (N-1)k_{N,A}P_N, \tag{1.51}$$

by taking the first element and summing the last $N-1$ elements of $\mathbf{P}$[21]. This simultaneous equation allows for the calculation of a closed-form solution,

$$k_{D,A} = \frac{\exp(-E_{1D}/k_{\mathrm{B}}T)}{k_{N,A}^{-1} + k_{1,D}^{-1} + (N-1)k_b^{-1}}, \tag{1.52}$$

the calculation of which may be found in section 16.13 of ref[21].

The exponential sensitivity to the energy difference between bridge and donor is an Arrhenius rate, with a barrier height E_{1D}, while the denominator consists of three terms: the lifetime of an electron on the Nth bridge state being transferred to the acceptor, $k_{N,A}^{-1}$; the lifetime of an electron on the first bridge state being backtransferred to the donor, $k_{1,D}^{-1}$, and the lifetime of states on the bridge, $(N-1)k_b^{-1}$. This last term gives an overall rate that is inversely proportional to the length of the bridge for large N.

While sequential hopping bridge-mediated transfer involves the charge being transferred to the bridge, in superexchange the effect of the bridge can be considered as a change to the effective coupling between donor and acceptor, affecting the tunnelling rate between the two states. Again, we consider a system consisting of a donor, a bridge consisting of N elements, and an acceptor. To keep notation consistent, we define the donor-bridge-acceptor Hamiltonian H such that the diagonal elements are $H_{1,1} = E_{\mathrm{D}}$, $H_{n,n} = E_{n-1}$ for $2 \leq n \leq N+1$, and $H_{N+2,N+2} = E_{\mathrm{A}}$. Using only nearest-neighbour couplings, we define $H_{1,2} = V_{\mathrm{D},1} = H_{1,\mathrm{D}}^{\star}$, $H_{n,n+1} = V_{n-1,n} = H_{n+1,n}^{\star}$ for $2 \leq n \leq N+1$, and $H_{N+1,N+2} = V_{N,\mathrm{A}} = H_{N+2,N+1}^{\star}$, with all other elements zero.

Using $H|\psi\rangle = E|\psi\rangle$, where E is the lowest energy eigenvalue and ψ is an eigenstate of the Hamiltonian, we expand $|\psi\rangle$ explicitly as a vector,

$$(H - E\mathbf{I})(\psi_{\mathrm{D}}, \psi_1, \ldots, \psi_N, \psi_{\mathrm{A}})^T = \mathbf{0}. \tag{1.53}$$

Repeating this process on the bridge subspace, denoted with subscript b, we write

$$(H_b - E\mathbf{I}_b)|\psi_b\rangle = -(V_{1\mathrm{D}}\psi_{\mathrm{D}}, 0, \ldots, 0, V_{NA}\psi_{\mathrm{A}})^T, \tag{1.54}$$

and consequently

$$|\psi_b\rangle = G(V_{1D}\psi_1, 0, \ldots, 0, V_{NA}\psi_N)^T, \tag{1.55}$$

where the Green's function $G = (E\mathbf{I}_b - H_b)^{-1}$. This Green's function is the solution to the coefficients of the bridge subspace (ψ_1 to ψ_N), allowing us to use Equation 1.54 to write the simultaneous equations

$$(\tilde{E}_\mathrm{D} - E)\,\psi_\mathrm{D} + \tilde{V}_\mathrm{DA}\,\psi_\mathrm{A} = 0 \tag{1.56}$$

$$(\tilde{E}_\mathrm{A} - E)\,\psi_\mathrm{A} + \tilde{V}_\mathrm{AD}\,\psi_\mathrm{D} = 0, \tag{1.57}$$

with perturbed energies

$$\tilde{E}_D = E_D + V_{D1}G_{11}V_{1D}, \tag{1.58}$$

$$\tilde{E}_A = E_A + V_{AN}G_{NN}V_{NA}, \tag{1.59}$$

and effective coupling

$$\tilde{V}_{DA} = V_{D1}G_{1N}V_{NA}. \tag{1.60}$$

The rate of charge transfer with superexchange is given by

$$k_{D\to A} = \frac{2\pi}{\hbar}\frac{|\tilde{V}_{DA}|^2}{\sqrt{4\pi k_\mathrm{B}T\lambda}}\exp\left(\frac{-(\Delta\tilde{E}_{AD}+\lambda)^2}{4k_\mathrm{B}T\lambda}\right). \tag{1.61}$$

A closed-form solution is generated by taking the coupling between bridge units to be identically V_b and writing the characteristic bridge energy E_b. Then we may take the lowest order Dyson expansion in G and write[21]

$$\tilde{V}_{AD} = \frac{V_{D1}V_{NA}}{E_D - E_b}\left(\frac{V_b}{E_D - E_b}\right)^{N-1}. \tag{1.62}$$

This solution holds for weak coupling, $V_{n,n+1} \ll E_b - E_D$. For larger couplings, higher orders in the Dyson expansion must be used.

Adiabatic charge transfer

In deriving Marcus theory, we made the assumption that the electronic coupling between sites was weak relative to the coupling to the environment. This is known as the diabatic (or nonadiabatic) regime, where the Hamiltonian describing the system has small off-diagonal terms in the site basis relative to the diagonal terms.

In the adiabatic limit, this assumption no longer holds. Returning to the parabolas introduced in Equations 1.15 and 1.16, we write the system Hamiltonian

$$H = W_\mathrm{R}(x)\,|\psi_\mathrm{R}\rangle\langle\psi_\mathrm{R}| + W_\mathrm{P}(x)\,|\psi_\mathrm{P}\rangle\langle\psi_\mathrm{P}| + V_\mathrm{RP}\,|\psi_\mathrm{R}\rangle\langle\psi_\mathrm{P}| + V_\mathrm{PR}\,|\psi_\mathrm{P}\rangle\langle\psi_\mathrm{R}|, \tag{1.63}$$

where we have introduced V_RP as the electronic coupling between $|\psi_\mathrm{R}\rangle$ and $|\psi_\mathrm{P}\rangle$. The PES generated by the eigenvalues of this Hamiltonian are

$$W_\pm(x) = \frac{1}{2}kx^2 + \frac{\varepsilon_\mathrm{R}+\varepsilon_\mathrm{P}}{2} \pm \sqrt{\frac{(\Delta E_\mathrm{PR} - Ax)^2}{4} + V_\mathrm{RP}^2}\,. \tag{1.64}$$

Instead of having a reactant and a product PES, we now have an upper (W_+) and a lower (W_-) PES, separated at the transition state by an energy gap of $2V_\mathrm{RP}$, shown in Figure 1.6. Since the adiabatic

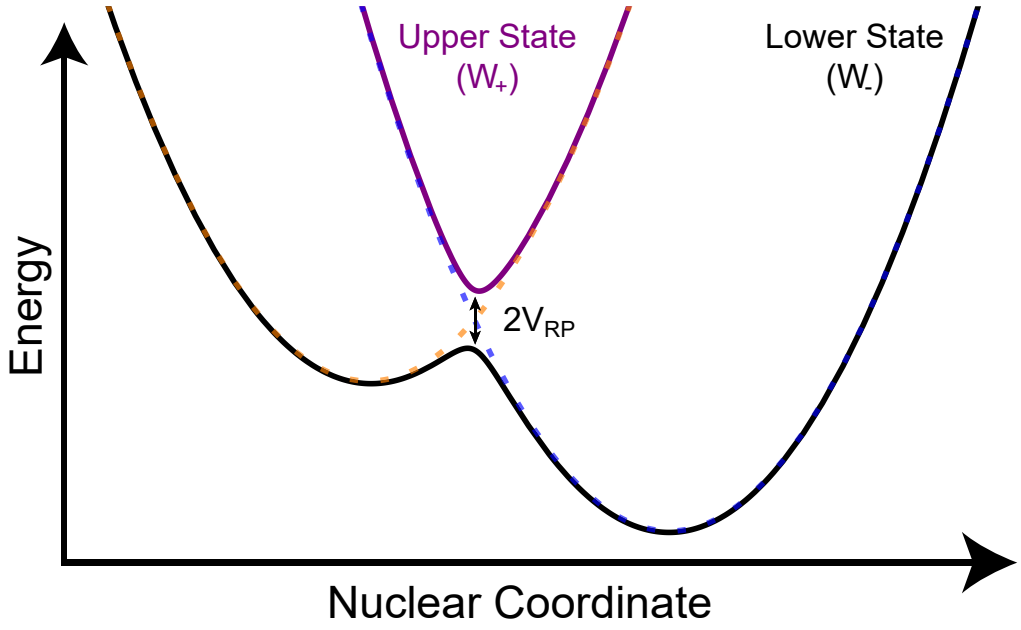

Figure 1.6: Upper (W_+, purple) and lower (W_-, black) adiabatic surfaces created by the coupling between the reactant (orange, dashed) and product (blue, dashed) states. At the closest approach ($x = x_T$) the distance between the surfaces is $2V_{\mathrm{RP}}$, and away from this point W_+ and W_- converge with the reactant and product states.

PES are not diagonal in the site basis, adiabatic transfer involves charge delocalisation over the donor and the acceptor in both the reactant and product states (to various degrees). The rate for adiabatic charge transfer still follows an Arrhenius expression,

$$k_{ab}^{\mathrm{adiabatic}} \propto e^{-\tilde{E}_A/k_{\mathrm{B}}T}, \tag{1.65}$$

with adiabatic activation energy $\tilde{E}_A = W_-(x_T) - W_-(x_a)$. Derivation of this rate equation may be found in the appendix, Section 1.4.1.

Delocalisation can be divided into three broad categories, using the Robin-Day classification scheme[22]. While this system was initially developed to describe charge transfer in mixed-valence metal ligands, it has since found broader application in both inorganic and organic mixed-valence systems[23]. The three classes are Class I, Class II, and Class III, which represent charge transfer between states that are localised, partially delocalised, and fully delocalised respectively, shown in Figure 1.7.

Class I systems have small electronic coupling between reactant and product states relative to the reorganisation energy for charge transfer. This leads to highly distinct states, and allows for the approximations of diabatic charge transfer to be used.

In Class II systems, the electronic coupling is intermediate, $0 < V < \lambda/2$. In these systems, there is separation between the adiabatic ground and excited states, but there are still distinct reactant and product wells, separated by some activation energy. In these systems adiabatic charge transfer techniques can be used.

Class III systems are fully delocalised, with $V \geq \lambda/2$. In this limit the adiabatic ground state forms a single potential well, and the charge is fully delocalised between the donor and acceptor.

Instead of adiabatic charge transfer between donor and acceptor, we can imagine the delocalisation

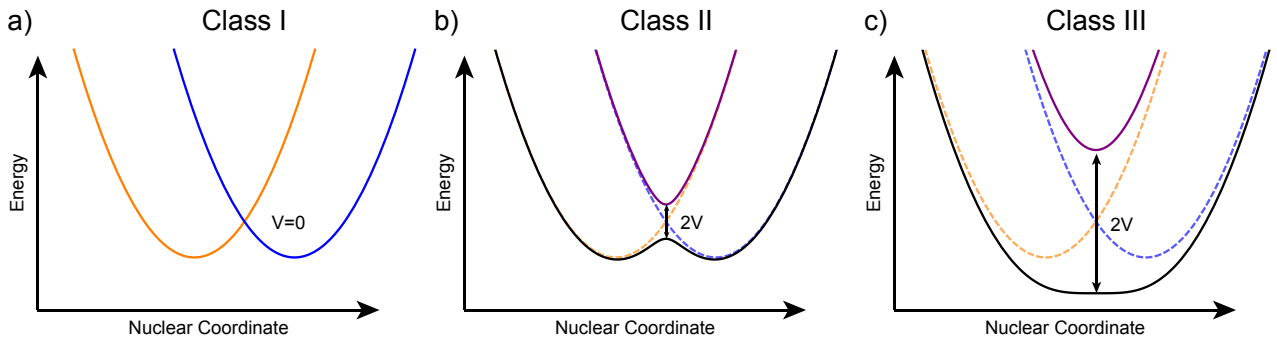

Figure 1.7: Robin-Day classification scheme. a) A class I system ($V = 0$) consists of two individual diabats, and can be treated in the same manner as Figure 1.2. These diabats are included as dashed lines in Figure 1.7b and Figure 1.7c for reference. b) A class II system ($0 \lesssim V < \lambda/2$) shows partial delocalisation due to the coupling between sites, separating the PES into a lower (black) and upper (purple) energy states, with a closest-approach separation of $2V$. Although the barrier between the left and right potential wells has been reduced, the two wells remain independent. c) A class III system ($V \geq \lambda/2$) shows full delocalisation, with the coupling so strong that the two potential wells have merged.

taking place between two donors. This too would generate adiabatic ground and excited states *à la* Class II and Class III systems, which raises a number of questions: how do we describe charge transfer from such a donor to an acceptor? What if the acceptor also experiences similar delocalisation? What if there are more than two sites? To describe such systems, we need a theory of delocalised CT.

We can gain inspiration for a CT theory by examining an analogous system where these questions have been answered: exciton transfer.

1.1.2 Exciton transfer

In 1921, Klein and Rosseland pointed out that if an unexcited atom could be excited by collision with an electron without emitting radiation, then the reverse process should also be possible[24]. This was the beginning of studies into *collisions of the second kind*, any process in which excitonic energy (energy from excited electrons still bound to their atoms/molecules) is transferred through collision, unaccompanied by the creation or annihilation of a photon[25]. This was used to explain particle-mediated excitation energy transfer (EET) in solids that could conduct electrons, but failed in those that could not[26]. At the same time, studies into fluorescence examining chromophores (light-sensitive molecules) in solution were unable to explain fluorescence quenching at a greater rate than predicted by photon-mediated EET[26]. It was noted in the 1940s that a successful theory would also help explain EET in plants and DNA[26].

A solution to this problem was developed by Theodor Förster, who derived a theory of EET that was mediated by neither the collision of matter nor the transmission of photons, but instead involved quantum tunnelling of the excitation energy from donor to acceptor[26] (Figure 1.8). This theory, Förster resonance energy transfer (FRET), determines the rate of EET using the Fermi golden rule rate

$$k = \frac{2\pi}{\hbar}|J_{\mathrm{DA}}|^2 F(E_{\mathrm{DA}}), \tag{1.66}$$

where $F(E_{\mathrm{DA}})$ is the Franck-Condon factor, which describes the overlap of vibrational wavefunctions. Fortunately, we have an easy way to describe these vibrational wavefunctions using the donor emission

spectrum, $L_D(E)$, and the acceptor absorption spectrum, $I_A(E)$. Their overlap can be evaluated using an overlap integral, allowing us to write Equation 1.66 as

$$k = \frac{2\pi}{\hbar}|J_{DA}|^2 \int_{-\infty}^{\infty} dE\, L_D(E) I_A(E), \tag{1.67}$$

where J is the coupling between donor and acceptor, mediated by the Coulomb mechanism, and E is the energy.

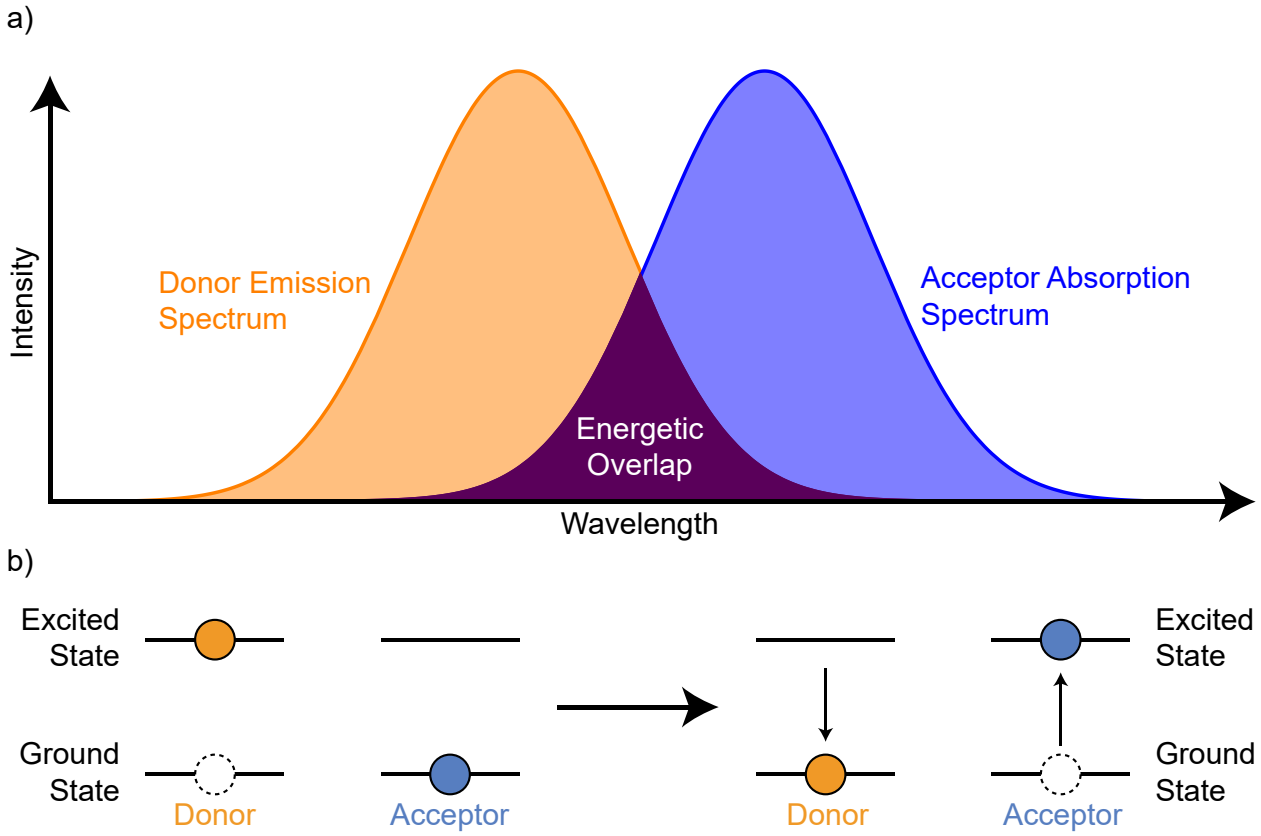

Figure 1.8: Exciton transfer between a donor molecule and acceptor molecule via Förster resonance energy transfer (FRET). a) FRET is caused by the overlap of donor and emission spectra, with the energetic overlap allowing an exciton (electron-hole pair) to tunnel from donor to acceptor. b) The exciton is initially on the donor. During FRET, the donor electron de-excites while simultaneously the acceptor electron excites, tunnelling the exciton from donor to acceptor. FRET is not mediated by a photon, but the process can be seen as the transfer of a virtual photon[27].

For distances greater than about 20 Å, J_{DA} may be approximated by treating the donor and acceptor as point dipoles[28],

$$J_{DA} = \frac{1}{4\pi\varepsilon r_{DA}^3}\left(\mathbf{d}_D \cdot \mathbf{d}_A - 3(\mathbf{d}_D \cdot \hat{\mathbf{r}}_{DA})(\mathbf{d}_A \cdot \hat{\mathbf{r}}_{DA})\right), \tag{1.68}$$

where ε is the absolute permittivity of the medium, $\mathbf{d}_D$ and $\mathbf{d}_A$ are the transition dipole moments of D and A respectively, and $\mathbf{r}_{DA}$ the vector describing their relative positions, with r_{DA} its magnitude and $\hat{\mathbf{r}}_{DA}$ the unit vector. Equation 1.68 is the lowest-order term in the multipole expansion of the Coulomb interaction[29].

Immediately noticeable in Equation 1.68 is the r_{DA}^{-3} dependence of J_{DA}, leading to a rate that is sensitive to the sixth power of distance, $k \propto r_{DA}^{-6}$. Writing the orientation factor $\kappa = \cos(\theta_{DA}) -$

$3\cos(\theta_{RD})\cos(\theta_{RA})$, where θ_{ab} is the angle between a and b, we can express Equation 1.67 as

$$k = \frac{\kappa^2}{8\pi\hbar\varepsilon^2 r_{DA}^6}\int_{-\infty}^{\infty} dE\, L'_D(E) I'_A(E), \tag{1.69}$$

where $L'_D(E) = d_D^2 L_D(E)$ and $I'_A(E) = d_A^2 I_A(E)$.

In the special case where the assumptions behind MT hold for EET, we can simplify this further using similar techniques (*e.g.* Landau-Zener theory, FGR), resulting in the rate equation

$$k = \frac{2\pi}{\hbar}\frac{|J_{DA}|^2}{\sqrt{2\pi k_B T S_{DA}}}\exp\left(\frac{-(\Delta E_{DA} - S_{DA}/2)^2}{2k_B T S_{DA}}\right), \tag{1.70}$$

where S_{DA} is the Stokes' shift (difference between the peak of the maxima of the absorption and emission spectra) between the donor and acceptor[11].

Important to note are the similarities between Equation 1.70 and MT (Equation 1.46); since the Stokes' shift in FRET is twice the reorganisation energy, these two theories are identical in the slow nuclear motion limit, with the exception of the coupling, which decays exponentially with distance in MT and with the sixth power of distance in FRET. This suggests that mathematical tools developed to describe EET could also be used to explore CT.

1.1.3 Transfer of delocalised excitons and charges

Strong inter-site coupling in molecular systems, relative to the environmental coupling, can cause exciton or charge wavefunctions to extend over multiple molecules, called an aggregate, at which the exciton or charge cannot be described as being on an individual site; we call such a charge or exciton delocalised. Transfer of charge from a delocalised state on one aggregate to delocalised state on another is called inter-aggregate charge transfer, and a closed-form description of inter-aggregate charge transfer could prove useful in many systems, such as organic semiconductors, the reaction centres of photosynthetic organisms, inorganic coordination complexes, and conductive metal-organic frameworks.

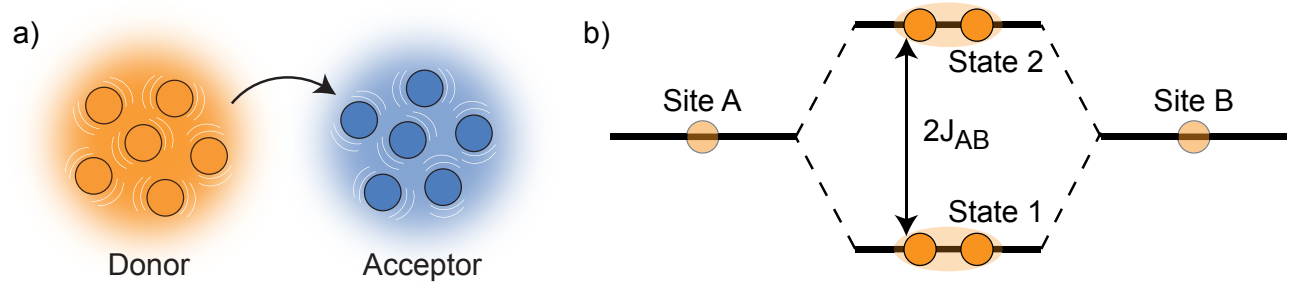

Figure 1.9: a) Delocalised transfer from a donor aggregate (orange) to an acceptor aggregate (blue). The charge or exciton to be transferred between aggregates is not located on an individual site, but its wavefunction extends across the entire aggregate. b) Strong coupling between sites A and B leads to energetic splitting proportional to the coupling, J_{AB}. The resulting states 1 and 2 are delocalised, with their wavefunction extending over both sites, and any charge or exciton transfer will take place from these delocalised states.

The problem of describing delocalised exciton transfer was first addressed with the development of generalised FRET (gFRET) by Sumi[30,31]. Developed to describe exciton transfer in photosynthetic

bacteria, this theory considers two aggregates of chromophores—the donor aggregate with N_D sites labelled $|D_j\rangle$, and the acceptor aggregate with N_A sites labelled $|A_k\rangle$—coupled to two separate phonon baths. The electronic coupling between the chromophores is given by

$$J_{AD} = \sum_{j}^{N_D} \sum_{k}^{N_A} |A_k\rangle J_{kj} \langle D_j| , \tag{1.71}$$

which is weak relative to both the intra-aggregate coupling and the aggregate-bath coupling. The Hamiltonian of this aggregate system is

$$H = H_D^0 + H_A^0 + J_{AD} + J_{DA} + H_{DE} + H_{AE} + H_E, \tag{1.72}$$

where H_D^0 and H_A^0 are the Hamiltonian of the donor and acceptor aggregates, H_{DE} and H_{AE} are the couplings between the donor aggregate and the bath and the acceptor aggregate and the bath (respectively), and $H_E = H_{E_D} + H_{E_A}$ is the Hamiltonian of the environment, which can be divided into donor and acceptor sub-systems. The lowest order perturbation in J_{AD} gives a transfer rate of

$$k = \frac{2\pi}{\hbar} \int dE \sum_j \langle D_j| J_{DA} I_A(E) J_{AD} L_D(E) |D_j\rangle , \tag{1.73}$$

where $J_{DA} = J_{AD}^\dagger$, $I_A(E)$ is the acceptor absorption spectrum, and $L_D(E)$ is the donor emission spectrum. The spectra are written

$$I_A(E) = \sum_k \sum_{k'} |A_k\rangle I_{kk'}(E) \langle A_{k'}| , \tag{1.74}$$

$$L_D(E) = \sum_j \sum_{j'} |D_j\rangle e^{-E/k_B T} I_{jj'}(E) \langle D_{j'}| , \tag{1.75}$$

$$I_{kk'}(E) = c_{kk'} \int dF\, e^{-F/k_B T} \,\mathrm{Tr}_E \langle A_k| \delta(H_{AE} - E - F) |A_{k'}\rangle \delta(H_{E_A} - F), \tag{1.76}$$

where $c_{kk'}$ is a normalisation constant and Tr_E is the trace over the environmental modes. $I_{jj'}(E)$ is analogously defined on the donor. We can write the eigenstates of H_D^0 and H_A^0 as $|D_\alpha\rangle, |A_\beta\rangle$, which we refer to as the adiabatic basis. This allows us to write $J_{\beta\alpha} = \langle A_\beta| J_{AD} |D_\alpha\rangle$. If the initial exciton population can be approximated as diagonal in the adiabatic basis on the donor aggregate, Equation 1.73 becomes

$$k = \frac{2\pi}{\hbar} |J_{\alpha\beta}|^2 \int dE\, \langle A_\beta| I_A(E) |A_\beta\rangle \langle D_\alpha| L_D(E) |D_\alpha\rangle . \tag{1.77}$$

This equation for gFRET illustrates that in the case that donor molecules are more strongly attracted to each other than the acceptor molecules, and *vice versa*, we can stop seeing transfer as occurring between individual donor and acceptor molecules but between a donor aggregate and an acceptor aggregate. This delocalised transfer is important, because it allows for the constructive or destructive interference between individual site transfer pathways. This can be illustrated by considering a system of one donor (D) and two acceptors (A_1 and A_2); if the two acceptors have negligible coupling to each other, we can write:

$$k_{\mathrm{FRET}} \propto \frac{1}{2} |J_{DA_1}|^2 + \frac{1}{2} |J_{DA_2}|^2, \tag{1.78}$$

i.e. the exciton has a 50-50 chance of being transferred to either acceptor at a rate proportional to their coupling. If we take $J_{DA_1} = J_{DA_2} = J_{DA}$, we can see $k \propto |J_{DA}|^2$, identical to the rate of exciton transfer from a donor to a single acceptor. However, if the acceptors are strongly coupled, transfer will occur to a delocalised state:

$$k_{\text{gFRET}} \propto \left| \frac{J_{DA_1} + J_{DA_2}}{\sqrt{2}} \right|^2, \tag{1.79}$$

and in the case of $J_{DA_1} = J_{DA_2} = J_{DA}$, $k_{\text{gFRET}} = 2k_{\text{FRET}}$. Similarly, we could posit $J_{DA_1} = -J_{DA_2} = J_{DA}$, which would result in $k_{\text{gFRET}} = 0$. When the transfer is enhanced in this manner, the process is known as *supertransfer*, and when it is slowed, *subtransfer*.

Delocalised exciton transfer was further generalised into multi-chromophoric FRET (MC-FRET), which includes time-dependent internal dynamics within the donor aggregates[32],

$$k = \sum_{jj'} \sum_{kk'} \frac{J_{jk} J_{j'k'}}{\pi \hbar^2} \int_{-\infty}^{\infty} d\omega \, L_{jj'}(t, \omega) I_{kk'}(\omega), \tag{1.80}$$

$$I_{kk'}(\omega) = \int_{-\infty}^{\infty} dt \, e^{i\omega t} \, \text{Tr}_E \, e^{iH_{E_A} t/\hbar} \langle A_k | e^{-iH_A t/\hbar} | A_{k'} \rangle \rho_A, \tag{1.81}$$

$$L_{jj'}(t, \omega) = \text{Re} \int_0^t d\tau e^{-i\omega\tau} \, \text{Tr}_E \, e^{-iH_{E_D}\tau/\hbar} \langle D_j | e^{-iH_D(t-\tau)/\hbar} | E \rangle \langle E | \rho_D e^{-iH_D t/\hbar} | D_{j'} \rangle, \tag{1.82}$$

where $H_A = H_A^0 + H_{AE}$ and $H_D = H_D^0 + H_{DE}$, ρ_A and ρ_D the initial state of A and D, and $|E\rangle\langle E|$ the initial excitation of the donor aggregate, such as through a laser pulse. Equation 1.73 is the stationary limit of Equation 1.80. A closed form expression for MC-FRET was developed in the high temperature, slow bath limit[33]

$$k = \sum_{\alpha\beta} \frac{\rho_\alpha}{2\pi} \frac{|J_{\alpha\beta}|^2}{\sqrt{4\pi k_{\text{B}} T S_{\alpha\beta}}} e^{-(S_{\alpha\beta} + \Delta E_{\beta\alpha})^2 / 4 k_{\text{B}} T S_{\alpha\beta}}, \tag{1.83}$$

where $S_{\alpha\beta}$ is the Stokes shift, and ρ_α is the initial exciton distribution on α. Being similar in form to the MT rate equation, Equation 1.83 offers one immediate qualitative prediction, which has yet to be experimentally verified: the existence of an inverted regime for multi-chromophoric exciton transfer.

While Equation 1.83 describes inter-aggregate exciton transfer, no such closed-form expression existed for charge transfer, which would provide significant qualitative insight into the behaviour of charge transfer in delocalised molecular systems, such as whether or not an inverted regime exists. While quantum chemical simulations would allow aggregates to be treated as supermolecules to allow the use of MT, this approach is computationally expensive (scaling up to exponentially with system size) and inflexible (any modification of the system, such as the removal of a single molecule, would necessitate a recalculation of the entire system). We introduce a theory of delocalised charge transfer in Chapter 2.

One system where delocalisation occurs is the photosynthetic reaction centre (RC), which accepts excitonic energy from an antenna system that absorbs light, and uses this energy for charge separation at a pair of molecules known as the special pair (SP). The RC is a dimer, with each monomer contributing one molecule to the SP, and the strong coupling between SP molecules ensures that the charge is transferred from a delocalised state. However, in most organisms the charge proceeds down only one branch of the RC[34], leading to the question: why is the RC dimeric? In order to explore how delocalisation contributes to charge transfer rate in the RC, we enter the field of quantum biology.

1.2 Quantum Biology

Quantum biology is the field of study examining how biological systems exploit quantum physical effects to function. While even early founders of quantum theory, such as Bohr[35] and Schrödinger[36], recognised that quantum effects would play an important role in biological systems, the effects then-recognised were trivial (*e.g.* molecules are described using quantum theory, biological systems are made of molecules, ergo biological systems are described by quantum theory), or direct interactions with light (photochemistry is an inherently quantum phenomenon)[37], and by the 1960s the idea that quantum physics played only a trivial role in biology was so common as to be considered "pedestrian"[38].

That isn't to say that there were no investigations into non-trivial quantum effects into biology before the 1960s: it was recognised as early as the 1930s and '40s that quantum effects may be important in systems such as energy transfer within photosynthetic structures and DNA[26], or in olfaction exploiting vibrational mechanisms[39]. With the advent of modern experimental tools and techniques, quantum biology—the study of how biological systems exploit quantum physical effects to attain or enhance functionality[40]—has begun to attract broader scientific interest[41]. This has included research into features as disparate as quantum coherence in photosynthesis[30,42,43], radical pairs in magnetoreception[44–46], inelastic tunnelling in olfaction[47–49], and proton tunnelling in enzymatic reactions[50–52].

In some systems, it has been suggested that the hot (room temperature) and noisy (disordered) nature of the environment and systems help, rather than hinder, quantum transport effects through a set of mechanisms collectively known as environment-assisted quantum transport (ENAQT)[53–56].

Perhaps the most studied systems in quantum biology have been the light-harvesting apparatus in photosynthetic organisms, in which the photosynthetic reaction centre is buried.

1.2.1 Light-harvesting systems

Brief evolutionary overview

It is uncertain when photosynthesis first evolved, but light-harvesting organisms were among the earliest forms of life[57]. Geological evidence points to the Archæan as the origin of photosynthesis, with isotopic evidence of autotrophy (fixation of inorganic carbon) as far back as 3.8 Ga (giga annum, or billion years ago)[57,58], although dates for the origin of photosynthesis earlier than 3.5 Ga are highly contentious[59–61]. Microfossil and stromatolite (fossilised bacterial biofilms) evidence suggests an origin for photosynthesis 3.3 Ga to 3.5 Ga[57–62]. Evidence of oxygenic photosynthesis, in the form of banded iron formations (BIFs), begin as early as 3.7 Ga, but these can also be explained by anoxygenic ferrous-driven photosynthetic organisms[58,63].

Unambiguous evidence of oxygenic photosynthesis from cyanobacteria dates from 2.7 Ga to 2.8 Ga, coinciding with an increase in deposition of BIFs which likely served as a buffer to keep atmospheric oxygen levels low[58]. Once the soluble iron had been oxidised, oxygen gradually started building in

the atmosphere, reaching up to 2% by 2.0 Ga; by this date, molecular evidence for both cyanobacteria and purple bacteria is established[63].

Sometime between 1.5 Ga to 1.8 Ga the first photosynthesising eukaryotes appeared[65,66]. This was due to an endosymbiosis event, whereby a eukaryotic cell incorporated a cyanobacterium into itself[67,68], gaining the ability to photosynthesise. As such, the fundamental nature of the light-harvesting apparatus of plants, green algae, and cyanobacteria are extremely similar[63]. Differences have evolved over time, however, to such a degree that cyanobacteria and eukaryotic light-harvesting complexes cannot be considered interchangeable.

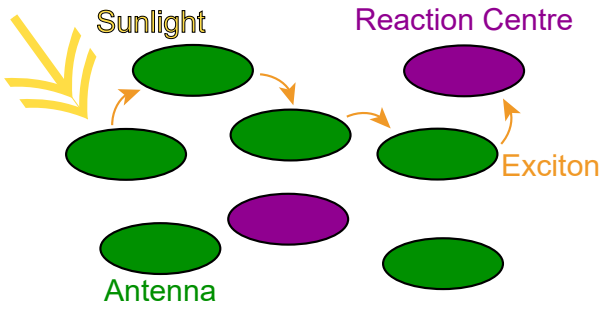

Figure 1.10: A simplified model of a photosynthetic complex, based on purple bacteria. Sunlight (yellow) is absorbed by an antenna complex (green), creating an exciton (orange). The exciton is transferred between antenna complexes until it arrives at the reaction centre (purple). This transfer is highly efficient, taking place with near-unity quantum efficiency[64].

There are six major extant lineages of photosynthetic complex: cyanobacteria (including plants and green algae), acidobacteria (phylum *Acidobacteria*), heliobacteria (family *Heliobacteriaceae*), green sulphur bacteria (phylum *Chlorobi*), filamentous anoxygenic phototrophs (FAPs) (photosynthetic members of phylum *Chloroflexi*), and purple bacteria (photosynthetic members of phylum *Proteobacteria*); all of which are differentiated by the structure of their light harvesting complexes[63,69–71] but despite their differences all function with near-unity quantum efficiency from photon absorption to charge separation[34,72] (although significantly lower thermal efficiency[73], the total energy output compared to the energy of the incident light). Light harvesting complexes consist broadly of two components: an antenna, which absorbs photons to create electronic energy in the form of excitons; and a reaction centre (RC), which converts excitons into chemical energy in the form of an electron to perform reduction (Figure 1.10). These two structures vary significantly amongst extant organisms (Table 1.1), and are described independently below.

Antennae

Antenna systems vary wildly between organisms, but all are pigment-protein complexes that employ pigments known as chlorophylls (Chl) for cyanobacteria and eukaryotic organisms, and bacteriochlorophylls (BChl) for the remaining bacterial lineages. How these are arranged depends on the organism, but can be divided into two classes: extrinsic antennae, which do not cross the organisms' lipid bilayer membrane; and integral antennae, which span the membrane and can be buried deep within it. The integral membrane antennas can be further divided into two groups: peripheral antennae, which serve to harvest light in organisms without an extrinsic antenna, and core antennae which can either be separable from or fused to the reaction centre. Heliobacteria are unique amongst photosynthetic organisms in that they completely lack both an extrinsic and a peripheral antenna complex, instead relying on the fused core antenna for all light harvesting[74].

		Integral Membrane Protein			
		Antenna		Reaction Centre	
Organism	Extrinsic Antenna	Peripheral	Core	Type I	Type II
Acidobacteria	Chlorosome, baseplate, FMO	—	Fused	✓	—
Cyanobacteria	Phycobilisome	—	CP43, CP47	✓	✓
FAPs	Chlorosome, baseplate	—	LH1	—	✓
Green sulphur bacteria	Chlorosome, baseplate, FMO	—	Fused	✓	—
Heliobacteria	—	—	Fused	✓	—
Purple bacteria	—	LH2	LH1	—	✓
Eukaryote	—	LHC-II	CP43, CP47	✓	✓

Table 1.1: Light-harvesting complexes of the photosynthetic lineages, divided into extrinsic (does not span the membrane) and intrinsic membrane proteins. FAPs = filamentous anoxygenic phototrophs; FMO = Fenna-Matthews-Olson complex; LH1 & 2 = light-harvesting complex 1 & 2 (bacteria); LHC-II = light-harvesting complex II (eukaryote). Details of the antennae and reaction centres can be found in their respective sub-sections. *Fused* indicates that the core antenna complex are subunits of the same protein structure that includes the reaction centre.

Extrinsic antennae

Acidobacteria, green sulphur bacteria, and FAPs have chlorosome-based extrinsic antennae, which is a sac-like organelle that contains a large number of BChl pigments, most of which are not bound by proteins. When excited by a photon, the chlorosome funnels the energy (in the form of an exciton) to the baseplate, a two-dimensional array of BChl in a protein matrix[75]. In FAPs, the energy is then transferred directly to the core antenna, while in acidobacteria and green sulphur bacteria it is transferred to the RC *via* the Fenna-Matthews-Olson complex (FMO), a trimer consisting of three monomers each containing eight BChl supported by a protein scaffold[76,77]. From the FMO the exciton is transferred to the RC.

Cyanobacteria also contain an extrinsic antenna, although rather than the sac-like chlorosome it's a protein-pigment structure called the phycobilisome[63]. This consists of rods of a pigment-protein complex phycoerythrin (not present in all organisms) to absorb short-wavelength light; attached to the base of these rods is a phycocyanin pigment-protein structure, which absors mid-wavelength light; and connecting the rest of the antenna to the RC is the allophycocyanin, which absorbs long-wavelength light. The respective absorption maxima helps the phycobilisome act like an energetic funnel, with lower energies closer to the RC and higher farther away. Red algae, although they are eukaryotes, have an antenna system similar to cyanobacteria[34].

Peripheral antennae

Peripheral antennae are integral membrane protein-pigment complexes that collect light but do not transport it to the RC, instead either transporting the energy between peripheral antenna structures or

to the core antenna system.

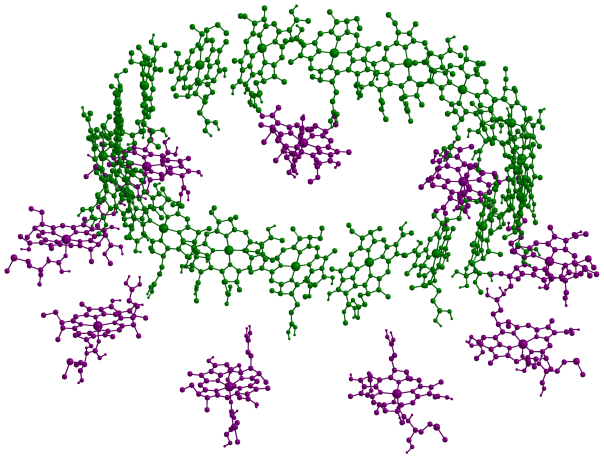

Figure 1.11: Crystallographic structure of light-harvesting complex 2 (LH2) of purple bacteria[78]. The B800 ring (purple) absorbs light, and transfers the energy to the B850 ring (green) in under 1 ps. The exciton is delocalised across the B850 ring due to tight coupling between the BChl molecules[79]. Supporting structures and BChl tails removed for clarity.

In purple bacteria, the peripheral antenna consists of light-harvesting complex II (LH2), which consist of nine subunits of three BChl bound and a carotenoid bound to a protein[63]. Each LH2 complex contains two rings of BChl: B800, containing nine BCHl; and B850, containing eighteen BChl. These rings are named after their peak absorption wavelength (800 nm and 850 nm respectively), and are stacked atop one another. As the B800 ring is higher in energy, it transfers the excitonic energy to the B850 ring, which then transfers the energy edge-to-edge with either another LH2 complex, or to the core antenna complex.

The peripheral antenna of eukaryotes is a supercomplex containing light-harvesting complex II (LHC-II) units. These units consist of twelve Chl molecules which serve to act as an antenna to absorb light, and transport it to the core antenna complex[81].

Core antennae

In FAP and purple bacteria, the RC is surrounded by a ring of BChl called the light-harvesting complex I (LH1). This ring consists of approximately sixteen subunits, each with two BChl pigments supported by a protein and carotenoid[63]. This ring surrounds the bacterial RC, and can absorb light directly or accept energy in the form of an exciton from an LH2 unit, whereupon it transfers the energy to the RC.

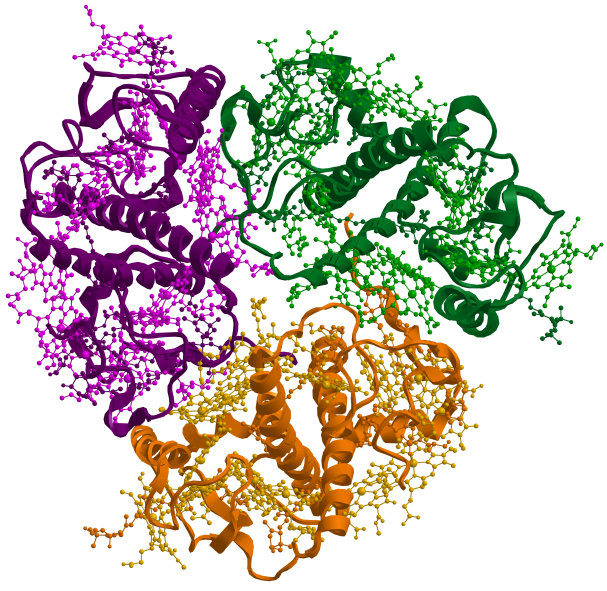

Figure 1.12: Crystallographic structure of light-harvesting complex II (LHC-II) trimer in plants[80].

In eukaryotes and cyanobacteria, CP43 and CP47 are the protein-pigment structures that act as the core antenna. These sit on either side of the reaction centre complex, and consist of ten to twelve (CP43) or twelve to fourteen (CP47) Chl molecules in a protein backbone. When energy is transferred to CP43/47, the structure acts as an energetic funnel to direct the energy to the RC. This structure is homologous to the fused core antennae of acidobacteria, green sulphur bacteria, and heliobacteria, but are coded for in separate genes to the RC.

Reaction centre

All extant RCs are dimeric integral membrane pigment-protein complexes, with the cofactor dimer made of two monomers that couple at a pair of (B)Chl known as the special pair (SP)[34]. Excitons from the antenna are transferred to SP, where they are delocalised across both constituent molecules. The charge is then transferred from this delocalised state on the SP to the primary acceptor (which may be a (B)Chl or a (bacterio)phaeophytin (BPhe) depending on organism), and from there it is transferred to the ultimate charge acceptor. The delocalisation across the SP molecules is universal in all light-harvesting organisms, and the reason this evolved is a mystery[34].

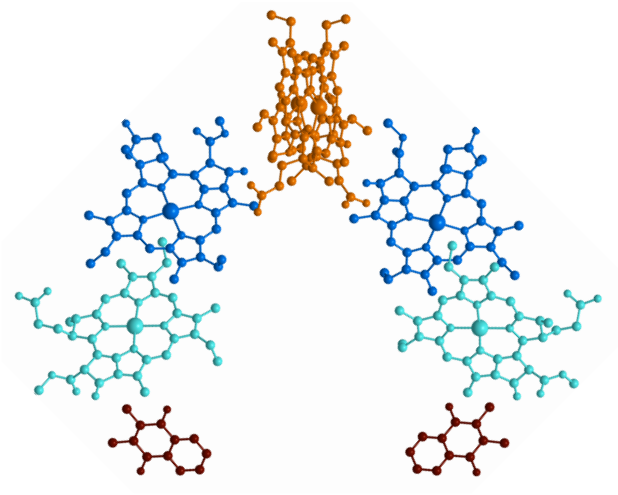

Figure 1.13: Crystallographic structure[82] of a Type II photosynthetic reaction centre, with protein scaffold and tails removed for clarity. The RC is a dimer consisting of two monomers, each of which contains a special pair (bacterio)chlorophyll (orange), accessory (B)Chl (dark blue), and (bacterio)phaeophytin (cyan). Type II RCs use quinones (brown) as charge acceptors, while Type I use iron-sulphur complexes.

RCs are divided into two classes, depending on the nature of this ultimate acceptor: type I, or iron-sulphur (FeS) type, reduce a ferrodoxin to create chemical energy, while type II, or quinone type (Q-type), reduce a quinone to a quinol. The structure of these RCs is shown in Figure 1.13.

In anoxygenic organisms, there is only one type of RC, as shown in Table 1.1, which provides an electron to drive metabolic function. In oxygenic photosynthesis, the two different RCs perform two different functions: the Type II RC uses the exciton's energy to oxidise water (using a system known as the oxygen-evolving complex (OEC)), and transfers the electron to the Type I RC (via the cytochrome), where it is excited by another exciton and used to drive metabolism.

The two branches of the RC can be symmetric, as is the case in heliobacteria[34,74,83], with identical probability of charge transfer down either; however, in most organisms the RC is asymmetrical, with charge preferably travelling down one branch, called the active branch[34]. This is accomplished by by differences in electronic coupling between SP and the primary charge acceptor on each branch[84], and energetic asymmetries between the branches, which also has the effect of affecting the charge delocalisation on SP—the charge ranges from fully delocalised across both (B)Chl in P[84–86], to being strongly asymmetrical[87].

The fact that in many organisms charge transfer occurs down one branch only raises the question: why is the RC dimeric? As delocalisation is an inherently quantum phenomenon, we must examine quantum effects in photosynthesis.

1.2.2 Quantum effects in photosynthesis

Delocalisation is a quantum effect that occurs in the RC and other photosynthetic systems. To better understand how quantum effects affect the RC, we will first examine quantum effects known in other light-harvesting systems.

Quantum effects in photosynthesis can broadly be divided into two categories: incoherent transfer, first proposed in the 1940s[26], and coherent transfer, proposed in the 1930s[41,88]. However, it was not until a number of advances were made in EET and CT theory, new experimental tools and techniques were developed, and the structure of light-harvesting structures were better understood that these theories could be tested.

In the late 20th century, gFRET was developed to describe incoherent exciton transfer between the two BChl rings in LH2 of purple bacteria and transfer to the SP from the LH1 ring[30]. The transfer between delocalised states lead to supertransfer at a rate 20–30 times that predicted by FRET, due to the interference of exciton-transfer pathways from different sites[30,79,89]. Further, the enhancement is significantly greater than would be expected if the transition dipoles of the BChls in the ring were randomly oriented, indicating that supertransfer may have been evolutionarily selected for[90,91].

At the same time as gFRET was being used to describe incoherent transfer in the LH complexes of bacteria, pump-probe spectroscopy was showing unusual oscillations in FMO. This was explained by coherent superpositions of electronic states evolving in time[92], and was supported in 2007 using two-dimensional electronic spectroscopy (2DES) at cryogenic temperatures[42], and again at room temperature by two independent groups in 2010[89,93]. This explanation proposed that wave-like oscillations were important for the (near-unity) efficiency of excitonic transfer through the FMO. Critics of this theory questioned whether such wave-like oscillations can occur in incoherent sunlight[94], whether the coherence serves to enhance exciton transfer[95,96], and ultimately whether the transfer was indeed between excitonic states[43,97–100].

While it is now generally accepted that the oscillations in FMO are due to vibronic (vibrational and electronic) coherences[41,101], rather than electronic ones, the importance of these coherences are still a matter of active study in both FMO[40,96,102] and other light-harvesting systems[41,96,101], especially the bilisomes of marine algae[101].

Research demonstrating that coherent excitonic states are not excited *in vivo* by incoherent sunlight, but that stationary states (states that are diagonal or nearly diagonal in the energy basis) are[94,103,104], has still left open the possibility of quantum effects being important through incoherent transfer within LH structures, between LH structures, and from LH structures to the RC. While the LH structures of bacteria are highly ordered and symmetrical complexes, the antennae of many other organisms are quasi-disordered to the point of almost appearing random[41]. Recent work has suggested that the degree of delocalisation, determined by static disorder, is the dominant term in describing exciton transfer in a number of photosynthetic systems[96], including FMO. Since delocalisation of excitons across multiple molecules is important in many photosynthetic systems, including energy transport to the RC, supertransfer plays a role in enhancing transport[94,96]. Further, ENAQT can interrupt coherent effects that localise the exciton (*e.g.* Anderson localisation), allowing the delocalisation to persist on

exciton transfer timescales[94].

With this established, we can now turn our attention to the RC. Coherent dynamics in the RC is still an active area of investigation, due to the high efficiency and speed of charge separation and transfer. The coupling of charge transfer states to nuclear modes was suggested to play a functional role in the efficiency of charge transfer since the 1990s[105,106], and recent work with 2DES has detected quantum beats at a number of frequencies that correlate with charge transfer, exciton, and vibrational states at room temperature[106–108]. As such, vibronic coherences have been suggested to play an active role in charge separation at physiological temperatures in both bacterial and oxygenic photosynthesis[43,98,106–109]. Although the mere presence of quantum beating doesn't mean that coherence is playing a functional role in charge separation, this is an active field study that is currently seeing much activity.

1.3 Thesis Outline

We have now isolated two key problems: (1) how does delocalisation in molecular systems affect charge transfer; and (2) why did the photosynthetic reaction centre dimerise? Chapter 2 will answer the first question by introducing generalised Marcus theory, which offers a way to calculate the rate of transfer of delocalised charges between aggregates of molecules using the known charge transfer properties of the constituent molecules. Chapter 3 will answer the second question by using generalised Marcus theory from Chapter 2 to demonstrate dimerisation diminished charge transfer within the reaction centre but enhanced excitonic transfer to the reaction centre, likely improving overall efficiency. Future research opportunities offered by the results of these chapters are discussed in Chapter 4.

1.4 Appendix

1.4.1 Derivation of Landau-Zener rate

To derive the Landau-Zener rate, we start from Equation 1.24,

$$H_{ab}(x) = W_a(x)\,|\phi_a\rangle\langle\phi_a| + W_b(x)\,|\phi_b\rangle\langle\phi_b| + V_{ab}\,|\phi_a\rangle\langle\phi_b| + V_{ba}\,|\phi_b\rangle\langle\phi_a|, \tag{1.84}$$

with initial population entirely in state $|\phi_a\rangle$. At the transition state $x = x_T$, $W_a = W_b$; away from the transition state, $|W_a(x) - W_b(x)| \gg |V_{ab}|$. In order to understand what happens at this transition, we examine the potential energy surface near the transition point,

$$W_a(x) = W_a(x_T) + \left.\frac{\partial W_a(x)}{\partial x}\right|_{x=x_T}(x - x_T), \tag{1.85}$$

and similarly for $W_b(x)$. We note two things about this situation: first, that a particle trying to cross between the surfaces will experience an effective force on surface a of $F_a = -\left.\frac{\partial W_a(x)}{\partial x}\right|_{x=x_T}$ (and similarly for b), and since the probability of transition decreases exponentially with barrier height (*cf.*

Equation 1.5, the Arrhenius rate), the transition occurs only when $x - x_T$ is small, and so we write $x - x_T \approx v_T t$, where v_T is the velocity (crossing attempt frequency per unit time) at the transition point. This allows us to write the time-dependent Hamiltonian

$$H_{ab}(x_T,t) = -F_a v_T t \left|\phi_a\right\rangle \left\langle\phi_a\right| - F_b v_T t \left|\phi_b\right\rangle \left\langle\phi_b\right|. \tag{1.86}$$

We can use Equation 1.86 to construct a time-evolution operator, $U(t,t')$ from $H_{ab}(t) + V_{ab}\left|\phi_a\right\rangle \left\langle\phi_b\right| + V_{ba}\left|\phi_b\right\rangle \left\langle\phi_a\right|$,

$$U(t,t') = U_0(t,t')S(t,t'), \tag{1.87}$$

where the unitary operator, $U_0(t,t')$, and the scattering matrix, $S(t,t')$, are defined through perturbation expansions:

$$U_0(t,t') = T\exp\left(\frac{-i}{\hbar}\int_{t'}^{t} d\tau H_{ab}(\tau)\right); \tag{1.88}$$

$$S(t,t') = T\exp\left(\frac{-i}{\hbar}\int_{t'}^{t} d\tau U_0^{\dagger}(t,t')\hat{V}U_0(t,t')\right), \tag{1.89}$$

where $\hat{V} = V_{ab}\left|\phi_a\right\rangle \left\langle\phi_b\right| + V_{ba}\left|\phi_b\right\rangle \left\langle\phi_a\right|$, and T is the time-ordering operator.

As $H_{ab}(x_T,t)$ consists of two terms that commute, Equation 1.88 evaluates to[11]

$$U_0(t,t') = e^{iv_T F_a(t^2-t'^2)/2\hbar}\left|\phi_a\right\rangle \left\langle\phi_a\right| + e^{iv_T F_b(t^2-t'^2)/2\hbar}\left|\phi_b\right\rangle \left\langle\phi_b\right|, \tag{1.90}$$

which allows the evaluation of $S(t,t')$.

The probability of remaining on the reactant state is $P_a(t=\infty)$. Assuming that the population was initially ($t=-\infty$) on the reactant state, we can use the time evolution operator, Equation 1.87 to evaluate $P_a = \left|\left\langle\phi_a\right| U(-\infty,\infty)\left|\phi_a\right\rangle\right|^2 = e^{-\Gamma}$, where the Massey parameter

$$\Gamma = \frac{2\pi}{\hbar}|V_{ab}|^2 \frac{1}{v_T|F_a - F_b|}\bigg|_{x=x_T}. \tag{1.91}$$

The probability of crossing from $\left|\phi_a\right\rangle$ to $\left|\phi_b\right\rangle$ at the transition state with velocity v_T for a single crossing attempt is $1 - e^{-\Gamma}$.

At this point it is useful to find $H_{ab}(x_T)$. The two eigenvalues of the Hamiltonian are

$$W_{\pm}(x) = \frac{W_a(x) + W_b(x)}{2} \pm \sqrt{|V_{ab}|^2 + \frac{1}{4}(W_a(x) - W_b(x))^2}, \tag{1.92}$$

and since $W_a(x_T) = W_b(x_T)$, we can write

$$W_{\pm}(x_T) = W_a(x_T) \pm |V_{ab}|. \tag{1.93}$$

Since the probability of crossing from the lower state, $W_-(x)$, to the upper state, $W_+(x)$, is P_a for a single crossing attempt, we can calculate the probability of ending up in the reactant side of the $W_-(x)$. Once on the upper surface, the probability of crossing back to the reactant side of the lower state in a single attempt is P_a, meaning there's a $1 - P_a$ chance of staying on the upper surface. This means that the probability of a second attempt occurring is $(1 - P_a)^2$ which has a P_a chance of success, since the

particle has to fail to cross to the lower barrier twice before another attempt is made. As such, we can write the probability of transitioning from the reactant to product sides of $W_-(x)$ as

$$P_{ab} = 1 - e^{-\Gamma}(e^{-\Gamma} + (1-e^{-\Gamma})^2 e^{-\Gamma} + (1-e^{-\Gamma})^4 e^{-\Gamma} + \cdots) \tag{1.94}$$

$$= 1 - e^{-2\Gamma}. \tag{1.95}$$

We examine the case where $W_a(x)$ and $W_b(x)$ are harmonic potentials, $W_a(x) = m_a\omega_a^2(x-x_a)^2/2$ and $W_b(x) = m_b\omega_b^2(x-x_b)^2/2$, and share the same curvature, $m_a\omega_a^2 = m_b\omega_b^2 = m\omega_{\text{vib}}^2$, as per Equations 1.10 and 1.11. If we consider the distribution of transition velocities, $P(v_T)$, to be thermal, we can express $P(v_T)$ as a Boltzmann distribution

$$P(v_T) = Q^{-1} e^{-mv_T^2/2k_\text{B}T} \cdot Z^{-1} e^{-\tilde{E}_A/k_\text{B}T}, \tag{1.96}$$

where we have defined the adiabatic activation energy, $\tilde{E}_A = W_-(x_T) - W_-(x_a)$, and Q and Z are the partition functions,

$$Q = \int_{-\infty}^{\infty} dv_T\, e^{-mv_T^2/2k_\text{B}T} \tag{1.97}$$

$$= \sqrt{\frac{2\pi k_\text{B}T}{m}} \tag{1.98}$$

$$Z = \int_{-\infty}^{x_T} dx\, e^{-\tilde{E}_A/k_\text{B}T} \tag{1.99}$$

$$= \sqrt{\frac{\pi k_\text{B}T}{2m\omega_{\text{vib}}^2}} \left(1 + \text{erf}\left(\frac{\tilde{E}_A}{k_\text{B}T}\right)\right), \tag{1.100}$$

where $\text{erf}(z)$ is the Gauss error function. In the limit where $\tilde{E}_A$ is large relative to $k_\text{B}T$, the error function in Equation 1.100 approaches 1 and so we can write

$$P(v_T) = \frac{m\omega_{\text{vib}}}{2\pi k_\text{B}T} e^{-mv_T^2/2k_\text{B}T} \cdot e^{-\tilde{E}_A/k_\text{B}T}. \tag{1.101}$$

With P_{ab} and $P(v_T)$ defined, we can write the transition rate

$$k_{ab} = \int_0^{\infty} dv_T\, v_T P(v_T) P_{ab}. \tag{1.102}$$

While this cannot be expressed with a closed-form solution, we can examine two limits: adiabatic (large V_{ab} such that $\Gamma \gg 0$) and diabatic (small V_{ab} such that $\Gamma \approx 0$). In the adiabatic limit, Γ increases much faster than any other term, and so we can approximate $P_{ab} = 1 - e^{-\Gamma} \approx 1$. In this limit, Equation 1.102 is:

$$k_{ab}^{\text{adiabatic}} = \frac{\omega_{\text{vib}}}{2\pi} e^{-\tilde{E}_A/k_\text{B}T}, \tag{1.103}$$

In the diabatic limit, we expand P_{ab} to first-order in Γ before evaluating Equation 1.102,

$$k_{ab}^{\text{diabatic}} = \frac{2\pi}{\hbar} \frac{|V_{ab}|^2}{\sqrt{\pi k_\text{B}T}} \frac{\sqrt{m\omega_{\text{vib}}^2/2}}{|F_a - F_b|_{x=x_T}} e^{-E_A/k_\text{B}T}, \tag{1.104}$$

where the diabatic activation energy $E_A = W_a(x_T) - W_a(x_a)$. Since we now have expressions for $W_a(x)$ and $W_b(x)$, we can evaluate $|F_a - F_b|_{x=x_T} = m\omega_{vib}^2|x_a - x_b|$. The energy required to go from $W_a(x_a)$ to $W_a(x_b)$ is $W_a(x_b) - W_a(x_a) = m\omega_{vib}^2(x_b - x_a)/2 \equiv \lambda$. This lets us write Equation 1.104:

$$k_{ab}^{\text{diabatic}} = \frac{2\pi}{\hbar}\frac{|V_{ab}|^2}{\sqrt{4\pi k_{\text{B}} T\lambda}} e^{-E_A/k_{\text{B}}T}. \tag{1.105}$$

Chapter 2

Generalised Marcus Theory

The following publication has been incorporated as Chapter 2, with minor modifications:

Generalised Marcus theory for multi-molecular delocalised charge transfer, *Chem. Sci.*, **9**, 2942 (2018), DOI: 10.1039/C8SC00053K[110].

Natasha B. Taylor[1] and Ivan Kassal[1,2].

[1]*Centre for Engineered Quantum Systems and School of Mathematics and Physics, The University of Queensland, Brisbane, Queensland 4072, Australia*

[2]*The University of Sydney Nano Institute and School of Chemistry, The University of Sydney, New South Wales 2006, Australia*

2.1 Abstract

Although Marcus theory is widely used to describe charge transfer in molecular systems, in its usual form it is restricted to transfer from one molecule to another. If a charge is delocalised across multiple donor molecules, this approach requires us to treat the entire donor aggregate as a unified supermolecule, leading to potentially expensive quantum-chemical calculations and making it more difficult to understand how the aggregate components contribute to the overall transfer. Here, we show that it is possible to describe charge transfer between groups of molecules in terms of the properties of the constituent molecules and couplings between them, obviating the need for expensive supermolecular calculations. We use the resulting theory to show that charge delocalisation between molecules in either the donor or acceptor aggregates can enhance the rate of charge transfer through a process we call supertransfer (or suppress it through subtransfer). The rate can also be enhanced above what is possible with a single donor and a single acceptor by judiciously tuning energy levels and reorganisation energies. We also describe bridge-mediated charge transfer between delocalised molecular aggregates. The equations of generalised Marcus theory are in closed form, providing qualitative insight into the impact of delocalisation on charge dynamics in molecular systems.

2.2 Introduction

Theories of charge-transfer rates underpin our understanding of a wide variety of chemical reactions and charge-transport processes, not only in chemistry, but also in biology and materials science[11,111–113]. In most of the well-studied cases, the charge is being transferred from one molecule to another. However, in many systems—including organic semiconductors[114,115], the reaction centres of photosynthetic organisms[116,117], inorganic coordination complexes[118], and conductive metal-organic frameworks (MOFs)[119]—the charge to be transferred is delocalised across multiple donor molecules (or is to be received by states delocalised over multiple acceptor molecules). The usual theoretical approaches can be applied to these cases if the donor or acceptor aggregates are treated as single supermolecules, but doing so is often computationally prohibitive, requires a complete re-calculation if any part is changed, and, most importantly, offers limited qualitative insight into how the component molecules and the interactions between them affect the inter-aggregate charge transfer.

Although delocalisation in charge transfer has been studied extensively, most studies have focused on cases of delocalisation between the donor and acceptor, as opposed to delocalisation within donor or acceptor aggregates. In particular, donor-acceptor delocalisation is critical to understanding adiabatic electron transfer, as first emphasised by Hush[120,121], and extended by numerous authors since[122–124]. For example, intervalence transitions in mixed-valence compounds are a clear manifestation of delocalisation between two molecules[125].

Here, we study the problem of charge transfer from one delocalised molecular aggregate to another. In order to be able to speak of two distinct aggregates, we assume that the coupling between the aggregates (i.e., between any donor molecule and any acceptor molecule) is small compared to the strength of their coupling to the environment. Furthermore, to ensure that charges within either aggregate (or both) are delocalised among the constituent molecules, we assume that the couplings between the molecules are stronger than their coupling to the environment.

Because the overall donor-acceptor coupling is weak, the charge transfer will be incoherent, i.e., with no coherence between the donor and acceptor states. Apart from the delocalisation within the aggregates, this situation is described by non-adiabatic electron transfer, which we take as our starting point. Although we will follow convention in calling it Marcus theory[10] (MT), the standard expression for non-adiabatic charge transfer between one donor D and one acceptor A was derived by Levich and Dogonadze[18]:

$$k_{D\to A} = \frac{2\pi}{\hbar}\frac{|V_{DA}|^2}{\sqrt{4\pi k_B T \lambda_{DA}}}\exp\left(\frac{-(\Delta E_{DA}+\lambda_{DA})^2}{4k_B T\lambda_{DA}}\right), \tag{2.1}$$

where, at temperature T, three parameters control the transfer rate: the donor-acceptor electronic coupling, V_{DA}, determined by the overlap of their electronic wavefunctions; the reorganisation energy, λ_{DA}, which is the energy required to reorganise the environment from equilibrium about the reactant to equilibrium about the product without changing the electronic state; and the energy difference between the final and initial states, ΔE_{DA}.

Here, we show that it is possible to generalise non-adiabatic MT to describe charge transfer between molecular aggregates in terms of the properties of individual molecules and couplings between them.

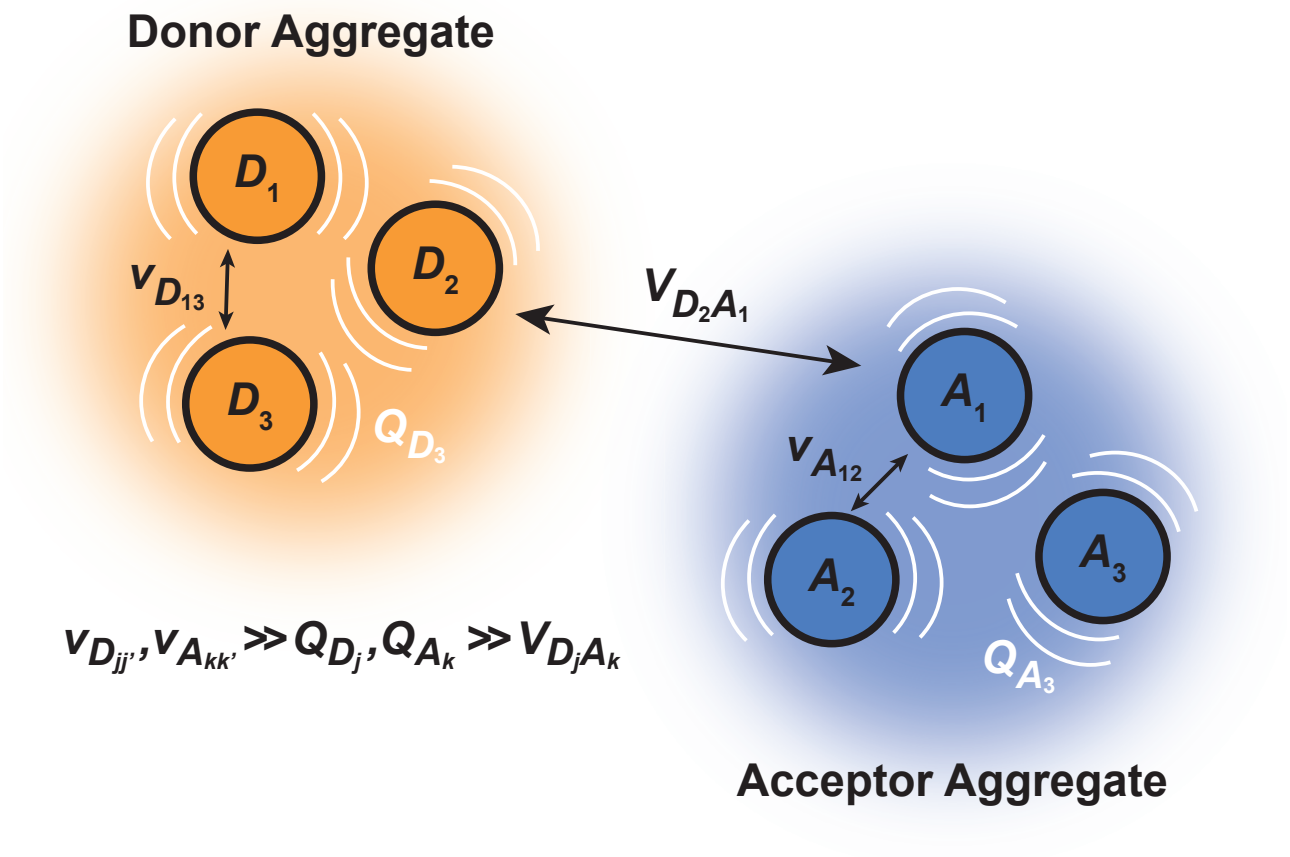

Figure 2.1: The model system for generalised Marcus theory. The model describes charge transfer between two delocalised aggregates if the couplings v between molecules constituting the donor (or acceptor) are strong compared to the coupling to the environment Q, while the couplings V between molecules in the donor with those in the acceptor are relatively weak.

Our theory is both computationally cheap – avoiding the need for supramolecular quantum-chemical simulations – and offers intuitive insight into how the charge transfer rates are affected by changes to molecules in either aggregate.

Our approach is inspired by developments in Förster resonance energy transfer (FRET), which describes the exciton transfer rate between two chromophores and is, like MT, derived from second-order perturbation theory in the donor-acceptor coupling. Sumi developed generalised FRET (gFRET) to describe the transfer of excitons between delocalised aggregates in photosynthetic antenna complexes[30,31], and his approach has since been used to study exciton transfer in a wide range of molecular aggregates[90,91,126]. Following Sumi, we name our theory 'generalised Marcus theory' (gMT).

MT also allows a description of bridge-mediated charge transfer, where the donor and acceptor are not directly coupled, but a coupling between them is mediated by intervening 'bridge' molecules, whose states are sufficiently high in energy to prevent actual charge transfer from the donor to the bridge[11,111,112]. A bridge enables charge transfer to occur over longer distances, although the rate typically decreases exponentially with the number of bridge elements. After deriving gMT in Section 2.3.1, we show that it is also easily extended to describe bridge-assisted charge transfer between delocalised aggregates in Section 2.3.2.

	Marcus theory	Generalised Marcus theory	Bridge-mediated generalised Marcus theory
Donor & acceptor indices	Sites $\lvert D_j\rangle$, $\lvert A_k\rangle$	Eigenstates $\lvert D_\alpha\rangle = \sum_j c_{\alpha j}\lvert D_j\rangle$, $\lvert A_\beta\rangle = \sum_k c_{\beta k}\lvert A_k\rangle$	Eigenstates $\lvert D_\alpha\rangle = \sum_j c_{\alpha j}\lvert D_j\rangle$, $\lvert A_\beta\rangle = \sum_k c_{\beta k}\lvert A_k\rangle$
Electronic coupling	V_{jk}	$V_{\alpha\beta} = \sum_{j,k} c_{\alpha j} c^*_{\beta k} V_{jk}$	$\hat{V}_{\alpha\beta} = \sum_{j,k} c_{\alpha j} c^*_{\beta k} V_{jB_1} G_B^{1N} V_{kB_N}$
Reorganisation energy (separable environments)	$\lambda_j + \lambda_k$	$\lambda_{\alpha\beta} = \sum_j \lvert c_{\alpha j}\rvert^4 \lambda_j + \sum_k \lvert c_{\beta k}\rvert^4 \lambda_k$	$\lambda_{\alpha\beta} = \sum_j \lvert c_{\alpha j}\rvert^4 \lambda_j + \sum_k \lvert c_{\beta k}\rvert^4 \lambda_k$
Energy difference (ΔE)	$E_{A_k} - E_{A_j}$	$E_\beta - E_\alpha$	$\hat{E}_\beta - \hat{E}_\alpha = E_\beta + \sum_{k,k'} c_{\beta k} c^\star_{\beta k'} V_{kB_N} V_{B_N k'} G_B^{NN} - E_\alpha - \sum_{j,j'} c_{\alpha j} c^\star_{\alpha j'} V_{jB_1} V_{B_1 j'} G_B^{11}$

Table 2.1: The equations of generalised Marcus theory (gMT) and bridge-mediated gMT have the same form as ordinary Marcus theory, provided that relevant parameters are replaced as provided in this table. E_α and E_β are the eigenstates of the donor and acceptor aggregate Hamiltonians, H_D^0 and H_A^0 respectively. Bridge-mediated gMT contains a bridge of N sites, with site B_1 coupling to the donor aggregate and B_N to the acceptor. The couplings V_{jB_1} and V_{kB_N} are the coupling of the jth donor site to B_1, and the coupling of the kth acceptor site to B_N, respectively. Green's function G_B, given by Equation 2.37, describes transport through the bridge.

2.3 Results

2.3.1 Generalised Marcus theory

We generalise Marcus theory by considering an aggregate of N_D donor molecules and an aggregate of N_A acceptor molecules, with each molecule coupled to an independent environment of thermalised harmonic oscillators. Three approximations make it possible to define two distinct aggregates (Figure 2.1): first, the coupling between molecules in each aggregate is much stronger than their coupling to the environment, ensuring that the delocalised eigenstates of each aggregate are the appropriate basis for perturbation theory; second, the system-environment coupling is much stronger than the inter-aggregate coupling, implying that inter-aggregate charge transfer is incoherent (hopping); and third, because we assume each site is coupled to its own environment, no environmental mode connects a donor and an acceptor molecule. Where applicable, we follow the derivation of multi-chromophoric FRET (MC-FRET)[32], which reduces to generalised FRET in the appropriate limit. While gFRET can also be derived using Fermi's golden rule[127], we used a time-dependent derivation because some of our intermediate results may be useful in more general contexts.

The full Hamiltonian is $H = H_D^0 + H_A^0 + H_C + H_{DE} + H_{AE} + H_E$, and we introduce each term here as well as in Figure 2.1. The donor-aggregate and acceptor-aggregate Hamiltonians are, respectively,

$$H_D^0 = \sum_{j=1}^{N_D} E_j \left|D_j\right\rangle \left\langle D_j\right| + \sum_{j\neq j'} v_{jj'} \left|D_j\right\rangle \left\langle D_{j'}\right|, \tag{2.2}$$

$$H_A^0 = \sum_{k=1}^{N_A} E_k \left|A_k\right\rangle \left\langle A_k\right| + \sum_{k\neq k'} v_{kk'} \left|A_k\right\rangle \left\langle A_{k'}\right|, \tag{2.3}$$

where $|D_j\rangle$ and $|A_k\rangle$ are the states where the charge is localised on molecules D_j and A_k respectively. Throughout this work we index donor sites with j and acceptor sites with k: $\sum_j$ should be read as a sum over only the donor sites, and $\sum_k$ only over acceptors. The donor and acceptor molecules have site energies E_j and E_k, and intra-aggregate couplings are $v_{jj'}$ (in the donor) and $v_{kk'}$ (in the acceptor).

We refer to the eigenstates of H_D^0 and H_A^0 as the aggregate basis, being, respectively, $|D_\alpha\rangle = \sum_j c_{\alpha j} |D_j\rangle$ and $|A_\beta\rangle = \sum_k c_{\beta k} |A_k\rangle$, with energies E_α and E_β. Similar to site indices j and k, index α is consistently used to denote only donor eigenstates, and β acceptor eigenstates.

Inter-aggregate coupling is described by the Hamiltonian

$$H_C = \sum_{j=1}^{N_D} \sum_{k=1}^{N_A} V_{jk} \left(\left|D_j\right\rangle \left\langle A_k\right| + \left|A_k\right\rangle \left\langle D_j\right| \right), \tag{2.4}$$

where V_{jk} is the coupling between the jth donor and kth acceptor molecules.

The environment is described by a set of harmonic oscillators:

$$H_E = \sum_\xi \hbar\omega_\xi (b_\xi^\dagger b_\xi + 1/2), \tag{2.5}$$

where ω_ξ is the frequency of the ξth environment mode, with creation operator $b_\xi^\dagger$. We can also write $H_E = H_{E_D} + H_{E_A}$, with the environment modes partitioned between those that couple to donor and acceptor molecules.

The donor-environment and acceptor-environment interaction Hamiltonians are, respectively,

$$H_{DE} = \sum_{j=1}^{N_D} Q_j \left|D_j\right\rangle \left\langle D_j\right|, \tag{2.6}$$

$$H_{AE} = \sum_{k=1}^{N_A} Q_k \left|A_k\right\rangle \left\langle A_k\right|, \tag{2.7}$$

with $Q_j = \sum_\xi \hbar\omega_\xi g_{j\xi}(b_\xi + b_\xi^\dagger)$, where $g_{j\xi}$ is the dimensionless coupling of the ξth environment mode to the charged jth donor molecule, relative to the uncharged state. Q_k is defined analogously. The assumption of a local environment means that, for a fixed ξ, only one of $g_{j\xi}$ can be non-zero.

The charge-transfer rate is the rate of change of the charge population on the acceptor,

$$k_{D\to A}(t) = \frac{d}{dt}\mathrm{Tr}_E \sum_k \left\langle A_k\right| \rho(t) \left|A_k\right\rangle, \tag{2.8}$$

where $\rho(t)$ is the density matrix of the system, and Tr_E is the trace over the environmental modes. As detailed in the Appendix, $k_{D\to A}$ can be calculated using second-order perturbation theory in H_C and, because we assumed separable environments, generates a time-dependent transfer rate

$$k_{D\to A}(t) = \sum_{j,j'}\sum_{k,k'} \frac{V_{jk}V_{j'k'}}{\hbar^2}\cdot 2\mathrm{Re}\int_0^t d\tau\, \mathrm{Tr}_E\big(\left\langle A_k\right| e^{-i(H-H_C)(t-\tau)/\hbar}\left|A_{k'}\right\rangle \left\langle D_{j'}\right| e^{-i(H-H_C)\tau/\hbar}\rho(0)e^{i(H-H_C)t/\hbar}\left|D_j\right\rangle\big). \tag{2.9}$$

To proceed, we consider the rate in the aggregate basis. The requirement that V_{jk} be weaker than all other couplings means that the donor aggregate will relax to a thermal state faster than the charge transfer. In other words, we assume that the initial density operator of the system $\rho(0)$ will, before charge transfer takes place, relax to a state ρ_{th} in which both the donor and acceptor aggregates are in equilibrium with their own environments (see Appendix for details). This gives a time-independent transfer rate,

$$k_{D\to A} = \sum_{\alpha,\beta} \frac{|V_{\alpha\beta}|^2}{2\pi\hbar^2}\int_{-\infty}^{\infty} d\omega\, \mathscr{D}_D^{\alpha\alpha}(\omega)\mathscr{A}_A^{\beta\beta}(\omega), \tag{2.10}$$

where

$$V_{\alpha\beta} = \sum_{j,k} c_{\alpha j}^* c_{\beta k} V_{jk}, \tag{2.11}$$

$$\mathscr{D}_D^{\alpha\alpha}(\omega) = \int_{-\infty}^{\infty} dt\, e^{-i\omega t}\mathrm{Tr}_{E_D}\big(e^{-iH_{E_D}t/\hbar}\left\langle D_\alpha\right| e^{iH_Dt/\hbar}\rho_D\left|D_\alpha\right\rangle\big), \tag{2.12}$$

$$\mathscr{A}_A^{\beta\beta}(\omega) = \int_{-\infty}^{\infty} dt\, e^{i\omega t}\mathrm{Tr}_{E_A}\big(e^{iH_{E_A}t/\hbar}\left\langle A_\beta\right| e^{-iH_At/\hbar}\left|A_\beta\right\rangle\rho_A\big), \tag{2.13}$$

and where ρ_{th} is split into donor and acceptor components, $\rho_{\mathrm{th}} = \rho_D \otimes \rho_A$. Because the donor-environment coupling is weak, the thermal state of the donor will approximately factorise to $\rho_D = (\sum_\alpha \rho_{\alpha\alpha}\left|D_\alpha\right\rangle\left\langle D_\alpha\right|)\otimes\rho_{E_D}$, where $\rho_{\alpha\alpha} = \exp(-E_\alpha/k_BT)/(\sum_\alpha \exp(-E_\alpha/k_BT))$ is the electronic population distribution, and the thermal environment is $\rho_{E_D} = \exp(-H_{E_D}/k_BT)/\mathrm{Tr}_{E_D}(\exp(-H_{E_D}/k_BT))$. The thermal state of the acceptor is $\rho_A = \rho_{E_A} = \exp(-H_{E_A}/k_BT)/\mathrm{Tr}_{E_A}(\exp(-H_{E_A}/k_BT))$. Finally, we have also written $H_D = H_D^0 + H_{DE} + H_{E_D}$, and similarly for H_A.

Equations 2.10–2.13 are analogous to the MC-FRET treatment of delocalised exciton transfer[32]. In particular, the rate of MC-FRET depends on the (weighted) overlap of the donor emission spectrum with the acceptor absorption spectrum, which resembles the form of Equation 2.10. However, in gMT, Equation 2.12 describes the spectrum of charge disassociation from the donor and Equation 2.13 the charge association spectrum for the acceptor. Furthermore, the inter-aggregate coupling in Equation 2.10 is determined by the overlap of electronic wavefunctions, while in MC-FRET the couplings are from the interactions of transition dipole moments.

Evaluating Equations 2.12–2.13 for independent harmonic environments gives (see Appendix for details)

$$\mathscr{D}_D^{\alpha\alpha}(\omega) = \rho_{\alpha\alpha} \int_{-\infty}^{\infty} dt\, e^{-i\omega t} e^{iE_\alpha t/\hbar + G_\alpha(t) - G_\alpha(0)}, \tag{2.14}$$

$$\mathscr{A}_A^{\beta\beta}(\omega) = \int_{-\infty}^{\infty} dt\, e^{i\omega t} e^{-iE_\beta t/\hbar + G_\beta(t) - G_\beta(0)}, \tag{2.15}$$

with the lineshape function

$$G_\alpha(t) = \sum_\xi g_{\alpha\xi}^2 \big(\cos(\omega_\xi t)(1+2n(\omega_\xi)) - i\sin(\omega_\xi t)\big), \tag{2.16}$$

and $G_\beta(t)$ analogously defined. For a thermally populated environment, the occupation of environmental modes is given by the Bose-Einstein distribution $n(\nu) = (\exp(\hbar\nu/k_BT)-1)^{-1}$.

The preceding equations are appropriate at a wide range of temperatures and environmental spectral densities. Although we could stop here, to obtain a clear comparison with MT, we now make two additional approximations that are also made in deriving ordinary Marcus theory. To do so, we assume that the spectral density $J(\omega) = \sum_\xi g_{\alpha\xi}^2 \delta(\omega - \omega_\xi)$ goes rapidly to zero beyond a cut-off frequency ω_c. Then, we first assume the high-temperature limit $k_BT \gg \hbar\omega_c$, so that $n(\nu) \approx k_BT/\hbar\nu \gg 1$, giving

$$G_\alpha(t) = \sum_\xi g_{\alpha\xi}^2 \left(\frac{2k_BT}{\hbar\omega_\xi}\cos(\omega_\xi t) - i\sin(\omega_\xi t)\right), \tag{2.17}$$

Second, MT also assumes the slow-nuclear-mode limit, in which the charge-transfer occurs faster than the characteristic timescales of the environment: $t \ll 1/\omega_c \lessapprox 1/\omega_\xi$. With $\omega_\xi t \ll 1$, we expand the trigonometric functions in Equation 2.17 to leading order:

$$G_\alpha(t) = \sum_\xi g_{\alpha\xi}^2 \left(\frac{2k_BT}{\hbar\omega_\xi} - \frac{t^2 k_BT\omega_\xi}{\hbar} - i\omega_\xi t\right). \tag{2.18}$$

We now define the reorganisation energy for the donor sites as $\lambda_j = \sum_\xi \hbar\omega_\xi g_{j\xi}^2$, and similarly for the acceptor sites, λ_k. The change of basis $g_{\alpha\xi} = \sum_j |c_{\alpha j}|^2 g_{j\xi}$ gives the reorganisation energy of aggregate eigenstates

$$\lambda_\alpha = \sum_\xi \hbar\omega_\xi g_{\alpha\xi}^2 = \sum_\xi \hbar\omega_\xi \left(\sum_j |c_{\alpha j}|^2 g_{j\xi}\right)\left(\sum_{j'} |c_{\alpha j'}|^2 g_{j'\xi}\right). \tag{2.19}$$

Since each site has an independent environment, no mode ξ couples to two different sites ($g_{j\xi}g_{j'\xi} = g_{j\xi}^2\delta_{jj'}$), giving

$$\lambda_\alpha = \sum_\xi \hbar\omega_\xi \sum_j |c_{\alpha j}|^4 g_{j\xi}^2, \tag{2.20}$$

and similarly for λ_β.

Substituting Equations 2.18 and 2.20 into Equations 2.14-2.15 we find

$$\mathscr{D}_D^{\alpha\alpha}(\omega) = \rho_{\alpha\alpha}\frac{2\pi\hbar}{\sqrt{4\pi k_B T\lambda_\alpha}}\exp\left(\frac{-(E_\alpha-\hbar\omega-\lambda_\alpha)^2}{4k_BT\lambda_\alpha}\right), \tag{2.21}$$

$$\mathscr{A}_A^{\beta\beta}(\omega) = \frac{2\pi\hbar}{\sqrt{4\pi k_B T\lambda_\beta}}\exp\left(\frac{-(E_\beta-\hbar\omega+\lambda_\beta)^2}{4k_BT\lambda_\beta}\right). \tag{2.22}$$

Consequently, the overlap integral in Equation 2.10 becomes

$$k_{D\to A} = \sum_{\alpha,\beta}\frac{2\pi}{\hbar}\frac{\rho_{\alpha\alpha}|V_{\alpha\beta}|^2}{\sqrt{4\pi k_B T\lambda_{\alpha\beta}}}\exp\left(\frac{-(\Delta E_{\alpha\beta}+\lambda_{\alpha\beta})^2}{4k_BT\lambda_{\alpha\beta}}\right), \tag{2.23}$$

where $\Delta E_{\alpha\beta} = E_\beta - E_\alpha$ and $\lambda_{\alpha\beta} = \lambda_\alpha + \lambda_\beta$, demonstrating that gMT takes the same form as MT, with all parameters defined analogously to—and expressible in terms of—their site-basis counterparts. These results are also summarised in Table 2.1, and in the limit of a single-molecule donor and single-molecule acceptor, Equation 2.23 reduces to the ordinary MT rate, Equation 2.1. The ability to recast gFRET in a form analogous to Equation 2.23[33] further illustrates the deep similarities between charge and exciton transfer.

2.3.2 Generalised bridge-mediated charge transfer

Like MT, gMT can be expanded to include the case where the coupling between the donor and the acceptor aggregates is not direct, but is instead mediated by a bridge consisting of higher-lying states of intervening molecules. We consider a bridge of N molecules, each modelled as a single site, where the donor molecules only couple to the first bridge state, B_1, the acceptor molecules only couple to the last bridge state, B_N, and each bridge molecule only couples to its two nearest neighbours in the chain, as shown in Figure 2.2. Usually, the bridge site energies E_{B_l} are considered energetically distinct from the donor and acceptor aggregates, i.e.,

$$(E_{B_k} - E_{B_l}), |V_{B_lB_{l+1}}| \ll E_{B_l} - E_{\alpha/\beta}, \tag{2.24}$$

where $V_{B_lB_{l+1}}$ are the intra-bridge couplings and $E_{\alpha/\beta}$ is the characteristic energy of donor and acceptor eigenstates (for concreteness, it could be taken as the highest eigenvalue of either H_D^0 or H_A^0).

We define the donor-bridge-acceptor Hamiltonian $H_{DBA} = H_B + H_D^0 + H_{DB} + H_A^0 + H_{AB}$ using H_D^0 and H_A^0 as above and adding the bridge Hamiltonian H_B and the coupling of the bridge to the donor, H_{DB}, and acceptor, H_{AB},

$$H_B = \sum_{l=1}^{N} E_{B_l}|B_l\rangle\langle B_l| + \sum_{l=1}^{N-1} V_{B_lB_{l+1}}|B_l\rangle\langle B_{l+1}| + \text{h.c.}, \tag{2.25}$$

$$H_{DB} = \sum_j V_{jB_1}|D_j\rangle\langle B_1| + \text{h.c.}, \tag{2.26}$$

$$H_{AB} = \sum_k V_{kB_N}|A_k\rangle\langle B_N| + \text{h.c.}, \tag{2.27}$$

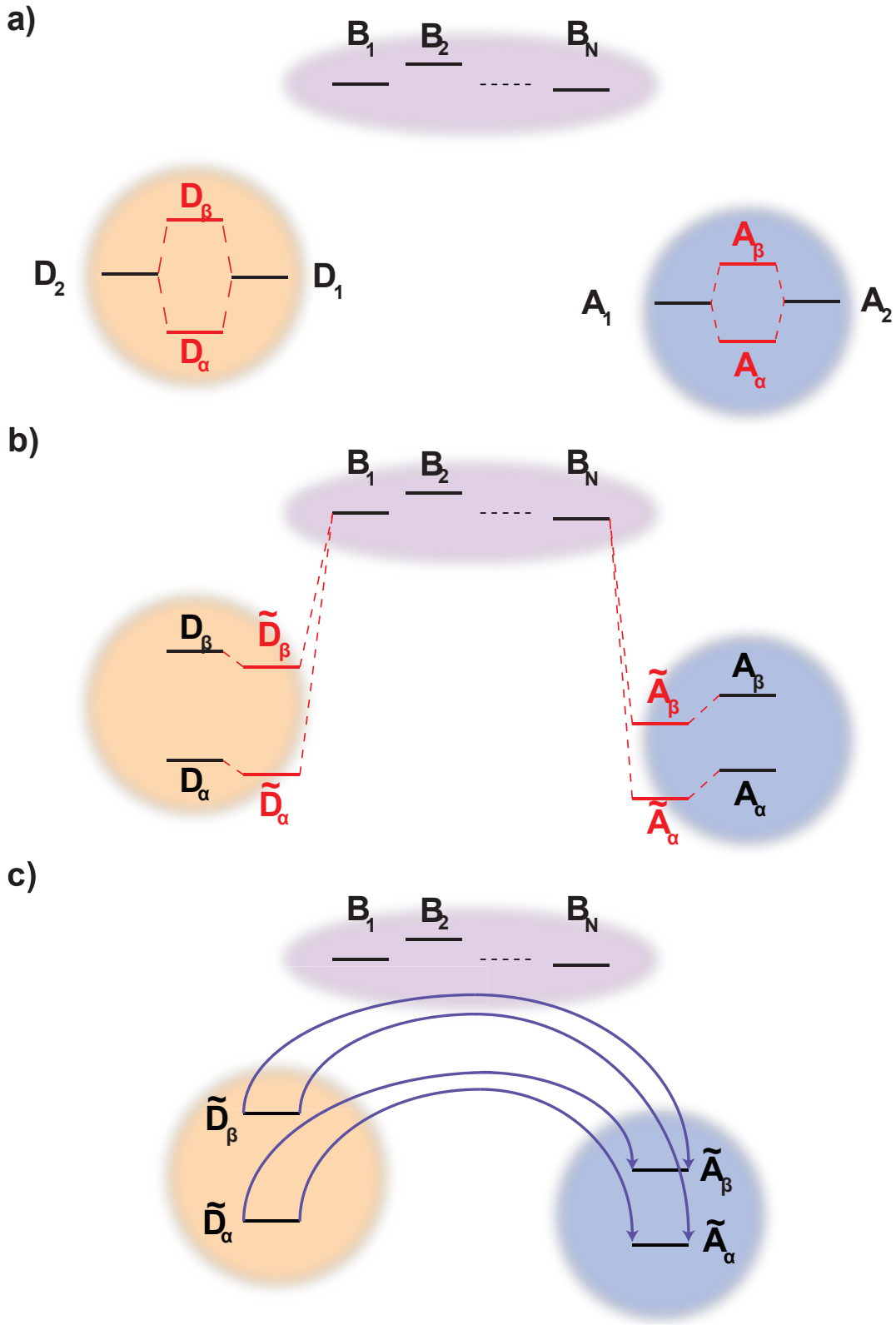

Figure 2.2: Generalised bridge-assisted charge transfer, shown with two donor molecules, D_1 and D_2, two acceptor molecules, A_1 and A_2, and N bridge molecules, $B_1 \ldots B_N$. a) The eigenstates of each aggregate are calculated. b) The energies of these eigenstates are then perturbed by the coupling to the bridge (perturbation of the bridge levels is neglected, see text). c) Charge transfer occurs directly between donor and acceptor aggregate eigenstates, assisted by virtual bridge states.

where $|B_l\rangle$ is the state of a charge being located on bridge site B_l.

Instead of thinking of B_1 and B_N as coupling to donor and acceptor sites, we can also consider them as coupling to the aggregate eigenstates. In the aggregate basis, H_{DBA} becomes

$$H_{DBA} = H_B + \sum_\alpha \left(E_\alpha |D_\alpha\rangle\langle D_\alpha| + V_{\alpha B_1} |D_\alpha\rangle\langle B_1| + \text{h.c.}\right) + \sum_\beta \left(E_\beta |A_\beta\rangle\langle A_\beta| + V_{\beta B_N} |A_\beta\rangle\langle B_N| + \text{h.c.}\right), \quad (2.28)$$

where $V_{\alpha B_1} = \sum_j c_{\alpha j} V_{jB_1}$ and $V_{\beta B_N} = \sum_k c_{\beta k} V_{kB_N}$.

We calculate the rate of charge transfer from each donor eigenstate $|D_\alpha\rangle$ to each acceptor eigenstate $|A_\beta\rangle$ independently, using the mathematics already established for single-site bridge-mediated transfer[21]. In other words, instead of considering the entire donor-bridge-acceptor system, we consider separately the subspace of each donor and acceptor eigenstate with the bridge,

$$\begin{aligned} H_{DBA}(\alpha,\beta) = H_B &+ E_\alpha |D_\alpha\rangle\langle D_\alpha| + V_{\alpha B_1} |D_\alpha\rangle\langle B_1| + \text{h.c.} \\ &+ E_\beta |A_\beta\rangle\langle A_\beta| + V_{\beta B_N} |A_\beta\rangle\langle B_N| + \text{h.c.} \end{aligned} \quad (2.29)$$

We denote the lowest-eigenvalue eigenvector of $H_{DBA}(\alpha,\beta)$ as $\mathbf{d}_{DBA} = (d_\alpha, d_{B_1}, \ldots, d_{B_N}, d_\beta)$, with eigenvalue E_{DBA}.

Since $(H_{DBA}(\alpha,\beta) - \mathbf{I}E_{DBA})\mathbf{d}_{DBA} = 0$, we find that

$$(E_\alpha - E_{DBA})d_\alpha + V_{\alpha B_1} d_{B_1} = 0, \quad (2.30)$$

$$(E_\beta - E_{DBA})d_\beta + V_{\beta B_N} d_{B_N} = 0. \quad (2.31)$$

The values of d_{B_1} and d_{B_N} can be found by considering the bridge subspace, $(H_B - \mathbf{I}E_{DBA})\mathbf{d}_B = -(V_{B_1\alpha} d_\alpha, 0, \ldots, 0, V_{B_N\beta} d_\beta)$ where $\mathbf{d}_B$ consists of the bridge elements of $\mathbf{d}_{DBA}$ in the same order. The solution of this equation is $\mathbf{d}_B = G_B(V_{B_1\alpha} d_\alpha, 0, \ldots, 0, V_{B_N\beta} d_\beta)$, using Green's function $G_B = (\mathbf{I}E_{DBA} - H_B)^{-1}$.

By substituting this solution for d_{B_1} and d_{B_N} into Equations 2.30 and 2.31, we find

$$(\hat{E}_\alpha - E_{DBA})d_\alpha + \hat{V}_{\alpha\beta} d_\beta = 0, \quad (2.32)$$

$$(\hat{E}_\beta - E_{DBA})d_\beta + \hat{V}_{\beta\alpha} d_\alpha = 0, \quad (2.33)$$

where $\hat{E}$ are the perturbed energies of aggregate eigenstates due to coupling with the bridge,

$$\hat{E}_\alpha = E_\alpha + V_{\alpha B_1} G_B^{11} V_{B_1\alpha}, \quad (2.34)$$

$$\hat{E}_\beta = E_\beta + V_{\beta B_N} G_B^{NN} V_{B_N\beta}, \quad (2.35)$$

and $\hat{V}$ is the effective coupling between the donor and acceptor eigenstates, mediated by the bridge,

$$\hat{V}_{\alpha\beta} = V_{\alpha B_1} G_B^{1N} V_{B_N\beta}. \quad (2.36)$$

To find the Green's function, we expand G_B in terms of a Dyson series. Because $|V_{B_l B_{l+1}}|$ is small (see Equation 2.24), we keep only the lowest-order term[21],

$$G_B^{1N} = (E_{DBA} - E_{B_1})^{-1} V_{B_1 B_2} (E_{DBA} - E_{B_2})^{-1} V_{B_2 B_3} \times \ldots \times (E_{DBA} - E_{B_{N-1}})^{-1} V_{B_{N-1} B_N} (E_{DBA} - E_{B_N})^{-1}. \quad (2.37)$$

While E_{DBA} is an eigenvalue of the entire donor-bridge-acceptor system, we are only interested in the donor/acceptor subspace. Because $E_{B_l} - E_{\alpha/\beta}$ is large relative to inter-site couplings and energy differences (Equation 2.24), we can approximate $E_{DBA} - E_{B_l} \approx E_{\alpha/\beta} - E_B$, for average bridge energy E_B. This allows us to simplify Equation 2.36 using the geometric mean of the bridge couplings V_{BB},

$$\hat{V}_{\alpha\beta} = \frac{V_{\alpha B_1} V_{B_N \beta}}{E_{\alpha/\beta} - E_B} \left(\frac{V_{BB}}{E_{\alpha/\beta} - E_B} \right)^{N-1}. \quad (2.38)$$

As in ordinary bridge-assisted charge transfer, the effective coupling decays exponentially with bridge length because $V_{BB} < E_{\alpha/\beta} - E_B$ (Equation 2.24). Substituting Equations 2.34–2.37 into Equation 2.23, we have the rate of bridge-assisted gMT:

$$k_{D \to A} = \sum_{\alpha,\beta} \frac{2\pi}{\hbar} \frac{\rho_{\alpha\alpha} |\hat{V}_{\alpha\beta}|^2}{\sqrt{4\pi k_B T \lambda_{\alpha\beta}}} \exp\left(\frac{-(\Delta \hat{E}_{\alpha\beta} + \lambda_{\alpha\beta})^2}{4 k_B T \lambda_{\alpha\beta}} \right). \quad (2.39)$$

2.4 Discussion

The summary of results in Table 2.1 shows that gMT—whether bridged or not—follows the same functional form as ordinary Marcus theory. This allows intuition gained from studying MT to continue to be useful when studying aggregates instead of single molecules (provided that the parameters are redefined as shown in Table 2.1). Further, gMT allows known values of relevant parameters (couplings, energy differences, and reorganisation energies) of individual molecules to be used to calculate the effective parameters for aggregates, saving computational time by avoiding expensive supramolecular quantum-chemical simulations.

However, the presence of delocalisation in aggregates leads to significant differences between MT and gMT. We can analyse the influence of delocalisation on charge transfer by separating its impact on the electronic and nuclear components of the MT rate.

The gMT electronic coupling factor $|V_{\alpha\beta}|^2 = |\sum_{j,k} c_{\alpha j} c^*_{\beta k} V_{jk}|^2$ includes a coherent sum involving electronic amplitudes in each of the donor and acceptor aggregates, allowing both constructive and destructive interference to affect the transfer rate. If the interferences is constructive, leading to enhanced transfer rates, we call the effect *supertransfer*, and if it is destructive, *subtransfer*, borrowing terminology from the similar problem of MC-FRET[128].

For illustration, we consider an aggregate of two identical coupled donors, D_1 and D_2, with a charge delocalised between them in the $|D_\alpha\rangle = (|D_1\rangle + |D_2\rangle)/\sqrt{2}$ state. The donors are coupled to a single acceptor A with strengths $V_{D_1 A}$ and $V_{D_2 A}$ respectively. If we were to apply Marcus theory between each donor and the acceptor independently, we would expect a transfer rate proportional to the

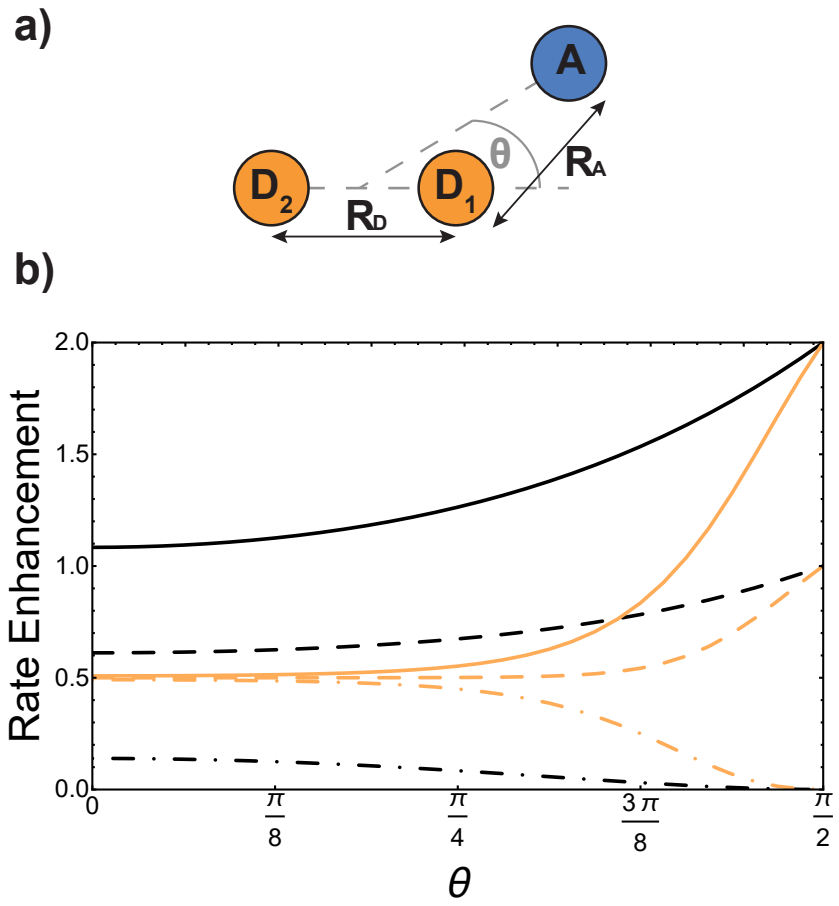

Figure 2.3: Example of generalised Marcus theory (gMT) and supertransfer, showing only the impact of electronic component $|V_{\alpha\beta}|^2$ on the charge transfer rate. a) Geometric arrangement of two donors and one acceptor, changing from collinear ($\theta = 0$) to an isosceles triangle ($\theta = \pi/2$). b) Rates of charge transfer from the donors to the acceptor are displayed as ratios of the rate that would be found if only donor D_1 were present and the charge initially localised on it. Black and orange lines indicate, respectively, geometries with $R_A = 3R_D$ or $R_A = R_D$ (at a constant $R_A = 5\,\text{Å}$). In both cases, the rates are computed for three initial donor states: the bright state $(|D_1\rangle + |D_2\rangle)/\sqrt{2}$ (solid), the dark state $(|D_1\rangle - |D_2\rangle)/\sqrt{2}$ (dot-dashed), and the fully mixed state of $|D_1\rangle$ and $|D_2\rangle$ (dashed). These three states are obtained as ground states of the donor Hamiltonian by assuming $V_{D_1D_2} = -100\,\text{meV}$ (bright), $V_{D_1D_2} = 100\,\text{meV}$ (dark), or $V_{D_1D_2} = 0\,\text{meV}$ (mixed). The transfer rates are independent of R_A and R_D when θ reaches $\pi/2$, where both donors are equidistant from the acceptor. At that point, constructive interference ensures that the transfer from the bright state is twice as fast as it would be from either site alone, while transfer from the dark state is completely suppressed by destructive interference caused by the opposite signs of the wavefunction at D_1 and D_2. The difference between the two geometries is apparent at smaller θ. When R_D is large compared to R_A (orange), the rate is half the single-site rate for all initial states, indicating that the acceptor is interacting primarily with D_1 until θ becomes considerable. By contrast, when both donors are close enough to the acceptor to interact with it strongly (black), supertransfer and subtransfer can occur at all values of θ, resulting in rate enhancements different from 0.5 at all angles. Other calculation parameters: $V_{DA}(r) = 50\,\text{meV}\exp(1 - r/2\,\text{Å})$.

square of each coupling, $k_{MT} \propto \frac{1}{2}|V_{D_1A}|^2 + \frac{1}{2}|V_{D_2A}|^2$, with the factors of $1/2$ indicating the population on each donor. However, this naive approach fails to include coherent effects of the superposition. These are treated correctly by gMT, which predicts a transfer rate of $k_{gMT} \propto |(V_{D_1A} + V_{D_2A})/\sqrt{2}\,|^2$. The presence of rate-enhancement due to supertransfer is apparent if $V_{D_1A} = V_{D_2A}$, which implies $k_{gMT} = 2k_{MT}$. In contrast, if the two transfer pathways interfere destructively, $V_{D_1A} = -V_{D_2A}$, gMT predicts subtransfer with $k_{gMT} = 0$. We refer to states that enhance the charge-transfer rate through supertransfer as *bright*, while those that retard it as *dark*, in analogy to the terms used in the literature on superradiance[129]. The relative populations of the bright and dark states will strongly influence the rate of charge transfer in delocalised systems.

Supertransfer is also sensitive to the system's geometry. Changing the distance and orientations between donors and acceptors will affect the electronic wavefunction overlaps due to the exponential decay of electronic wavefunctions with distance, consequently modifying the electronic couplings. To explore the consequences of this geometric sensitivity, we consider a model consisting of two donor molecules transferring a unit of charge to an acceptor molecule, shown in Figure 2.3. These calculations demonstrate that rate enhancement/retardation is weakest when the acceptor is co-linear with the donors. This is because the farther donor is so far away that the acceptor is only affected by the nearer donor. The impact is most significant when the acceptor is equidistant from the two donors, where supertransfer from the bright state amplifies the transfer rate by a factor of two, while the dark state provides no transfer.

We can compare these results with gFRET, the analogous theory of excitation-energy transfer between molecular aggregates[32]. Bright and dark states also exist in gFRET, but exciton transfer is not as sensitive to small changes in the separation between molecules. While the transfer rate in gMT is determined by the overlap of electronic wavefunctions, which decay exponentially with distance, the MC-FRET rate depends on the coupling of transition dipole moments, which decays with the cube of the distance. In addition, both gMT and gFRET are strongly affected by the relative orientations of the molecules. The orientational dependence of gFRET is easier to predict, especially in the large-separation limit where it can be represented by the interaction of two dipoles. By contrast, the orientational dependence of electronic couplings depends on the shape of the orbitals, which varies from molecule to molecule. Given that the geometric dependence of gFRET can lead to substantially different outcomes in light-harvesting complexes[90,91], the stronger dependence of gMT on geometry provides an opportunity to engineer molecular systems that perform charge transfer better than single sites.

The nuclear factor in gMT (also referred to as the Franck-Condon weighted density factor), $(4\pi k_B T \lambda_{\alpha\beta})^{-1/2} \exp(-(\Delta E_{\alpha\beta} + \lambda_{\alpha\beta})^2 / 4 k_B T \lambda_{\alpha\beta})$, has several features in common with ordinary MT. For example, for a fixed $\lambda_{\alpha\beta}$, the nuclear factor is maximised when $-\Delta E_{\alpha\beta} = \lambda_{\alpha\beta}$, and the inverted regime is possible when $-\Delta E_{\alpha\beta} > \lambda_{\alpha\beta}$. However, the nuclear term also possesses features not predicted by ordinary MT, allowing for both enhancement or retardation of the transfer rate.

The nuclear factor depends on two energies, $\Delta E_{\alpha\beta}$ and $\lambda_{\alpha\beta}$, which are affected by delocalisation in different ways. On the one hand, $\Delta E_{\alpha\beta}$ is the difference between eigenvalues of H_D^0 and H_A^0. If the extent of delocalisation in, say, the donor is increased, E_α will not change dramatically, remaining close (up to several times the intermolecular coupling) to a value of typical site energies. On the other hand, $\lambda_{\alpha\beta}$ is reduced by delocalisation. Since $\lambda_\alpha = \sum_j |c_{\alpha j}|^4 \lambda_j$, for a state purely localised on j, $\lambda_\alpha = \lambda_j$. However, in a fully delocalised state ($c_{\alpha j} = 1/\sqrt{N_D}$) of N_D identical donors ($\lambda_j = \lambda$), the reorganisation energy is decreased N_D-fold:

$$\lambda_\alpha = \sum_{j=1}^{N_D} \left| \frac{1}{\sqrt{N_D}} \right|^4 \lambda_j = \frac{\lambda}{N_D}. \tag{2.40}$$

In general, the reduction is by a factor equal to the inverse participation ratio $\mathrm{IPR} = (\sum_j |c_{\alpha j}|^4)^{-1}$. A reduction in λ leads to an exponential narrowing of both $\mathscr{D}_D^{\alpha\alpha}(\omega)$ and $\mathscr{A}_A^{\beta\beta}(\omega)$. Therefore, because

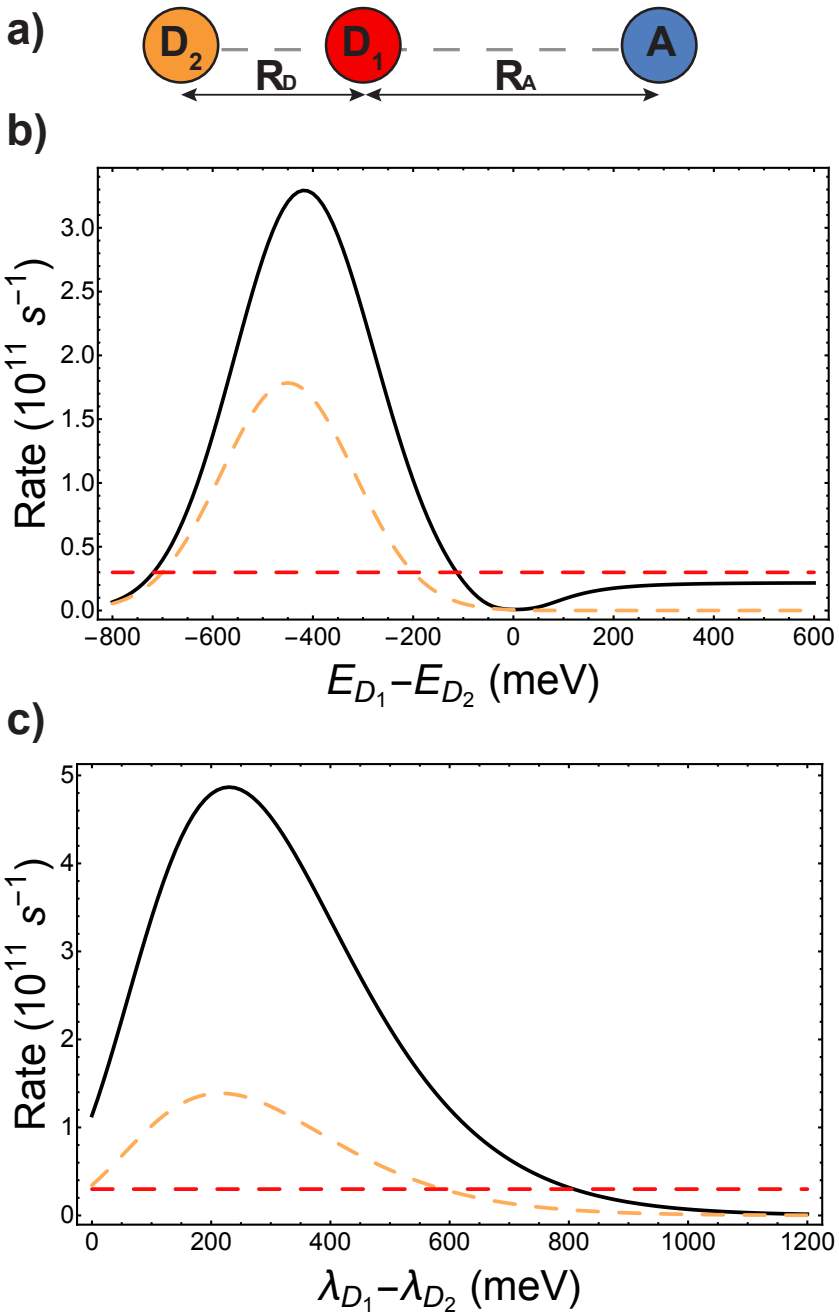

Figure 2.4: Tuning energy offsets and reorganisation energies can enhance charge-transfer rates beyond what is possible with either donor site alone. a) Two donors and one acceptor in a collinear geometry, with different colours (orange/red) indicating inequivalent donors. b) Energetic detuning: the charge transfer rate from the aggregate to the acceptor (solid line) is compared to the rate if only D_1 (dashed red) or D_2 (dashed orange) were present, as a function of the energy difference between D_1 and D_2. Even with the effects of supertransfer removed (the aggregate rate is shown divided by the electronic supertransfer enhancement of 1.42), energetic tuning can make the aggregate transfer faster than would be possible with either donor alone. In particular, the presence of D_2, which itself is weakly coupled to A, can enhance the transfer rate above the rate from D_1 alone. c) Reorganisation energies: plot as in b), but the rates are shown as a function of the difference in reorganisation energies between D_1 and D_2. Here as well, adding D_2 with a favourable reorganisation energy can enhance the rate above what is possible with either donor alone. Calculation parameters: $V_{D_1D_2} = -37\,\text{meV}$, $V_{D_1A} = 18\,\text{meV}$, $V_{D_2A} = 2.5\,\text{meV}$, $\lambda_A = 200\,\text{meV}$, $\lambda_{D_1} = 150\,\text{meV}$, $E_{D_1} = 700\,\text{meV}$, $E_A = 0\,\text{meV}$, $k_BT = 25\,\text{meV}$. In addition, b) uses $\lambda_{D_2} = 150\,\text{meV}$ and c) has $E_{D_2} = 600\,\text{meV}$.

the charge-transfer rate depends on the overlap of the two spectra (Equation 2.10), the reduction in λ will reduce the transfer rate between most pairs of eigenstates, the exception being ones where $\Delta E_{\alpha\beta} = -\lambda_{\alpha\beta}$.

The presence of different processes affecting the nuclear factor means that delocalisation can have a complicated effect on the charge-transfer rate, even apart from supertransfer. Critical to the rate is the relative size of $\Delta E_{\alpha\beta}$ and $\lambda_{\alpha\beta}$, because of the rate's exponential sensitivity to $(\Delta E_{\alpha\beta} + \lambda_{\alpha\beta})^2$. The different effects are illustrated with another example, shown in Figure 2.4a, where acceptor A is strongly coupled to donor D_1, whose site energy and reorganisation energy are such that the transfer from D_1 to A is very slow ($-\Delta E_{D_1A} \gg \lambda_{D_1A}$). Another donor D_2 is then introduced, but is weakly coupled to A due to its distance. A naive application of classical MT might suggest that, because D_2 hardly interacts with A, it would serve to only steal charge density from D_1, reducing the already slow transfer rate. Generalised MT, however, shows that it is possible to choose the energy and reorganisation energy of D_2, as well as its coupling to D_1, so that a coherent superposition between D_1 and D_2 will enhance the total transfer rate above what is possible with *either* D_1 or D_2 alone. This is true even if supertransfer is neglected, as shown in Figures 2.4b and c. Indeed, for two donors, supertransfer can enhance the rate by at most a factor of two, while there is no limit to how much the nuclear factor can be enhanced by judiciously tuning $\Delta E_{\alpha\beta}$ and $\lambda_{\alpha\beta}$ to minimise $(\Delta E_{\alpha\beta} + \lambda_{\alpha\beta})^2$. This result shows that even if an unfavourable donor must be used in a donor-acceptor system (for whatever reason), another donor can be added to tune the nuclear term's contribution to the charge transfer rate.

Our results also extend gMT to treat bridge-mediated charge transfer, showing that the usual equations still apply when considering delocalised aggregates. Indeed, including the effects of bridge-mediated charge transfer on gMT does not qualitatively change the effects of supertransfer and energetic tuning, except that the coherent effects depend on the geometry of the donor aggregate with respect to the first bridge molecule, and the acceptor aggregate with respect to the last. In particular, the results shown in Figures 2.3 and 2.4 would remain unchanged if the couplings were mediated by a bridge.

2.5 Conclusion

The theory presented in this work is the first description of charge transfer between delocalised molecular aggregates. Therefore, we anticipate that it will have broad applications in fields where charge transfer and electronic coherence intersect, including organic photovoltaics, photosynthesis, and inorganic complexes.

The major prediction of gMT is that delocalisation within an aggregate can significantly affect charge transfer rates through two mechanisms: supertransfer and nuclear tuning. The first is a consequence of the constructive interferences of charge-transfer pathways, while the latter is the ability of a charge-transfer rate to be modified by adjusting effective energy levels and reorganisation energies by delocalising electronic states over different molecules.

Both of these predictions are suited to being tested experimentally. The simplest approach would be to construct covalently linked donors and acceptors in geometries that approximate those in Figures 2.3 and 2.4. Tuning the couplings and energy levels through chemical modification would permit the adjustment of the parameters relevant for gMT, allowing the theory to be tested.

In this work, we restricted ourselves to deriving the delocalised generalisation of the simplest Marcus-theory formula. We are confident that many of the subsequent advances that have occurred in charge-transfer theory can also be incorporated as extensions to gMT. Indeed, our derivation is more general than the final result, and some of the approximations needed to derive an MT-like equation (e.g., high temperature, slow environmental modes) can be omitted and more general intermediate results used directly (e.g., Equations 2.10–2.13). Although it is not clear whether a simple, closed-form expression could be derived, a number of improvements to gMT can be envisaged, including adiabatic charge transfer, quantum-mechanical vibrational corrections[130], coherent multistep charge transfer[131], shared intra-aggregate environmental modes[132], and off-diagonal system-environment couplings. Inspiration could also be taken from advances in MC-FRET to obtain generalisations able to treat system-environment entanglement or other parameter regimes outside the approximations used here[127,133,134].

2.6 Appendix

Here we give the full derivation of Equations 2.14–2.15 from Equation 2.8, indexing the sum with k'' for future convenience:

$$k_{D\to A}(t) = \frac{d}{dt}\mathrm{Tr}_E \sum_{k''} \langle A_{k''}|\,\rho(t)\,|A_{k''}\rangle\,. \tag{2.41}$$

Since the inter-aggregate coupling H_C is weak compared to all other terms in H, we take it as a perturbation. Taking $H_0 = H - H_C$, and using tildes to denote the interaction picture, we write $\tilde{H}_C(t) = e^{iH_0t/\hbar}H_C e^{-iH_0t/\hbar}$ and express $\dot{\tilde{\rho}}(t)$ to second order in perturbation theory:

$$\dot{\tilde{\rho}}(t) \approx -\frac{1}{\hbar^2}\int_0^t d\tau\,\mathrm{Tr}_E\left[\tilde{H}_C(t),\left[\tilde{H}_C(\tau),\rho(0)\right]\right], \tag{2.42}$$

where $[\cdot,\cdot]$ is the commutator, and Tr_E is the trace over the environment degrees of freedom. Substituting into Equation 2.41,

$$\begin{aligned} k_{D\to A}(t) &= -\frac{1}{\hbar^2}\sum_{k''}\langle A_{k''}|\int_0^t d\tau\,\mathrm{Tr}_E\left[\tilde{H}_C(t),\left[\tilde{H}_C(\tau),\rho(0)\right]\right]|A_{k''}\rangle &(2.43)\\ &= -\frac{1}{\hbar^2}\sum_{k''}\langle A_{k''}|\int_0^t d\tau\,\mathrm{Tr}_E\big(\tilde{H}_C(t)\tilde{H}_C(\tau)\rho(0)+\rho(0)\tilde{H}_C(\tau)\tilde{H}_C(t)\\ &\quad -\tilde{H}_C(\tau)\rho(0)\tilde{H}_C(t)-\tilde{H}_C(t)\rho(0)\tilde{H}_C(\tau)\big)\,|A_{k''}\rangle\,. &(2.44)\end{aligned}$$

Since the charge is initially on the donor aggregate, $\rho(0)\,|A_{k''}\rangle = \langle A_{k''}|\,\rho(0) = 0$, the first two terms vanish, giving

$$\begin{aligned} k_{D\to A}(t) &= \frac{1}{\hbar^2}\sum_{k''}2\mathrm{Re}\,\langle A_{k''}|\int_0^t d\tau\,\mathrm{Tr}_E\big(\tilde{H}_C(\tau)\rho(0)\tilde{H}_C(t)\big)\,|A_{k''}\rangle &(2.45)\\ &= \sum_{j,j'}\sum_{k,k',k''}\frac{V_{jk}V_{j'k'}}{\hbar^2}\cdot 2\mathrm{Re}\int_0^t d\tau\,\mathrm{Tr}_E\big(\,\langle A_{k''}|\,e^{iH_0\tau/\hbar}\,|A_{k'}\rangle\\ &\quad \langle D_{j'}|\,e^{-iH_0\tau/\hbar}\rho(0)e^{iH_0t/\hbar}\,|D_j\rangle\,\langle A_k|\,e^{-iH_0t/\hbar}\,|A_{k''}\rangle\,\big)\,. &(2.46)\end{aligned}$$

Using the cyclic property of the trace gives

$$k_{D\to A}(t) = \sum_{j,j'}\sum_{k,k'} \frac{V_{jk}V_{j'k'}}{\hbar^2} \cdot 2\mathrm{Re}\int_0^t d\tau\, \mathrm{Tr}_E\big(\langle A_k| e^{-iH_0(t-\tau)/\hbar}|A_{k'}\rangle \langle D_{j'}| e^{-iH_0\tau/\hbar}\rho(0)e^{iH_0 t/\hbar}|D_j\rangle\big). \quad (2.47)$$

Defining $\tau' = t-\tau$, we can write

$$k_{D\to A}(t) = \sum_{j,j'}\sum_{k,k'} \frac{V_{jk}V_{j'k'}}{\hbar^2} \cdot \int_{-t}^t d\tau'\, \mathrm{Tr}_E\big(\langle A_k| e^{-iH_0\tau'/\hbar}|A_{k'}\rangle \langle D_{j'}| e^{iH_0(\tau'-t)/\hbar}\rho(0)e^{-iH_0(\tau'-t)/\hbar}e^{iH_0\tau'/\hbar}|D_j\rangle\big). \quad (2.48)$$

To simplify further, we consider the term $e^{iH_0(\tau'-t)/\hbar}\rho(0)e^{-iH_0(\tau'-t)/\hbar}$, which describes the time-evolution of the donor aggregate (because H_0 induces no donor-acceptor transitions). Because the aggregate-environment coupling is much stronger than the inter-aggregate coupling, the donor aggregate will thermalise with the environment on timescales much shorter than the charge-transfer timescale. Therefore, for times t much longer than the donor thermalisation time (but much shorter than the charge-transfer time), we can consider the long-time limit,

$$\lim_{t\to\infty} e^{iH_0(\tau'-t)/\hbar}\rho(0)e^{-iH_0(\tau'-t)/\hbar} = \rho_{\mathrm{th}}, \quad (2.49)$$

where for a large, weakly coupled environment, the state $\rho_{\mathrm{th}} = \rho_D \otimes \rho_A$, of donor and acceptor aggregates independently thermalised with their own environments, is independent of $\rho(0)$. In this limit, we may also extend the limits of integration in Equation 2.48 to infinity to give a time-independent rate:

$$k_{D\to A} = \sum_{j,j'}\sum_{k,k'} \frac{V_{jk}V_{j'k'}}{\hbar^2} \cdot \int_{-\infty}^{\infty} d\tau'\, \mathrm{Tr}_E\big(\langle A_k| e^{-iH_0\tau'/\hbar}|A_{k'}\rangle \langle D_{j'}|\rho_{\mathrm{th}}e^{iH_0\tau'/\hbar}|D_j\rangle\big). \quad (2.50)$$

Writing $H_D = H_D^0 + H_{DE} + H_{E_D}$ and $H_A = H_A^0 + H_{AE} + H_{E_A}$ and using Plancherel's theorem, we can rewrite Equation 2.50 as

$$k_{D\to A} = \sum_{j,j'}\sum_{k,k'} \frac{V_{jk}V_{j'k'}}{2\pi\hbar^2} \int_{-\infty}^{\infty} d\omega\, \mathscr{D}_D^{jj'}(\omega)\mathscr{A}_A^{kk'}(\omega), \quad (2.51)$$

$$\mathscr{D}_D^{jj'}(\omega) = \int_{-\infty}^{\infty} dt\, e^{-i\omega t}\mathrm{Tr}_{E_D}\big(e^{-iH_{E_D}t/\hbar}\langle D_{j'}| e^{iH_D t/\hbar}\rho_D|D_j\rangle\big), \quad (2.52)$$

$$\mathscr{A}_A^{kk'}(\omega) = \int_{-\infty}^{\infty} dt\, e^{i\omega t}\mathrm{Tr}_{E_A}\big(e^{iH_{E_A}t/\hbar}\langle A_k| e^{-iH_A t/\hbar}|A_{k'}\rangle \rho_A\big), \quad (2.53)$$

where we have renamed τ' to t. Changing to the aggregate basis, Equation 2.51 becomes

$$k_{D\to A} = \sum_{\alpha,\beta}\sum_{\alpha',\beta'} \frac{V_{\alpha\beta}V_{\alpha'\beta'}}{2\pi\hbar^2} \int_{-\infty}^{\infty} d\omega\, \mathscr{D}_D^{\alpha\alpha'}(\omega)\mathscr{A}_A^{\beta\beta'}(\omega), \quad (2.54)$$

$$\mathscr{D}_D^{\alpha\alpha'}(\omega) = \int_{-\infty}^{\infty} dt\, e^{-i\omega t}\mathrm{Tr}_{E_D}\big(e^{-iH_{E_D}t/\hbar}\langle D_{\alpha'}| e^{iH_D t/\hbar}\rho_D|D_\alpha\rangle\big), \quad (2.55)$$

$$\mathscr{A}_A^{\beta\beta'}(\omega) = \int_{-\infty}^{\infty} dt\, e^{i\omega t}\mathrm{Tr}_{E_A}\big(e^{iH_{E_A}t/\hbar}\langle A_\beta| e^{-iH_A t/\hbar}|A_{\beta'}\rangle \rho_A\big), \quad (2.56)$$

Equation 2.54 reduces to Equation 2.10 if $\mathscr{D}_D^{\alpha\alpha'}$ and $\mathscr{A}_A^{\beta\beta'}$ can be assumed to be diagonal in the aggregate basis. In general, this is not the case, because H_{DE} and H_{AE} do not commute with H_D^0 and H_A^0 respectively. However, it is an appropriate approximation in the limit, assumed here, of weak system-environment coupling, where the environment does not significantly perturb the thermal equilibrium of the system. The same approximation was considered and discussed in detail in the context of MC-FRET[32,127], where it can be used to reduce the excitonic analogue of Equation 2.54 to a diagonal version. Of course, Equation 2.54 can be used directly, at the cost of intuitive parallels with MT being obscured.

Equations 2.12–2.13 can be evaluated in the particular case of a thermalised environment of independent harmonic oscillators to yield Equations 2.14–2.15. Assuming that $\mathscr{D}_D^{\alpha\alpha'}$ and $\mathscr{A}_A^{\beta\beta'}$ are diagonal is equivalent to assuming that the electronic Hamiltonians commute with the environmental ones, meaning that $\exp(iH_Dt/\hbar) = \exp(iH_D^0t/\hbar)\exp(i(H_{DE}+H_{E_D})t/\hbar)$, so that Equation 2.12 becomes

$$\mathscr{D}_D^{\alpha\alpha}(\omega) = \int_{-\infty}^{\infty} dt\, e^{-i\omega t} e^{iE_\alpha t/\hbar} \rho_{\alpha\alpha} \mathrm{Tr}_{E_D}\left(e^{-iH_{E_D}t/\hbar} \langle D_\alpha| e^{i(H_{DE}+H_{E_D})t/\hbar} |D_\alpha\rangle \rho_{E_D}\right). \tag{2.57}$$

The Hamiltonian $H_{DE}+H_{E_D}$ can be diagonalised using the polaron transformation, which describes the displacement of the environment oscillators by the presence of a charge:

$$\langle D_\alpha| e^{i(H_{DE}+H_{E_D})t/\hbar} |D_\alpha\rangle = S_\alpha^\dagger e^{iH_{E_D}t/\hbar} S_\alpha, \tag{2.58}$$

where $S_\alpha = \exp\left(\sum_\xi g_{\alpha\xi}(b_\xi - b_\xi^\dagger)\right)$. Using this fact in Equation 2.57 gives

$$\mathscr{D}_D^{\alpha\alpha}(\omega) = \int_{-\infty}^{\infty} dt\, e^{-i\omega t} e^{iE_\alpha t/\hbar} \rho_{\alpha\alpha} \mathrm{Tr}_{E_D}\left(e^{-iH_{E_D}t/\hbar} S_\alpha^\dagger e^{iH_{E_D}t/\hbar} S_\alpha \rho_{E_D}\right). \tag{2.59}$$

In Equation 2.59, the contributions of different aggregate eigenstates are explicitly uncoupled, meaning that the equation takes, for a particular α, the same form that occurs in the derivation of ordinary, single-site MT. Therefore, the trace can be evaluated for a harmonic environment using standard techniques (e.g., section 6.8.1 of ref.[11]), giving Equation 2.14.

2.7 Acknowledgements

We thank Tom Stace and the UQ Node EQuS Theory Group for helpful comments on the manuscript. We were supported by the Westpac Bicentennial Foundation through a Westpac Research Fellowship and by the Australian Research Council through a Discovery Early Career Researcher Award (DE140100433) and the Centre of Excellence for Engineered Quantum Systems (CE110001013), and by an Australian Government Research Training Program (RTP) Scholarship.

Chapter 3

Evolution of Dimerism in the Photosynthetic Reaction Centre

The following publication has been incorporated as Chapter 3, with minor modifications:

Why are photosynthetic reaction centres dimeric?, *Chem. Sci.*, **10**, 9576, (2019), DOI: 10.1039/C9SC03712H[135].

Natasha B. Taylor[1] and Ivan Kassal[2].

[1]*Centre for Engineered Quantum Systems and School of Mathematics and Physics, The University of Queensland, Brisbane, Queensland 4072, Australia*

[2]*The University of Sydney Nano Institute and School of Chemistry, The University of Sydney, New South Wales 2006, Australia*

3.1 Abstract

All photosynthetic organisms convert solar energy into chemical energy through charge separation in dimeric reaction centres. It is unknown why early reaction centres dimerised and completely displaced their monomeric ancestors. Here, we discuss several proposed explanations for reaction-centre dimerism and conclude—with only weak assumptions about the primordial dimerisation event—that the most probable explanation for the dimerism is that it arose because it enhanced light-harvesting efficiency by deepening the excitonic trap, i.e., by enhancing the rate of exciton transfer from an antenna complex and decreasing the rate of back transfer. This effect would have outweighed the negative effect dimerisation would have had on charge transfer within the reaction centre. Our argument implies that dimerisation likely occurred after the evolution of the first antennas, and it explains why the lower-energy state of the special pair is bright.

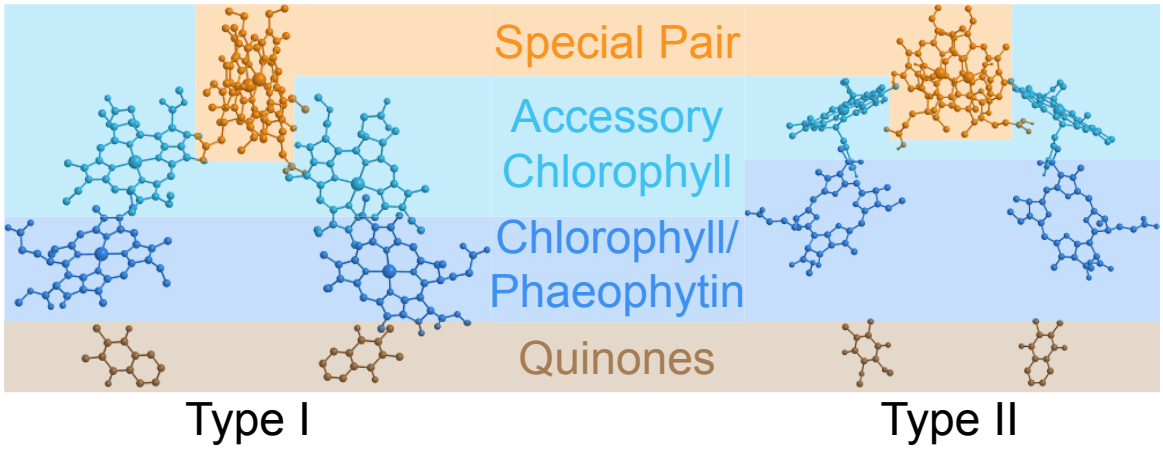

Figure 3.1: Photosynthetic reaction centres (RCs). All extant RCs are dimeric, comprising special pair chlorophylls, accessory chlorophylls, secondary chlorophylls or phaeophytins, and quinones. Bacteria use bacteriochlorophyll and bacteriophaeophytin instead. Shown are crystallographic structures[82,137], with chlorophyll tails and supporting protein removed for clarity.

3.2 Introduction

Photosynthetic energy conversion takes place in reaction centres (RC), where energy from the absorbed light drives charge separation. In all photosynthetic architectures, light is absorbed by an antenna complex to form an exciton, which is transferred to the RC. All extant RCs are dimeric pigment-protein complexes, the arrangement of whose core pigment cofactors is strongly conserved[34,136]. The most important feature of RC dimerism is that the monomers interact strongly at the special pair (P), a pair of tightly coupled (bacterio)chlorophylls, which is both the exciton acceptor and the primary charge donor[34] (Figure 3.1).

The ancestor of modern RCs is thought to be a monomeric pigment-protein complex containing the core RC cofactors[57], which we call the *primordial* RC. Prior to dimerisation, the primordial RC may have been photosynthetic, or it may have been appropriated from another membrane protein role, such as UV protection[138] or energetic metabolism[139]. Whatever its original purpose, the primordial RC dimerised, creating a homodimeric RC coded for by a single gene[57]. The homodimer gradually diverged into the ancestors of the modern RCs, all of which retain its general structure[60,140,141].

Our aim is to survey possible explanations for the dominance of RC dimerism and, especially, for the strong coupling between the two pigments in the special pair. As with any attempt to reconstruct reasons for long-ago evolutionary change, we cannot offer definite answers. Evolution rarely has an unambiguous explanation, with large differences in phenotype usually being end results of an undirected and disorderly process influenced by many kinds of selection pressures. More generally, evolutionary reasoning is often abductive, trying to find the best explanation (which may be a combination of multiple reasons) for a set of observations. Abductive conclusions are never logically certain and should be qualified as “most likely” or “best available”, and they may change in light of new evidence. So, to be more precise, our goal is to identify the most likely explanation(s) of the RC dimerism and of the strong coupling in P, given the current evidence.

This goal is hampered by over three billion years of evolutionary distance from the primordial

dimerisation event. Because there is little certainty about any detail of the primordial RC, our discussion and models are qualitative. We only seek general trends that hold across a broad range of possibilities about the primordial RC. Even so, we are able to conclude that the most likely explanation of dimerisation (or, at least, of the strong coupling in P) is that it improved exciton transfer from an antenna to the RC, possibly by a large margin, despite having a deleterious influence on charge transfer. On balance, the improvement to exciton transfer was likely more significant, leading to an overall increase in RC performance.

3.3 Possible explanations of reaction-centre dimerism

3.3.1 Evolutionary background

We reconstruct the primordial dimerisation event based on features of modern RCs. The generally accepted evolutionary relationships are shown in Figure 3.2. A monomeric RC dimerised to a homodimer, which diverged into several variants, some of which underwent gene duplication, allowing them to replace the homodimer with a heterodimer[57,60,74,140].

As a result, there is considerable diversity among modern RCs. A basic distinction is based on the final electron acceptor: in type I RCs, it is a ferredoxin, whereas in type II RCs, it is a quinone. Many organisms have only a single type of RC, but cyanobacteria, green algae, and plants have both type I and type II, present in photosystem I (PSI) and photosystem II (PSII), respectively. Type I RCs can be either homodimeric (e.g., in heliobacteria) or heterodimeric (e.g., PSI), unlike type II RCs, all of which are heterodimeric.

Despite differences in the final electron acceptor, the structures mediating initial exciton- and charge-transfer steps are remarkably conserved across all extant RCs. All RCs are dimeric, with two branches that only interact at a strongly coupled special pair (P) of chlorophyll (Chl) or bacteriochlorophyll (BChl) molecules. P is the dominant acceptor of excitons from antenna complexes and the primary charge donor[142–144]. From P, the charges are transferred down either branch in homodimeric RCs (such as heliobacteria[74,83]) or down only one branch in heterodimers. The pigments involved in the initial charge-transfer step always come from a small set of closely related tetrapyrroles (Chl, BChl, or (bacterio)phaeophytin, (B)Phe).

We emphasise that the purpose of discussing modern RCs is only to reconstruct features of the primordial one—we make no claims about the subsequent evolution and diversification, including the rise of heterodimers.

3.3.2 Candidate explanations

We group proposed explanations for RC dimerism into six categories.

1. *Explanation 1* is that that dimerisation was simply a random, fitness-neutral event that became fixed by genetic drift. We think this is unlikely, because fixation of a particular fitness-neutral

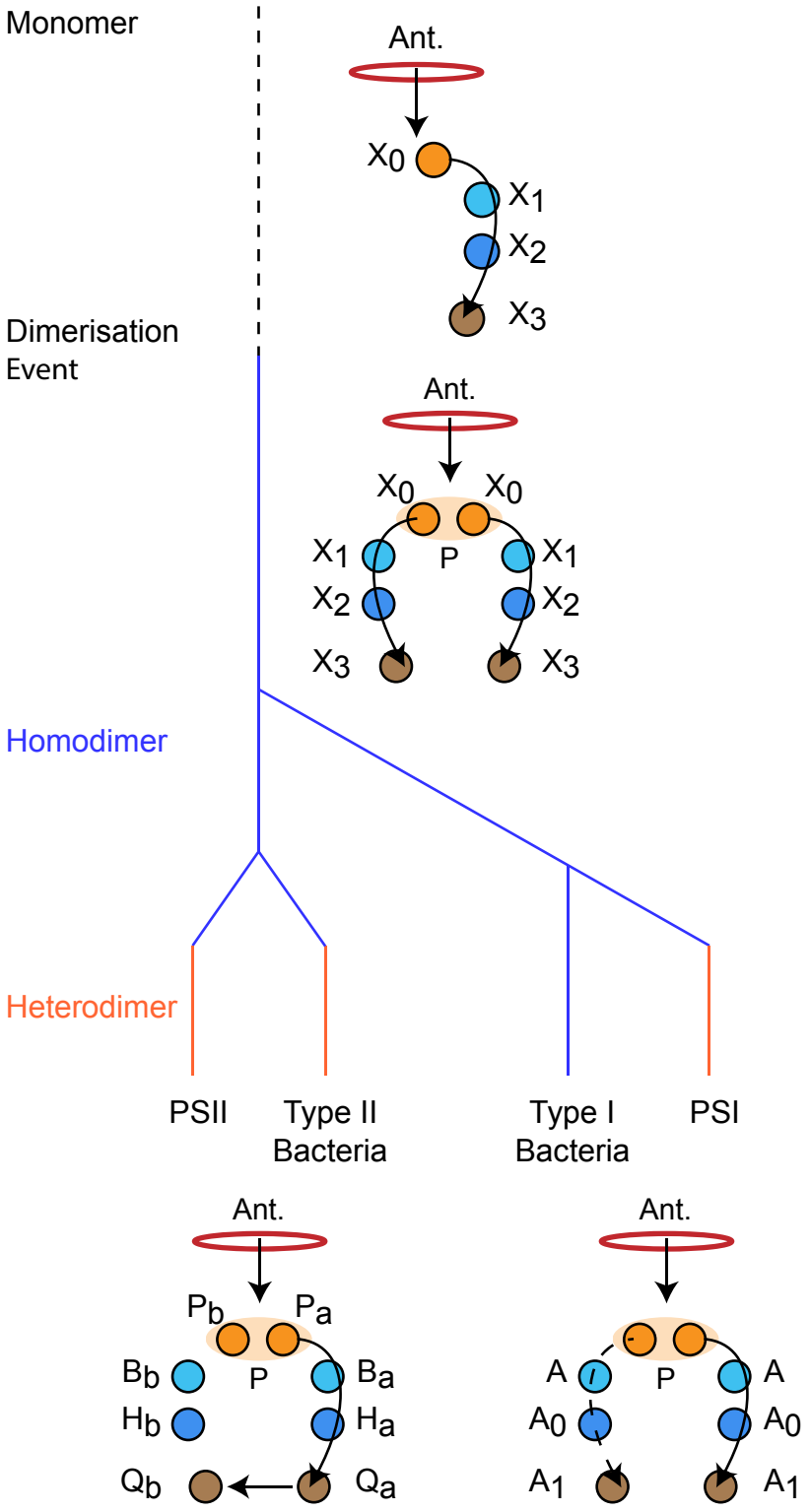

Figure 3.2: Evolution of reaction centres (RC)[34]. The primordial RC was monomeric, likely comprising three BChls (X_0, X_1, X_2) and a quinone (X_3). An antenna (Ant.) would transfer an exciton to X_0, which would also serve as the charge donor. The charge would transfer through X_1 and X_2 before arriving at X_3. The monomeric RC dimerised, producing a homodimer with two identical copies of the monomer, connected at the special pair (P). Excitons from the antenna could delocalise over P before charge separation, with charge transfer occurring along either branch. The homodimer subsequently diverged into type I and type II RCs, some of which experienced gene duplication events that led to heterodimerism. In modern type I RCs, each branch consists of three (B)Chls (P, A, and A_0) and a quinone (A_1). In heterodimeric PSI, charge transfer occurs exclusively down one branch, while in homodimeric systems (such as heliobacteria) charge can move down either branch with equal probability. In modern type II RCs, each branch consists of two (B)Chls (P and B), a phaeophytin (H) and a quinone (Q). Charge travels down one branch before being transferred to the inactive-branch quinone.

mutation is very improbable in large populations[145], such as those of bacteria. In other words, if dimerisation were fitness neutral, it would be difficult to explain the complete extinction of all competing, monomer-carrying organisms.

In contrast to *Explanation 1*, the remaining explanations assume that the initial dimerisation event conferred a fitness advantage. They differ in the proposed mechanism for this advantage, the central question being what can a dimer do that a monomer cannot.

2. *Explanation 2* is that dimerisation served a structural purpose. For example, by altering the structure of the supporting protein, it could have aided in assembly or in finding a particularly favourable packing of transmembrane helices[136]. This explanation, however, does not account for the strong coupling within P; similar large-scale structural changes could presumably have occurred even without the two P pigments coming into extremely close contact. It is possible that protein dimerisation occurred first and the strong coupling within P evolved later. If so, the problem is moved one step down the evolutionary timeline, and the interesting question becomes why the two weakly interacting branches of the dimer eventually evolved to have a strongly coupled P.

3. *Explanation 3*, offered in the context of Type II RCs, is that the presence of two quinones allows them to have different potentials and to stabilise the electron by transfer from Q_a to Q_b (see Figure 3.2)[146]. Transfer between quinones, however, is evolutionarily recent, requiring a heterodimeric RC. In the primordial dimer, the two quinones were symmetric (as in modern heliobacteria[83]), meaning that the quinones cannot explain the primordial dimerisation event[74].

Unlike the explanations above, the remaining explanations all assume that the strong coupling within P served an evolutionary purpose.

4. *Explanation 4* is that the coupling within P shifted its absorption peak to the red (see below), allowing it to harvest longer wavelengths. An organism with this mutation could survive in an environment where all shorter wavelengths were harvested by monomeric organisms. This mechanism would be particularly relevant if the primordial organisms lacked antennas and relied on RCs for light absorption as well. This explanation, however, does not account for the extinction of monomeric RCs; the success of dimeric organisms in the long-wavelength niche is consistent with the continuation of monomers using shorter wavelengths. Similarly, modern organisms with apparent long-wavelength adaptations (such as chlorophyll *f*[147]) have not displaced dominant species.

   Explanation 4 could only account for universal dimerism if the initial spectral-niche dimerism enabled a subsequent evolutionary advantage that allowed the dimers to displace the monomers. Although this sequence of events cannot be ruled out, it requires the conjunction of three circumstances, each of which appears quite uncertain: a) there were no antennas in the primordial

RC, b) the dimers arose to occupy the long-wavelength niche, and c) there was some future advantage, which could not have evolved directly.

5. *Explanation 5* proposes that the coupling within P increased its redox potential E_m, improving performance of donor-side electron transfer by making it easier for P^+ to be re-reduced. In oxygenic organisms, an increased E_m might facilitate water oxidation and reduce oxidative stress through the decreased lifetime of P^+ [146]. The primordial RC, however, was not oxygenic, and, like modern anoxygenic RCs, did not need a particularly high redox potential. Most importantly, the coupling within P would have actually hindered the re-reduction of P^+. The re-reduction occurs in the ground state, P_g, which is split by the coupling into two states, the higher-lying P_{g+} and the lower-lying P_{g-}. In the P^+ state that is to be re-reduced, the hole occupies the higher-energy state P_{g+}, i.e., the full state P^+ has a doubly occupied P_{g-} and a singly occupied P_{g+}. Because the coupling increases the energy of P_{g+}, there is a smaller driving force for electron transfer from the re-reductant to the dimer compared to the monomer, making the processes both kinetically and thermodynamically less favourable in the dimer.

6. *Explanation 6* is that dimerisation directly improved one of the two central functions of the RC. The first of these is the RC's role as an exciton acceptor, accepting optically generated excitations from pigments in the antenna. The second is charge separation, separating the electron and the hole onto separate pigment. The overall efficiency of the RC is the probability that an antenna exciton gives rise to charge separation before it is lost to recombination, and an improvement in the efficiency would confer a fitness advantage on the dimeric organism compared to the monomeric competition.

For the reasons given above, we view *Explanations 1–5* as unlikely to explain the origin of RC dimerism or, at least, of the strong coupling in P. Therefore, this chapter examines the plausibility of *Explanation 6*, which is considerably more complicated than the others. Readers unconvinced by our arguments against *Explanations 1–5* can read the rest of this chapter as an examination of how dimerism and the strong coupling in P affected the efficiency of the RC, an effect that would have contributed to RC performance even if one of *Explanations 1–5* were the dominant reason for the dimerisation.

Analysing *Explanation 6* requires understanding how the dimerisation affected the exciton- and charge-transfer functions in the RC. Intriguingly, the constituent pigments within P are the only ones in the RC close enough to influence each other, meaning that the part of the RC most affected by dimerisation is also both the ultimate acceptor of excitonic energy and the location of charge separation [142–144]. Therefore, to understand the role of dimerisation, we must consider how both exciton transfer to P and charge transfer out of it would have been affected by dimerisation.

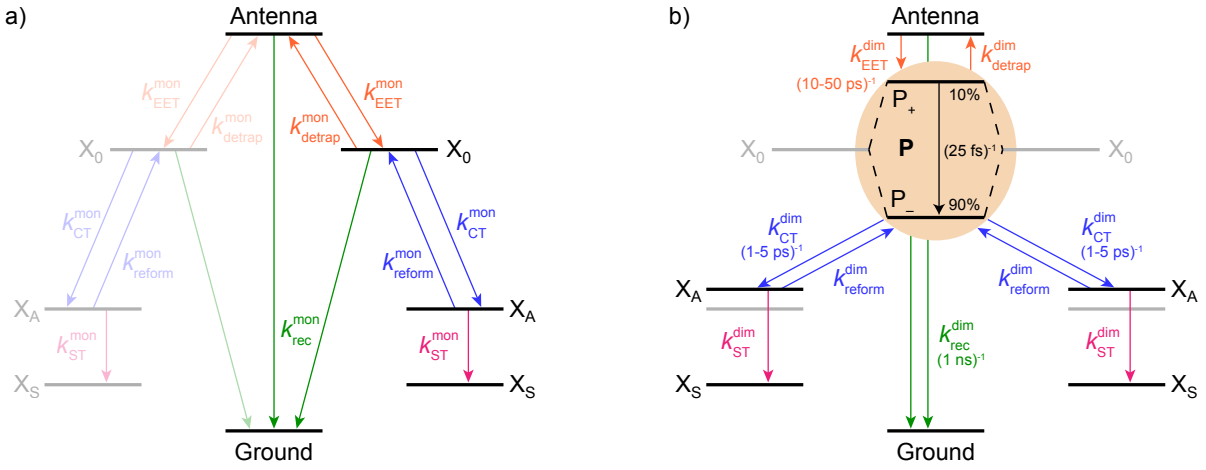

Figure 3.3: Energy and charge transfer pathways for **(a)** monomeric and **(b)** homodimeric reaction centres. Both diagrams show excitation energy transfer (orange) between the antenna and X_0/P, charge transfer (blue) between X_0/P and the primary electron acceptor X_A, subsequent charge transfer to X_S (pink), and exciton recombination (green). Rates found in modern systems are shown in parentheses, and the distribution of oscillator strengths in modern P is shown as percentages. The energy of an electron on X_A in the dimer is destabilised compared to the monomer due to the weaker electrostatic attraction to the delocalised hole on P.

3.4 Model

In the following, we model the primordial monomeric RC and the homodimer formed by the initial dimerisation, before studying how the dimerisation affected exciton transfer, charge transfer, and the overall efficiency. As the exact properties of the primordial RC are unknown, our model is necessarily general and qualitative. We are not looking for precise predictions of efficiencies, but for strong trends that hold across a broad parameter range.

3.4.1 Modelling the primordial dimerisation event

As the positions and orientations of the cofactors are well conserved across all RCs, we assume that the primordial homodimer had a similar structure to modern RCs. Therefore, the pigments of each branch are assumed to be too distant to strongly perturb each other, apart from the two composing P.

The precise identity of the pigments in the primordial RC are not important to our argument, and we agnostically refer to them as X_0 through X_3 in Figure 3.2. That said, these cofactors were most likely BChls, which is probably the most primitive of the modern RC tetrapyrroles[59,68,148], although this is not universally accepted[61].

We also make no assumptions about which pigment was the primary electron acceptor. In modern RCs, X_1 is either an electron acceptor itself or a bridge for transfer to X_2[83,149,150]. We only assume that one of the pigments is the primary acceptor—which we call X_A—and that it is lower in energy than P; whether charge transfer involves intermediate bridging states does not affect our argument.

We also assume an antenna (Ant.) that transfers excitons to P. The great diversity of modern antenna complexes[34] means we cannot say anything definitive about the structure of primordial antenna(s), so we treat them quite generally.

Finally, we assume the primordial monomer to be simply one half of the homodimer just described. Its antenna is assumed to be the same as the homodimer's.

We model the monomeric and dimeric RCs as multi-level systems governed by the rate processes shown in Figure 3.3. The rates for the monomer and dimer carry superscripts "mon" and "dim", respectively, and include the rate k_{EET} of excitation energy transfer (EET) from the antenna to X_0/P and the rate k_{detrap} of the reverse detrapping process. Charge transfer (CT) from P to the charge acceptor $\mathrm{X_A}$ is at rate k_{CT}, while the reverse process, exciton re-formation, occurs at rate k_{reform}. Subsequent transfer out of $\mathrm{X_A}$ to subsequent state(s) $\mathrm{X_S}$ occurs at rate k_{ST} and is assumed to be irreversible.

We also include exciton recombination to ground at rate $k_{\mathrm{rec}}^{\mathrm{mon}}$; in modern organisms, this rate is small ($\sim 1\,\mathrm{ns}^{-1}$)[151], and without knowing the structure of the primordial exciton donor, we take the modern value as representative.

The homodimer model also includes excitonic coupling J_{P} between the two X_0 molecules in P, resulting in two excitonic states, P_+ and P_-, which are respectively J_{P} higher and lower in energy than X_0 (Figure 3.4a). For modern plants, about 90% of the oscillator strength is in the lower state P_- [152]. We assume that the relaxation from P_+ to P_- is faster than any other process, occurring at a rate of $(25\,\mathrm{fs})^{-1}$ [143]. Therefore, even if P_+ is excited, rapid internal conversion to P_- ensures that all subsequent EET and CT take place from P_-.

3.4.2 Light-harvesting efficiency as figure of merit

The RC converts excitons into charges, and if dimerism increased fitness, it would have done so by increasing the efficiency of this fundamental process. As further CT from the primary charge $\mathrm{X_A}$ acceptor is identical in both the monomer and the dimer, we define the efficiency as the probability that an antenna exciton yields an electron on $\mathrm{X_S}$, as opposed to being lost to recombination.

The efficiency is maximised by having forward transfer rates k_{CT}, k_{EET}, and k_{ST} that are large relative to k_{rec}, k_{detrap}, and k_{reform}. Slow recombination implies high efficiency because recombination is the only way for the exciton to be lost, while slow detrapping ensures that the exciton, once it reaches P, has a chance to drive CT.

For both the monomer and the dimer, state populations obey a set of rate equations (superscripts "mon" and "dim" omitted from the rates):

$$\dot{A}(t) = X_0(t)k_{\mathrm{detrap}} - A(t)(k_{\mathrm{EET}} + k_{\mathrm{rec}}), \tag{3.1}$$

$$\dot{X}_0(t) = A(t)k_{\mathrm{EET}} + X_{\mathrm{A}}(t)k_{\mathrm{reform}} - X_0(t)(k_{\mathrm{detrap}} + k_{\mathrm{rec}} + k_{\mathrm{CT}}), \tag{3.2}$$

$$\dot{X}_{\mathrm{A}}(t) = X_0(t)k_{\mathrm{CT}} - X_{\mathrm{A}}(t)(k_{\mathrm{reform}} + k_{\mathrm{ST}}), \tag{3.3}$$

$$\dot{X}_{\mathrm{SA}}(t) = X_{\mathrm{A}}(t)k_{\mathrm{ST}}, \tag{3.4}$$

where $A(t)$, $X_0(t)$, $X_{\mathrm{A}}(t)$, and $X_{\mathrm{SA}}(t)$ are the populations of antenna excitons, X_0 excitons, $\mathrm{X_A}$ charges, and $\mathrm{X_{SA}}$ charges, respectively. The efficiency is the long-time ($t \to \infty$) population of $\mathrm{X_{SA}}$, given an

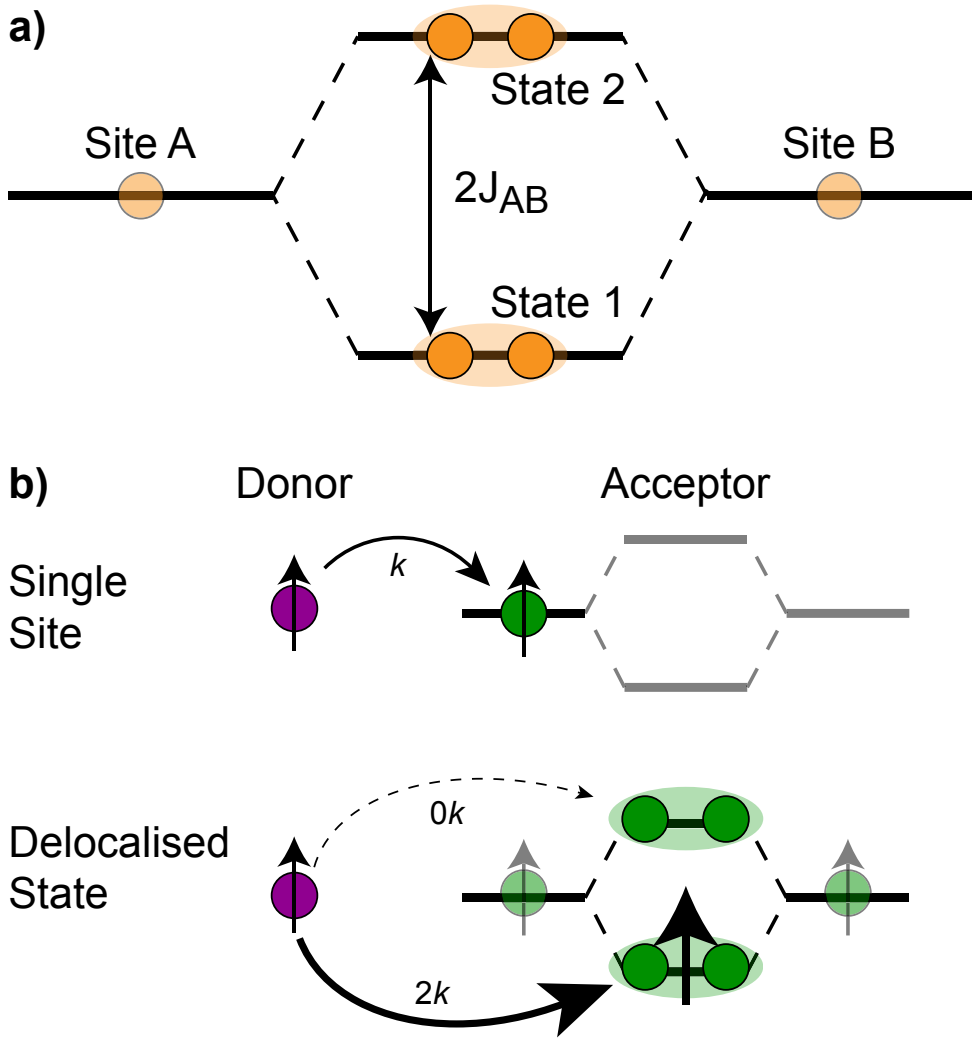

Figure 3.4: **a)** The coupling J_{AB} between two sites, A and B, gives rise to two delocalised (orange shading) eigenstates, 1 and 2, with an energetic splitting between them. In the RC, the two molecules in P couple to create a lower state, P_+, and an upper state, P_-. **b)** Example of exciton transfer and supertransfer, showing donors (purple), acceptors (green), and their transition dipole moments (arrows). Transfer from a single site to a single acceptor occurs at rate k, while transfer to delocalised acceptor states occurs at rate $2k$ (supertransfer from the bright state) or 0 (subtransfer from the dark state). Super- and subtransfer also occur in charge transfer, except that it is mediated by wavefunction overlap and not transition-dipole coupling.

initial antenna exciton (i.e., $A(0) = 1$ and $X_0(0) = X_A(0) = X_{SA}(0) = 0$),

$$\eta = \frac{k_{CT}k_{EET}k_{ST}}{k_{reform}k_{rec}(k_{detrap} + k_{EET} + k_{rec}) + k_{ST}k_{EET}k_{CT} + k_{ST}k_{rec}(k_{CT} + k_{detrap} + k_{EET} + k_{rec})}. \quad (3.5)$$

The monomer and dimer efficiencies η^{mon} and η^{dim} are calculated by placing the superscripts "mon" or "dim" on the rates in Equation 3.5.

We will generally calculate the relative efficiency η^{dim}/η^{mon}, which indicates whether dimerisation improved or diminished the light harvesting. The following sections survey how dimerisation would have affected the relative efficiency through changes in EET and CT.

3.4.3 Dimerism enhances excitation energy transfer (EET) to the special pair

The effect of EET on the relative efficiency $\eta^{\text{dim}}/\eta^{\text{mon}}$ is determined by how the EET rates in Equation 3.5 are affected by dimerisation. For high efficiency, k_{EET} should be large relative to k_{detrap} and k_{rec}, to allow the exciton to stay in X_0/P for as long as possible and increase the chance for CT to occur.

Coupling between RCs and their antennas is weak, meaning that both EET and detrapping can be described perturbatively, by Förster resonant energy transfer (FRET)[94,153]. If either the donor or the acceptor (or both) feature excitonic delocalisation, FRET should be replaced by generalised FRET (gFRET)[30], which describes EET in delocalised systems and has been widely used to describe photosynthetic systems[30,90,91,126]. In particular, it is necessary to use gFRET for modelling the dimeric RC because the excitonic states of P are delocalised. The gFRET transfer rate is

$$k_{\text{gFRET}} = \sum_{\alpha,\beta} \frac{2\pi}{\hbar} |J_{\alpha\beta}|^2 \int dE\, L_\alpha(E) I_\beta(E), \tag{3.6}$$

where $L_\alpha(E)$ is the emission spectrum of the α donor state, $I_\beta(E)$ the absorption spectrum of the β acceptor state, and $J_{\alpha\beta}$ the excitonic coupling between donor state α and acceptor state β.

Dimerisation can affect gFRET rates by two mechanisms: supertransfer and the creation of an energetic trap. The former affects the $|J_{\alpha\beta}|^2$ factor in Equation 3.6, and the latter the spectral overlap integral.

The first effect, supertransfer, is the enhancement of EET due to increases in $|J_{\alpha\beta}|^2$ in Equation 3.6, arising from the constructive interference between EET pathways, as discussed in Section 1.1.3. For example, in EET between a single donor D and a single acceptor A, the EET rate k_{single} is proportional to $|J_{\text{DA}}|^2$. By contrast, multi-site gFRET occurs between the delocalised eigenstates of the donor and the acceptor, rather than as a sum of rates between individual sites (Figure 3.4b). With two EET acceptors, supertransfer can accelerate EET up to a factor of two; if the transition dipoles of the donor and the acceptors are parallel, the acceptor state is fully delocalised over the two acceptor molecules, meaning that the donor couples to an effective acceptor transition dipole that is larger by a factor of $\sqrt{2}$, giving a gFRET rate of

$$k_{\text{delocal}} \propto \left| \frac{1}{\sqrt{2}} \left(J_{\text{DA}_1} + J_{\text{DA}_2}\right) \right|^2 \propto 2k_{\text{single}}. \tag{3.7}$$

The same enhancement factor of 2 can occur if there are two donor molecules with complete delocalisation between them, as would happen for exciton de-trapping back to the antenna. In cases where the two acceptor transition dipole moments are not perfectly parallel, the enhancement, which we denote γ, is less than 2. A reduction in γ can also occur due to environmental fluctuations or asymmetry between the two acceptor sites, either of which could partially localise the exciton. As we discuss in more detail below, we assume that γ in the primordial special pair was between 1.5 and 1.8, which we take as the supertransfer enhancement factor for both k_{EET} and k_{detrap}.

The second way that dimerisation affects EET is the creation of an energetic trap, which enters Equation 3.6 through the overlap integral. The coupling J_{P} between X_0 molecules in P means that P_-

is energetically stabilised relative to a single X_0. This energy shift affects EET in two ways: forward EET is accelerated by dimerisation because of the larger driving force and detrapping is slowed down because of the greater activation energy. Although the precise magnitude of these effects could be calculated using Equation 3.6 and a microscopic model, we focus only on the dominant effect, which is the change in detailed balance due to the energy shift. To do so, we assume the simplest case, that forward EET and detrapping are affected symmetrically, i.e., that forward EET is accelerated by a factor of $\exp(J_P/2k_BT)$, while detrapping is slowed down by a factor of $\exp(J_P/2k_BT)$. Our results would not be significantly different if, say, only forward EET were accelerated by $\exp(J_P/k_BT)$ or only detrapping slowed down by $\exp(J_P/k_BT)$. Finally, this approach is valid if, as is the case in all RCs, J_P is small compared to the widths of absorption and emission peaks; a very large J_P could eventually lead to a decrease in the overlap integral in Equation 3.6, but this is not biologically relevant.

We can combine the effects of supertransfer and energetic trapping to calculate the overall effect of dimerisation on EET rates and the efficiency. Dimerisation enhances the forward EET,

$$k_{EET}^{dim} = \gamma \exp(J_P/2k_BT) k_{EET}^{mon}. \tag{3.8}$$

By contrast, the detrapping rate is affected by both supertransfer and increased trapping, becoming

$$k_{detrap}^{dim} = \gamma \exp(-J_P/2k_BT) k_{detrap}^{mon}, \tag{3.9}$$

which can be more or less than k_{detrap}^{mon}, depending on γ and J_P. However, the ratio of forward to backward EET is enhanced by dimerisation, $k_{EET}^{dim}/k_{detrap}^{dim} = \exp(J_P/k_BT) k_{EET}^{mon}/k_{detrap}^{mon}$, a feature that enhances the overall dimer efficiency.

3.4.4 Dimerism diminishes charge transfer (CT) from the special pair

For high efficiency, k_{CT} should be high compared to k_{detrap} and k_{rec}. The smaller k_{CT} is relative to k_{detrap}, the longer the exciton spends in the antenna, offering more chance of recombination, while if k_{rec} is large, recombination can occur in P itself.

It is not clear what is the best theoretical model for CT in the primordial RCs. Unlike with EET—which always has weak antenna-RC couplings, making FRET the safe choice—CT couplings between modern special pairs and the primary charge acceptors are not weak, although they could have been in the past. The uncertainty in the strength of the primordial CT couplings translates to an uncertainty about the best theoretical description of primordial CT. The two extremes of CT are diabatic CT (also known as Marcus theory, and applicable for weak CT couplings) and adiabatic CT (applicable for strong CT couplings). Our approach is to carry out the calculations with both approaches; fortunately, it turns out that the final conclusions are not significantly affected by the choice.

First, we consider the diabatic limit. Just as describing EET in delocalised systems requires gFRET, diabatic CT in delocalised systems is described using our recently described generalised Marcus theory (gMT)[110], Chapter 2 of this thesis, which predicts a CT rate of

$$k_{gMT} = \sum_{\alpha,\beta} \frac{2\pi}{\hbar} \frac{|V_{\alpha\beta}|^2}{\sqrt{4\pi k_B T \lambda_{\alpha\beta}}} \exp\left(\frac{-(\Delta E_{\alpha\beta} + \lambda_{\alpha\beta})^2}{4k_B T \lambda_{\alpha\beta}} \right), \tag{3.10}$$

where $V_{\alpha\beta}$ is the electronic coupling between the αth delocalised state on the donor and βth delocalised state on the acceptor, $\lambda_{\alpha\beta} = \lambda_\alpha + \lambda_\beta$ is the reorganisation energy, and $\Delta E_{\alpha\beta} = E_\beta - E_\alpha$ is the energy difference.

Like gFRET, gMT allows for supertransfer through constructively interfering pathways[110]. However, it is more sensitive to geometry than gFRET because CT is mediated by wavefunction overlaps, which decay exponentially with distance[110]. In modern systems, the X_0 molecule that is more distant from the acceptor is so far away that its CT coupling to X_A would be negligible compared with the nearer X_0. Consequently, $|V_{P_-,X_A}|^2 = |V_{X_0,X_A}|^2/2$, leading to a halving of the CT rates.

Also similarly to gFRET, transfer from P to X_A is affected by changes in energy levels upon dimerisation, of which there are two kinds. Firstly, the coupling inside the special pair decreases the energy difference between P_- and X_A by J_P. Secondly, delocalisation also affects the electrostatics: since the two charges are closer together in the monomer state ${X_0}^-{X_A}^+$ than in the corresponding dimer state ${P_-}^+{X_A}^-$, the latter has weaker Coulomb binding and, therefore, a higher energy. This electrostatic energy difference also decreases the driving force for charge separation by an amount we call $\Delta E_{\mathrm{Coul,A}}$. Together, the two contributions imply that $\Delta E_{P_-,X_A} = \Delta E_{X_0,X_A} + \Delta E_{\mathrm{Coul,A}} + J_P$.

It is not immediately clear how energy changes affect the rates, because the Franck-Condon factor in Equation 3.10 also depends on the reorganisation energy, which is also affected by delocalisation: a donor (or acceptor) aggregate consisting of N molecules, each with reorganisation energy λ, has, in a fully delocalised state, $\lambda_\alpha = \lambda/N$[110]. For the RC, this implies $\lambda_{P_-,X_A} = \lambda_{X_0}/2 + \lambda_{X_A}$. Assuming that $\lambda_{X_0} \approx \lambda_{X_A}$, we have $\lambda_{P_-,X_A} = 3/4 \cdot \lambda_{X_0,X_A}$, where λ_{X_0,X_A} is the reorganisation energy for CT between X_0 and X_A.

Overall, the CT rate for the dimer becomes

$$k^{\mathrm{dim}}_{\mathrm{CT,gMT}} = \frac{1}{\sqrt{3}} k^{\mathrm{mon}}_{\mathrm{CT}} \exp\left(\frac{(\Delta E_{X_0,X_A} + \lambda_{X_0,X_A})^2}{4k_B T \lambda_{X_0,X_A}} - \frac{(\Delta E_{P_-,X_A} + \lambda_{P_-,X_A})^2}{4k_B T \lambda_{P_-,X_A}} \right), \tag{3.11}$$

which includes the ratio of pre-exponential factors, $|V_{P_-,X_A}|^2\sqrt{\lambda_{X_0,X_A}}\,/|V_{X_0,X_A}|^2\sqrt{\lambda_{P_-,X_A}} = 1/\sqrt{3}$. In most cases, dimerisation decreases the gMT rate; in particular, $k^{\mathrm{dim}}_{\mathrm{CT,gMT}} < k^{\mathrm{mon}}_{\mathrm{CT}}$ if, as in modern RCs, $J_P > 0$ and $\lambda_{X_0,X_A} \lesssim 220\,\mathrm{meV}$. Since gMT obeys detailed balance, the rate $k^{\mathrm{dim}}_{\mathrm{reform,gMT}}$ of charge back-transfer is calculated by reversing the signs of $\Delta E_{X_0,X_A}$ and $\Delta E_{P_-,X_A}$.

The second limit we consider is adiabatic charge transfer, which, in its simplest form[11], predicts a CT rate (whether forward or backward) of

$$k_{\mathrm{adiabatic}} = \frac{\omega_{\mathrm{vib}}}{2\pi} e^{-(E_A - |V_{DA}|)/k_B T}, \tag{3.12}$$

where ω_{vib} is the attempt frequency, E_A is the energy barrier, and V_{DA} the electronic coupling between donor and acceptor. The absolute value ensures that this rate describes transfer from the lower state regardless of the sign of V_{DA}.

Upon dimerisation, the electronic coupling V_{DA} is reduced by a factor of $\sqrt{2}$, and there are energetic shifts due to changes in the Coulomb binding. Analogously to our discussion of EET, we assume that forward CT is slowed down by the reduced driving force by a factor of $\exp(-\Delta E_{\mathrm{Coul,A}}/2k_B T)$,

Parameter	Symbol	Minimum	Maximum
Exciton recombination rate in monomer	$k_{\mathrm{rec}}^{\mathrm{mon}}$	$10^9\ \mathrm{s}^{-1}$	$10^9\ \mathrm{s}^{-1}$
Exciton transfer rate in monomer (antenna to RC)	$k_{\mathrm{EET}}^{\mathrm{mon}}$	$10^9\ \mathrm{s}^{-1}$	$10^{11}\ \mathrm{s}^{-1}$
Exciton detrapping rate in monomer (RC to antenna)	$k_{\mathrm{detrap}}^{\mathrm{mon}}$	$10^9\ \mathrm{s}^{-1}$	$10^{11}\ \mathrm{s}^{-1}$
Charge transfer rate in monomer	$k_{\mathrm{CT}}^{\mathrm{mon}}$	$10^9\ \mathrm{s}^{-1}$	$10^{12}\ \mathrm{s}^{-1}$
Excitonic coupling in special pair	J_{P}	10 meV	50 meV
Driving force for charge transfer in monomer	$\Delta E_{\mathrm{X_0,X_A}}$	$-\lambda_{\mathrm{X_0,X_A}}$	0 meV
Reorganisation energy for charge transfer in monomer	$\lambda_{\mathrm{X_0,X_A}}$	80 meV	270 meV
Electronic coupling for charge transfer in monomer	$V_{\mathrm{X_0,X_A}}$	1 meV	18 meV
Supertransfer enhancement factor in dimer	γ	1.5	1.8
Electrostatic energy shift of $\mathrm{X_A}$ upon dimerisation	$\Delta E_{\mathrm{Coul,A}}$	0 meV	30 meV
Electrostatic energy shift of $\mathrm{X_S}$ upon dimerisation	$\Delta E_{\mathrm{Coul,ST}}$	0 meV	10 meV

Table 3.1: The explored parameter space.

while the backward CT is accelerated by the reduced uphill barrier by a factor of $\exp(\Delta E_{\mathrm{Coul,A}}/2k_{\mathrm{B}}T)$. Overall, the rate of forward CT in the dimer becomes

$$k_{\mathrm{CT,adiabatic}}^{\mathrm{dim}} = k_{\mathrm{CT}}^{\mathrm{mon}} \exp\left(-\Delta E_{\mathrm{Coul,A}}/2k_{\mathrm{B}}T\right) \exp\left(\left(1-\sqrt{2}\,\right)\left|V_{\mathrm{X_0,X_A}}\right|/k_{\mathrm{B}}T\right). \tag{3.13}$$

As the exponentials are less than 1, dimerisation slows down the forward adiabatic CT, reducing the relative efficiency. Similarly, the back-transfer rate is taken to be

$$k_{\mathrm{reform,adiabatic}}^{\mathrm{dim}} = k_{\mathrm{reform}}^{\mathrm{mon}} \exp\left(\Delta E_{\mathrm{Coul,A}}/2k_{\mathrm{B}}T\right) \exp\left(\left(1-\sqrt{2}\,\right)\left|V_{\mathrm{X_0,X_A}}\right|/k_{\mathrm{B}}T\right), \tag{3.14}$$

where $k_{\mathrm{reform}}^{\mathrm{mon}}$ is given by detailed balance, $k_{\mathrm{reform}}^{\mathrm{mon}} = k_{\mathrm{CT}}^{\mathrm{mon}} \exp(\Delta E_{\mathrm{X_0,X_A}}/k_{\mathrm{B}}T)$.

Subsequent charge transfer is also affected by delocalisation due to changes in electrostatics. Because the subsequent transfer occurs farther from P, the energetic destabilisation is smaller than for transfer from P to $\mathrm{X_A}$, giving a net increase in the driving force, which we call $\Delta E_{\mathrm{Coul,ST}}$. In both gMT and adiabatic CT treatments, we include the effect through $k_{\mathrm{ST}}^{\mathrm{dim}} = \exp(\Delta E_{\mathrm{Coul,ST}}/k_{\mathrm{B}}T) k_{\mathrm{ST}}^{\mathrm{mon}}$.

Overall, dimerisation is expected to decrease the rate of CT whether it is described using gMT or adiabatic theory.

3.4.5 Parameter space

Our goal is to determine, over a plausible parameter space, whether and how the primordial dimerisation could have affected the RC efficiency. Table 3.1 lists the free parameters of the model and their ranges within the parameter space. The monomer rates were taken as fundamental, and dimer rates were calculated from monomer rates and the dimerisation parameters (J_{P}, $\Delta E_{\mathrm{X_0,X_A}}$, $\lambda_{\mathrm{X_0,X_A}}$, $V_{\mathrm{X_0,X_A}}$, γ, $\Delta E_{\mathrm{Coul,A}}$, and $\Delta E_{\mathrm{Coul,ST}}$) using Equations 3.8, 3.9, and 3.11 or 3.13.

We determined the limits of the parameter space by considering modern RCs. We assume that the monomer was no faster at EET or CT than modern RCs, implying that the monomer EET and CT rates are less than the natural rates: $k_{\mathrm{EET}}^{\mathrm{mon}} \leq 10^{11}\,\mathrm{s}^{-1}$ and $k_{\mathrm{CT}}^{\mathrm{mon}} \leq 10^{12}\,\mathrm{s}^{-1}$ [34,143,144,154]. We also assume that these rates are larger than the recombination rate $k_{\mathrm{rec}}^{\mathrm{mon}} = 10^{9}\,\mathrm{s}^{-1}$, which is assumed constant, essentially setting the timescale. We make no assumption about whether detrapping is faster than or comparable to forward EET (as in modern plants [155,156]) or slower (as in purple bacteria [157]), instead limiting $k_{\mathrm{detrap}}^{\mathrm{mon}}$ to at most $10^{11}\,\mathrm{s}^{-1}$, the maximal rate of $k_{\mathrm{EET}}^{\mathrm{mon}}$.

In modern RCs, J_{P} ranges between about 20 and 50 meV [83,85,158–160], setting the upper bound $J_{\mathrm{P}} \leq 50\,\mathrm{meV}$. As the coupling in the monomer may have been weaker than in modern RCs, we take 10 meV as the lower bound for J_{P}. Modern RCs have a coupling between the special pair and the charge acceptor of between 0.7 and 13 meV [84,85,87,161]; we compensate for the decrease in coupling through dimerisation by multiplying these values by $\sqrt{2}$ to find the range of $V_{\mathrm{X_0,X_A}}$. We assume CT takes place in the normal or activationless regime (as opposed to the inverted regime), meaning $\Delta E_{\mathrm{X_0,X_A}} \geq -\lambda_{\mathrm{X_0,X_A}}$, and that $E_{\mathrm{X_0}} \geq E_{\mathrm{X_A}}$, meaning $\Delta E_{\mathrm{X_0,X_A}} \leq 0$. The reorganisation energy $\lambda_{\mathrm{X_0,X_A}}$ is assumed to be between 80 and 270 meV, typical ranges for CT in biological structures [162–165].

We estimate γ, the supertransfer enhancement factor for EET, to have been between 1.5 and 1.8. As RC geometry is strongly conserved and EET depends on relative transition-dipole orientations in the special pair, we assume the distribution of oscillator strengths in the primordial dimer was similar to the modern cases. If, as in modern special pairs, $\mathrm{P_-}$ carried about 90% of the oscillator strength [152], $\gamma \approx 1.8$; the lower estimate of 1.5 allows for the primordial dimer to have been somewhat less efficient.

Finally, we consider the electrostatic energy differences $\Delta E_{\mathrm{Coul,A}}$ and $\Delta E_{\mathrm{Coul,ST}}$. We estimate the former as

$$\Delta E_{\mathrm{Coul,A}} = \frac{e^2}{4\pi\varepsilon_0\varepsilon_r}\left(\frac{1}{r_{\mathrm{X_AX_0}}^{\mathrm{mon}}} - \frac{1}{r_{\mathrm{X_AP}}^{\mathrm{dim}}}\right), \tag{3.15}$$

where ε_r is the relative permittivity, $r_{\mathrm{X_AX_0}}^{\mathrm{mon}}$ the distance between $\mathrm{X_A}$ and $\mathrm{X_0}$ in the monomer, and $r_{\mathrm{X_AP}}^{\mathrm{dim}}$ the distance between $\mathrm{X_A}$ and the centre of P in the dimer. $\Delta E_{\mathrm{Coul,ST}}$ is defined analogously, using distances between $\mathrm{X_0}$/P and the subsequent acceptors. For $\Delta E_{\mathrm{Coul,A}}$, we assume a range of 0 meV to 30 meV, based on the separations between pigments in several modern RCs, and on an effective ε_r ranging between 5 and 10. $\Delta E_{\mathrm{Coul,ST}}$ is smaller because of the larger distances, and we take it to be at most 10 meV.

3.5 Results

While we have shown above that dimerisation has opposite effects on EET and CT, enhancing the former and diminishing the latter, the total effect on the efficiency depends on which of these two effects is larger. We express the results of our parameter survey (Figure 3.5) as the relative efficiency of a dimer relative to a monomer, $\eta^{\mathrm{dim}}/\eta^{\mathrm{mon}}$.

Our results show that between about half and three-quarters of the parameter space (depending on whether CT is described using gMT or adiabatic theory) leads to improved relative efficiency

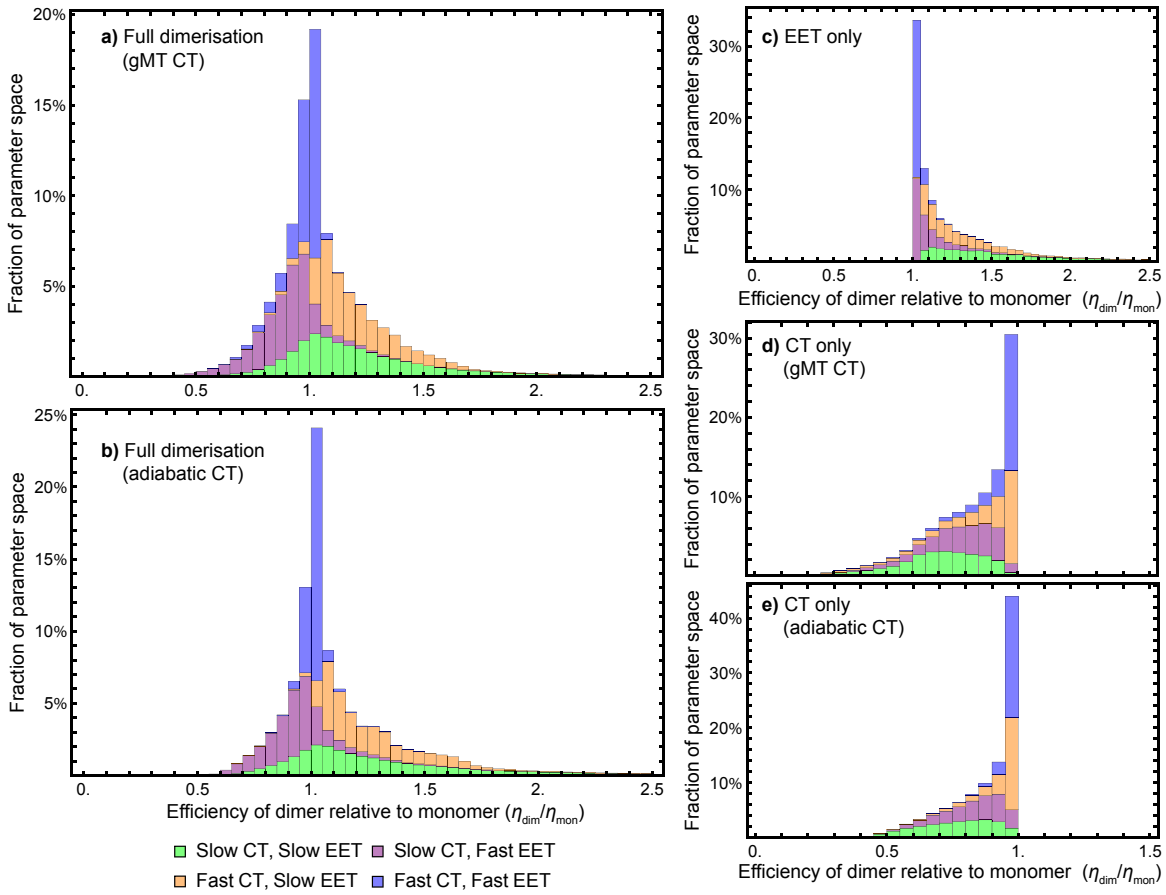

Figure 3.5: Efficiency of the dimer relative to the monomer across the parameter space of Table 3.1, if charge transfer (CT) is described using **(a)** generalised Marcus theory (gMT) or **(b)** adiabatic rates. **(c)** Relative efficiency if only exciton transfer (EET) effects are considered (i.e., assuming CT is unaffected by dimerisation), showing that dimerisation always enhances EET and the efficiency. **(d)** Relative efficiency if only CT effects are considered, modelled using gMT (i.e. assuming EET is unaffected by dimerisation), showing that dimerisation always diminishes CT and the efficiency. **(e)** As (d), but with CT described using adiabatic rates. In all cases, the recombination rate is $10^9\,\mathrm{s}^{-1}$; in the legend, 'slow' indicates rates comparable to recombination (below $10^{10}\,\mathrm{s}^{-1}$), and 'fast' those much faster (above $10^{10}\,\mathrm{s}^{-1}$). In all panels, the histograms are stacked.

(Figure 3.5a,b). When divided into individual contributions of EET (Figure 3.5c) and CT (Figure 3.5d,e) it can be seen that dimerisation enhances EET and is detrimental to CT. The differences in efficiency between the gMT and adiabatic treatments are caused by the fact that adiabatic CT rates are diminished less by dimerisation, meaning that the final efficiency can be increased more by the EET.

The results in Figure 3.5 are divided into four regimes, depending on whether EET and CT are fast (above $10^{10}\,\mathrm{s}^{-1}$, i.e., much faster than recombination), or slow (below $10^{10}\,\mathrm{s}^{-1}$, i.e., comparable to recombination). First, when both CT and EET are much faster than recombination, the exciton does not have time to recombine and the efficiency is high. In that case, small changes in rates due to dimerisation do not meaningfully affect the efficiency, making the relative efficiency close to 1. Second, if CT is much faster than recombination but EET is comparable to recombination, the exciton may recombine on the antenna. However, if it is transferred to X_0/P, the fast CT removes it before detrapping can occur. Since dimerisation improves EET, this regime consists largely of relative efficiencies greater than 1. Third, if CT is comparable to the recombination rate but EET is much faster, detrapping limits the amount of time CT has to occur and so the exciton spends much of its time

transferring between the antenna and X_0/P. Because dimerisation makes CT even slower, detrapping is more likely following dimerisation, and so this regime consists largely of relative efficiencies less than 1. Finally, the case where both CT and EET are comparable to the recombination rate has low efficiency, with recombination occurring in both X_0/P and the antenna. This regime is the most sensitive to small changes in EET and CT rate, and has the broadest distribution of relative efficiencies.

3.6 Discussion

Our results show that *Explanation 6* is a plausible account of the rise of RC dimerism. In a large fraction of the parameter space, the strong coupling in P would have caused changes in EET and CT that, overall, would have considerably increased the RC efficiency. In non-negligible regions of the parameter space, the enhancement was larger than 50%, a performance improvement that could have provided a sufficient fitness advantage to displace the monomeric competition.

We emphasise that the parameter space we surveyed was deliberately broad, whereas the actual dimerisation event corresponded to only one point in that space. Therefore, the panels of Figure 3.5 are *not* probability distributions for what would happen if evolution were repeated; rather, they reflect ignorance about the primordial RC and the rather arbitrary assumptions about the limits of the parameter space and of the distribution of each parameter (which we took to be uniform). To argue for a likely evolutionary explanation of dimerism, it suffices to establish that there is a large range of primordial parameters for which the argument holds.

While we surveyed a broad parameter space, we do think some areas of that space are more likely than others to represent the primordial RC. In particular, if the primordial RC was like modern RCs, it would fall in the orange panels of Figure 3.5, corresponding to fast CT and slow EET. Of the four domains in Figure 3.5, that is the one that shows the greatest efficiency enhancement.

If the efficiency enhancement was the actual driver of RC dimerism, it would tell us more about the early stages of the evolution of photosynthesis. First, because the efficiency enhancement is caused by improved EET from the antenna to P, the pre-dimerisation RC, like all modern RCs, would have had an antenna. In other words, antennas likely evolved before RC dimerism (or at least before the strong coupling in P). If the earliest antennas were poor at EET, as one might expect, the enhancement due to dimerism could have been very large. After the dimerisation event, the antennas diversified to the wide range seen today[34], but all RCs retained their dimerism.

Our argument also explains why the lower state of P is bright. Whether P^+ or P^- is lower in energy depends on the sign of J_P, which can change based on the alignment of the transition-dipole moments of the (B)Chls. One might think it would be better for the lower state to be dark, because that would slow down radiative relaxation (fluorescence), giving the exciton more time to dissociate, an idea called dark-state protection[166]. Indeed, if the RC were responsible for light absorption, the reversal of bright and dark states would improve the efficiency. However, if the driver of dimerisation was lowering the energy of the bright state of P relative to an antenna, then the bright state must have been the lower one.

3.7 Conclusion

We have used modern RCs to construct a model and a plausible parameter space for the primordial dimerisation event, finding that dimerisation could have increased RC efficiency, perhaps by as much as 50%, offering a good evolutionary explanation for the dimeric structure. The coupling between the two halves of P created an exciton trap, enhancing EET into the system and diminishing back transfer. While dimerisation decreased the forward CT rate, in large parts of the explored parameter space the slower CT was more than compensated for by the EET enhancement. In particular, if CT in the monomer was as fast as it is in modern dimers, the benefit to EET would have far exceeded the small decrease in efficiency due to the reduction in CT rates. Our findings could be experimentally tested through the engineering of fully monomeric RCs, which could also narrow the possible parameter regime through a combination of structural and more accurate computational studies.

3.8 Acknowledgements

We thank James Allen, Noel Hush, Kevin Redding, Jeffrey Reimers, and Thomas Renger for valuable feedback. We were supported by a Westpac Bicentennial Foundation Research Fellowship, by an Australian Government Research Training Program scholarship, and by a University of Sydney Nano Institute Grand Challenge.

Chapter 4

Conclusion

This thesis achieved two goals: (1) to derive a theory of delocalised charge transfer in molecular systems; and (2) to apply this theory to photosynthetic reaction centres to explain the impact of dimerisation on efficiency. Their implications for future research are summarised here.

4.1 Generalised Marcus Theory

Chapter 2 derived generalised Marcus theory (gMT) to describe delocalised charge transfer, that could be used in molecular systems such as organic semiconductors, the photosynthetic reaction centre, metal-organic framework, and inorganic coordination complexes.

To derive gMT, we used the time evolution of the Hamiltonian describing the system, environment, and system-environment interaction, using second-order in perturbation theory for inter-aggregate coupling to create equations of motion. The end result was a closed-form solution that allows predictions about the charge transfer properties of delocalised molecular systems. These include:

- charge supertransfer, the enhancement of delocalised charge transfer rate through constructive interference of charge-transfer pathways;
- reorganisation energy suppression, where the delocalisation reduces the environment displacement caused by the presence of a charge;
- the existence of an inverted regime, which was predicted by MT for charge transfer between individual sites; and
- nuclear tuning, where molecules can be arranged such that their delocalised charge transfer rate is greater than either alone.

These predictions are suited to be tested experimentally. As outlined in Chapter 2, the simplest test would be to construct covalently linked donors and acceptors in geometries such as those shown in Figures 2.3 and 2.4. Chemical modification would allow tuning of the couplings and energy levels, the parameters relevant for gMT, which would allow the theory to be tested.

Charge supertransfer in molecular systems was recently demonstrated experimentally[167] by constructing a covalently linked system of an electron donor (anthracene) equidistant from two electron acceptors (benzoquinones). When the electronic coupling between the acceptors was weak compared to the environment interactions (achieved by having the system at room temperature), the charge was transferred to a state localised on a single acceptor. However, with large coupling relative to the environment interactions (achieved by cooling the system to cryogenic temperatures), the electron was transferred to a delocalised state across the two acceptors. As gMT predicted, there was an enhancement of a factor of two in charge transfer rate to the delocalised state relative to the localised state.

As gMT is a general theory of delocalised charge transfer in molecular systems, future work could use gMT to on many systems of active research, such as organic semiconductors, conductive metal-organic frameworks, and inorganic coordination complexes.

While the closed-form solution of gMT is particular to the high-temperature stationary limit, intermediate solutions were also presented in Chapter 2, including a time-dependent expression that includes internal aggregate dynamics (Equation 2.9), to allow evaluation of aggregate charge transfer with fewer assumptions. However, like MT, gMT was derived in the strong-environment, weak donor-acceptor coupling limit, making it inapplicable in the Redfield regime (weak environment coupling, strong donor-acceptor coupling). Future work could use the same approach as gMT with the second-order perturbation being in the system-environment coupling, rather than the inter-aggregate coupling, or adapt low-temperature corrections to MT for use in gMT[168].

The closed-form solution presented in Chapter 2 is similar to the closed-form delocalised exciton transfer presented by Cleary and Cao[33]. This illustrates a deep similarity between charge and exciton transfer, and also leads to an open question: under what assumptions does this similarity break down, and in what limits is it maintained?

While gMT has been deliberately restricted to the delocalised generalisation of Marcus-theory, we are confident that future work on gMT could include developments in charge transfer subsequent to MT, such as adiabatic charge transfer, coherent multi-step charge transfer, quantum-mechanical vibrational corrections, off-diagonal system-bath couplings, and shared intra-aggregate environmental modes.

The goal of Chapter 2 was to derive a theory of delocalised charge transfer, which was successful with the derivation of gMT. This provided the last of the mathematical tools necessary to describe the effect of dimerisation on charge transfer within the photosynthetic RC.

4.2 Dimerism in Photosynthetic Reaction Centres

Chapter 3 explores reasons for the dimeric nature of photosynthetic reaction centres (RCs) using the results of Chapter 2. It was shown that, over a broad parameter regime, dimerisation of the RC from a monomeric ancestor likely improved overall RC quantum efficiency.

In Chapter 3 we constructed a model of the primordial monomeric RC, using extant organisms as a guide for a broad parameter regime of relative site energy levels, intersite coupling, and environment coupling. The dimerisation event led to a strong coupling between molecules where the two monomers connected, the special pair (SP), resulting in a delocalised state. Existing theories were able to describe exciton transfer to the SP (generalised Förster theory), and charge transfer out of the SP if the coupling strength between the SP and primary acceptor were greater than the coupling of either to the environment (adiabatic charge transfer), but were unsuited to describing charge transfer out of the SP when the coupling to the primary acceptor was weak relative to the intra-SP coupling or the environment (as is the case in modern systems). This was resolved by the derivation of generalised Marcus theory (gMT) in Chapter 2.

These theories were chosen for their capacity to describe delocalised charge and exciton transfer, enabling comparison of the monomer to a dimeric version of the primordial RC, and their computational efficiency allowing for assessment of RC efficiency across a broad parameter regime. This was necessary, as modern RCs are far removed from their monomeric ancestor, and the monomeric RC has not been preserved.

The main limitation of this work is that we cannot know for certain why dimeric RCs came to dominance over monomeric ones, as billions of years of evolution have led to highly derived photosynthetic systems, very removed from the monomer that underwent the initial dimerisation event. While certainty is inaccessible, we have demonstrated that dimerisation likely offered an enhancement to overall RC quantum efficiency, and this contributes to a body of work looking at the evolution of photosynthetic apparatuses.

Future work could greatly benefit from the research conducted in Chapter 3. Namely, the genetic engineering of a fully monomeric RC would allow these results to be experimentally verified by simulating the dimerisation event experimentally. Further, the construction of a monomer could help narrow the parameter regime explored in Table 3.1, allowing for more sophisticated and computationally-expensive quantum-chemical techniques to be feasibly used to examine the benefits and costs of dimerism relative to a monomeric reaction RC.

Bibliography

[1] S. R. Logan, J. Chem. Educ. **59**, 279 (1982).

[2] K. J. Laidler, J. Chem. Ed. **61**, 494 (1984).

[3] J. C. Maxwell, Philos. Trans. Royal Soc. , 49 (1867).

[4] L. Boltzmann, Vienna, part II **66**, 275 (1872).

[5] J. H. van't Hoff, *Etudes de dynamique chimique* (Frederik Muller & Co, Amsterdam, The Netherlands, 1884).

[6] S. A. Arrhenius, Z. Phys. Chem. **4**, 96 (1889).

[7] E. M. Conwell, Phys. Rev. **103**, 51 (1956).

[8] N. F. Mott, Can. J. Phys. **34**, 1356 (1956).

[9] A. Miller and E. Abrahams, Phys. Rev. **120**, 745 (1960).

[10] R. A. Marcus, J. Chem. Phys. **24**, 966 (1956).

[11] V. May and O. Kühn, *Charge and Energy Transfer in Molecular Systems*, 3rd ed. (Wiley-VCH, Weinheim, Germany, 2011).

[12] G. Schatz and M. Ratner, *Quantum Mechanics in Chemistry* (Dover, Mineola, New York, 2002).

[13] N. S. Hush, Trans. Faraday Soc. **57**, 557 (1961).

[14] L. D. Landau, Z. Sowjetunion **1**, 88 (1932).

[15] C. Zener, Proc. R. Soc. A Math. Phys. Eng. Sci. **137**, 696 (1932).

[16] E. C. G. Stückelberg, Helv. Phys. Acta **5**, 369 (1932).

[17] E. Majorana, Il Nuovo Cimento **9**, 43 (1932).

[18] V. Levich and R. Dogonadze, Dokl. Akad. Nauk. SSSR **124**, 123 (1959).

[19] M. Born and R. Oppenheimer, Ann. Phys. **389**, 457 (1927).

[20] E. W. Montroll and K. E. Shuler, J. Chem. Phys. **26**, 454 (1957).

[21] A. Nitzan, *Chemical Dynamics in Condensed Phases* (Oxford University Press, Oxford, UK, 2006).

[22] M. B. Robin and P. Day, in *Molecules into Materials* (Academic Press, 1968) pp. 142—317.

[23] M. Parthey and M. Kaupp, Chem. Soc. Rev. **43**, 5067 (2014).

[24] O. Klein and S. Rosseland, Zeitschrift für Physik **4**, 46 (1921).

[25] S. Dushman, J. Chem. Educ. **14**, 549 (1937).

[26] T. Förster, Ann. Phys. **437**, 55 (1948).

[27] K. D. B. Higgins, S. C. Benjamin, T. M. Stace, G. J. Milburn, B. W. Lovett, and E. M. Gauger, Nat. Commun. **5**, 4705 (2014).

[28] E. P. Kenny and I. Kassal, J. Phys. Chem. B **120**, 25 (2016).

[29] J. D. Jackson, *Classical Electrodynamics*, 3rd ed. (John Wiley & Sons, New York, USA, 1999).

[30] H. Sumi, J. Phys. Chem. B **103**, 252 (1999).

[31] H. Sumi, Chem. Rec. **1**, 480 (2001).

[32] S. Jang, M. Newton, and R. Silbey, Phys. Rev. Lett. **92**, 218301 (2004).

[33] L. Cleary and J. Cao, New J. Phys. **15**, 125030 (2013).

[34] R. Blankenship, *Molecular Mechanisms of Photosynthesis*, 2nd ed. (Wiley Blackwell, West Sussex, UK, 2014).

[35] N. Bohr, Nature **131**, 421 (1933).

[36] E. Schrödinger, *What Is Life? The Physical Aspect of the Living Cell* (Cambridge University Press, Cambridge, UK, 1944).

[37] M. Mohseni, Y. Omar, G. Engel, and M. Plenio, *Quantum Effects in Biology* (Cambridge University Press, Cambridge, 2014).

[38] H. Longuet-Higgins, Biophys. J. **2**, 207 (1962).

[39] G. M. Dyson, Perfum. Essent. Oil Rec **28**, 13 (1937).

[40] N. Lambert, Y. N. Chen, Y. C. Cheng, C. M. Li, G. Y. Chen, and F. Nori, Nat. Phys. **9**, 10 (2012).

[41] A. Marais, B. Adams, A. K. Ringsmuth, M. Ferretti, J. M. Gruber, R. Hendrikx, M. Schuld, S. L. Smith, I. Sinayskiy, T. P. J. Krüger, F. Petruccione, and R. van Grondelle, J. R. Soc. Interface **15**, 20180640 (2018).

[42] G. S. Engel, T. R. Calhoun, E. L. Read, T. K. Ahn, T. Mančal, Y. C. Cheng, R. E. Blankenship, and G. R. Fleming, Nature **446**, 782 (2007).

[43] E. Romero, J. Prior, A. W. Chin, S. E. Morgan, V. I. Novoderezhkin, M. B. Plenio, and R. van Grondelle, Sci. Rep. **7**, 2890 (2017).

[44] K. Schulten and P. Tavan, Nature **272**, 85 (1978).

[45] R. Wiltschko, K. Stapput, P. Thalau, and W. Wiltschko, J. R. Soc. Interface **7**, S163 (2010).

[46] P. J. Hore and H. Mouritsen, Annu. Rev. Biophys. **45**, 299 (2016).

[47] R. H. Wright, Nature **209**, 571 (1966).

[48] L. Turin, Chem. Senses **21**, 773 (1996).

[49] A. P. Horsfield, A. Haase, and L. Turin, Adv. Phys. X **2**, 937 (2017).

[50] K. L. Grant and J. P. Klinman, Biochemistry **28**, 6597 (1989).

[51] Z. D. Nagel and J. P. Klinman, Chem. Rev. **106**, 3095 (2006).

[52] D. R. Glowacki, J. N. Harvey, and A. J. Mulholland, Nat. Chem. **4**, 169 (2012).

[53] P. Rebentrost, M. Mohseni, I. Kassal, S. Lloyd, and A. Aspuru-Guzik, New J. Phys. **11**, 12 (2009).

[54] I. Kassal and A. Aspuru-Guzik, New J. Phys. **14**, 053041 (2012).

[55] T. V. Tscherbul and P. Brumer, Phys. Rev. Lett. **113**, 113601 (2014).

[56] D. N. Biggerstaff, R. Heilmann, A. A. Zecevik, M. Gräfe, M. A. Broome, A. Fedrizzi, S. Nolte, A. Szameit, A. G. White, and I. Kassal, Nat. Commun. **7**, 11282 (2016).

[57] R. E. Blankenship, Photosynth. Res. **33**, 91 (1992).

[58] J. M. Olson, Photosynth. Res. **88**, 109 (2006).

[59] J. M. Olson and R. E. Blankenship, in *Discov. Photosynth.* (Springer-Verlag, Berlin/Heidelberg, 2003) pp. 1073–1086.

[60] R. E. Blankenship, Plant Physiol. **154**, 434 (2010).

[61] L. O. Björn and Govindjee, *Photobiol. Sci. Light Life, Third Ed.*, edited by L. O. Björn (Springer New York, New York, 2015) Chap. 16, pp. 1–445.

[62] F. Westall, B. Cavalazzi, L. Lemelle, Y. Marrocchi, J. N. Rouzaud, A. Simionovici, M. Salomé, S. Mostefaoui, C. Andreazza, F. Foucher, J. Toporski, A. Jauss, V. Thiel, G. Southam, L. MacLean, S. Wirick, A. Hofmann, A. Meibom, F. Robert, and C. Défarge, Earth Planet. Sci. Lett. **310**, 468 (2011).

[63] M. F. Hohmann-Marriott and R. E. Blankenship, Annu. Rev. Plant Biol. **62**, 515 (2011).

[64] G. H. Richards, K. E. Wilk, P. M. G. Curmi, H. M. Quiney, and J. a. Davis, J. Phys. B At. Mol. Opt. Phys. **45**, 154015 (2012).

[65] H. S. Yoon, J. D. Hackett, C. Ciniglia, G. Pinto, and D. Bhattacharya, Mol. Biol. Evol. **21**, 809 (2004).

[66] H. C. Betts, M. N. Puttick, J. W. Clark, T. A. Williams, P. C. J. Donoghue, and D. Pisani, Nat. Ecol. Evol. **2**, 1556 (2018).

[67] L. Margulis, *Origin of eukaryotic cells: Evidence and research implications for a theory of the origin and evolution of microbial, plant and animal cells on the precambrian Earth* (Yale University Press, 1970).

[68] J. Xiong, Science **289**, 1724 (2000).

[69] R. S. Gupta, T. Mukhtar, and B. Singh, Mol. Microbiol. **32**, 893 (1999).

[70] R. S. Gupta, Photosynth. Res. **76**, 173 (2003).

[71] W. W. Fischer, J. Hemp, and J. E. Johnson, Annu. Rev. Earth Planet. Sci. **44**, 647 (2016).

[72] C. A. Wraight and R. K. Clayton, Biochim. Biophys. Acta - Bioenerg. **333**, 246 (1974).

[73] D. Mauzerall, Photosynth. Res. **116**, 363 (2013).

[74] G. S. Orf, C. Gisriel, and K. E. Redding, Photosynth. Res. **138**, 11 (2018).

[75] M. Ø. Pedersen, J. Linnanto, N. U. Frigaard, N. C. Nielsen, and M. Miller, Photosynth. Res. **104**, 233 (2010).

[76] B. W. Matthews and R. E. Fenna, Acc. Chem. Res. **13**, 309 (1980).

[77] J. M. Olson and C. A. Romano, Biochim. Biophys. Acta **59**, 726 (1962).

[78] V. Cherezov, J. Clogston, M. Z. Papiz, and M. Caffrey, J. Mol. Biol. **357**, 1605 (2006).

[79] J. Strümpfer and K. Schulten, J. Chem. Phys. **131**, 225101 (2009).

[80] X. Su, J. Ma, X. Wei, P. Cao, D. Zhu, W. Chang, Z. Liu, X. Zhang, and M. Li, Science. **357**, 815 (2017).

[81] F. Fassioli, R. Dinshaw, P. C. Arpin, and G. D. Scholes, J. Royal Soc. Interface **11**, (2013).

[82] S. Y. Netzer-El, I. Caspy, and N. Nelson, Front. Plant Sci. **9**, 1 (2019).

[83] A. Chauvet, J. Sarrou, S. Lin, S. P. Romberger, J. H. Golbeck, S. Savikhin, and K. E. Redding, Photosynth. Res. **116**, 1 (2013).

[84] D. Kolbasov and a. Scherz, J. Phys. Chem. B **104**, 1802 (2000).

[85] J. R. Durrant, D. R. Klug, S. L. Kwa, R. van Grondelle, G. Porter, and J. P. Dekker, Proc. Natl. Acad. Sci. U. S. A. **92**, 4798 (1995).

[86] L. Y. Zhang and R. A. Friesner, Proc. Natl. Acad. Sci. U. S. A. **95**, 13603 (1998).

[87] P. O. J. Scherer and S. F. Fischer, Chem. Phys. **131**, 115 (1989).

[88] J. Franck and E. Teller, J. Chem. Phys. **6**, 861 (1938).

[89] E. Collini, C. Y. Wong, K. E. Wilk, P. M. G. Curmi, P. Brumer, and G. D. Scholes, Nature **463**, 644 (2010).

[90] S. Baghbanzadeh and I. Kassal, J. Phys. Chem. Lett. **7**, 3804 (2016).

[91] S. Baghbanzadeh and I. Kassal, Phys. Chem. Chem. Phys. **18**, 7459 (2016).

[92] S. Savikhin, D. R. Buck, and W. S. Struve, Chem. Phys. **223**, 303 (1997).

[93] G. Panitchayangkoon, D. Hayes, K. A. Fransted, J. R. Caram, E. Harel, J. Wen, R. E. Blankenship, and G. S. Engel, Proc. Natl. Acad. Sci. **107**, 12766 (2010).

[94] I. Kassal, J. Yuen-Zhou, and S. Rahimi-Keshari, J. Phys. Chem. Lett. **4**, 362 (2013).

[95] D. M. Wilkins and N. S. Dattani, J. Chem. Theory Comput. **11**, 3411 (2015).

[96] K. Claridge, D. Padula, and A. Troisi, Faraday Discuss. , (2019).

[97] E. Romero, R. Augulis, V. I. Novoderezhkin, M. Ferretti, J. Thieme, D. Zigmantas, and R. van Grondelle, Nat. Phys. **10**, 676 (2014).

[98] V. Novoderezhkin, E. Romero, and R. van Grondelle, Phys. Chem. Chem. Phys. **17**, (2015).

[99] H. G. Duan, V. I. Prokhorenko, R. J. Cogdell, K. Ashraf, A. L. Stevens, M. Thorwart, and R. J. D. Miller, Proc. Natl. Acad. Sci. **114**, 8493 (2017).

[100] F. Ma, E. Romero, M. R. Jones, V. I. Novoderezhkin, and R. van Grondelle, Nat. Commun. **10**, 933 (2019).

[101] S. A. Oh, D. Coker, and D. Hutchinson, Faraday Discuss. (2019), 10.1039/C9FD00081J.

[102] J. C. Brookes, Proc. R. Soc. A Math. Phys. Eng. Sci. **473**, 20160822 (2017).

[103] X. Jiang and P. Brumer, J. Chem. Phys. **94**, 5833 (1991).

[104] T. Mančal and L. Valkunas, New J. Phys. **12**, 065044 (2010).

[105] M. H. Vos, F. Rappaport, J. C. Lambry, J. Breton, and J. L. Martin, Nature **363**, 320 (1993).

[106] F. Ma, E. Romero, M. R. Jones, V. I. Novoderezhkin, and R. van Grondelle, Nat. Commun. **10**, 933 (2019).

[107] V. Novoderezhkin, E. Romero, J. Prior, and R. van Grondelle, Phys. Chem. Chem. Phys. **19**, 5195 (2017).

[108] F. Ma, E. Romero, M. R. Jones, V. I. Novoderezhkin, and R. Van Grondelle, J. Phys. Chem. Lett. **9**, 1827 (2018).

[109] F. D. Fuller, J. Pan, A. Gelzinis, V. Butkus, S. S. Senlik, D. E. Wilcox, C. F. Yocum, L. Valkunas, D. Abramavicius, and J. P. Ogilvie, Nat. Chem. **6**, 706 (2014).

[110] N. B. Taylor and I. Kassal, Chem. Sci. **9**, 2942 (2018).

[111] R. Marcus and N. Sutin, Biochim. Biophys. Acta – Rev. Bioenerg. **811**, 265 (1985).

[112] P. F. Barbara, T. J. Meyer, and M. A. Ratner, J. Phys. Chem. **100**, 13148 (1996).

[113] J. Jortner and M. Bixon, *Electron Transfer-from Isolated Molecules to Biomolecules*, Vol. 106–107 (Adv. Chem. Phys., 1999).

[114] S. Few, J. M. Frost, and J. Nelson, Phys. Chem. Chem. Phys. **17**, 2311 (2015).

[115] A. Köhler and H. Bässler, *Electronic Processes in Organic Semiconductors: An Introduction* (John Wiley & Sons, 2015).

[116] J. P. Allen and J. C. Williams, FEBS Lett. **438**, 5 (1998).

[117] R. Blankenship, *Molecular Mechanisms of Photosynthesis*, 2nd ed. (Wiley Blackwell, Chichester, UK, 2014).

[118] D. M. D'Alessandro and F. R. Keene, Chem. Rev. **106**, 2270 (2006).

[119] D. M. D'Alessandro, J. R. R. Kanga, and J. S. Caddy, Aust. J. Chem. **64**, 718 (2011).

[120] N. S. Hush, J. Chem. Phys. **28**, 962 (1958).

[121] N. S. Hush, Trans. Faraday Soc. **57**, 557 (1961).

[122] R. J. Cave and M. D. Newton, Chem. Phys. Lett. **249**, 15 (1996).

[123] D. V. Matyushov and G. A. Voth, J. Phys. Chem. A **104**, 6470 (2000).

[124] J. E. Subotnik, S. Yeganeh, R. J. Cave, and M. A. Ratner, J. Chem. Phys. **129**, 244101 (2008).

[125] N. S. Hush, Prog. Inorg. Chem. **8**, 12 (1967).

[126] G. Scholes, X. Jordanides, and G. Fleming, J. Phys. Chem. B **105**, 1640 (2001).

[127] J. Ma and J. Cao, J. Chem. Phys. **142**, 094106 (2015).

[128] S. Jang and Y. C. Cheng, WIREs Comput. Mol. Sci. **3**, 84 (2013).

[129] A. Fruchtman, R. Gómez-Bombarelli, B. W. Lovett, and E. M. Gauger, Phys. Rev. Lett. **117**, 203603 (2016).

[130] J. Ulstrup and J. Jortner, J. Chem. Phys. **63**, 4358 (1975).

[131] A. Kuznetsov and J. Ulstrup, Electrochim. Acta **45**, 2339 (2000).

[132] T. Renger and R. A. Marcus, J. Chem. Phys. **116**, 9997 (2002).

[133] J. Ma, J. Moix, and J. Cao, J. Chem. Phys. **142**, 094107 (2015).

[134] J. M. Moix, J. Ma, and J. Cao, J. Chem. Phys. **142**, 094108 (2015).

[135] N. Taylor and I. Kassal, Chem. Sci. **10**, 9576 (2019).

[136] J. Allen and J. Williams, FEBS Lett. **438**, 5 (1998).

[137] A. W. Roszak, V. Moulisová, A. D. P. Reksodipuro, A. T. Gardiner, R. Fujii, H. Hashimoto, N. W. Isaacs, and R. J. Cogdell, Biochem. J. **442**, 27 (2012).

[138] A. Y. Mulkidjanian and W. Junge, Photosynth. Res. **51**, 27 (1997).

[139] T. Meyer, Biosystems **33**, 167 (1994).

[140] M. Büttner, D. L. Xie, H. Nelson, W. Pinther, G. Hauska, and N. Nelson, Proc. Natl. Acad. Sci. U. S. A. **89**, 8135 (1992).

[141] W. D. Schubert, O. Klukas, W. Saenger, H. T. Witt, P. Fromme, and N. Krauß, J. Mol. Biol. **280**, 297 (1998).

[142] F. Müh, M. Plöckinger, and T. Renger, J. Phys. Chem. Lett. **8**, 850 (2017).

[143] A. Niedringhaus, V. R. Policht, R. Sechrist, A. Konar, P. D. Laible, D. F. Bocian, D. Holten, C. Kirmaier, and J. P. Ogilvie, Proc. Natl. Acad. Sci. **115**, 3563 (2018).

[144] F. Ma, E. Romero, M. R. Jones, V. I. Novoderezhkin, and R. van Grondelle, J. Phys. Chem. Lett. **9**, 1827 (2018).

[145] D. L. Hartl and A. G. Clark, *Principles of Population Genetics*, 4th ed. (Sinauer Associates, 2006).

[146] H. Ishikita, W. Saenger, J. Biesiadka, B. Loll, and E. W. Knapp, Proc. Natl. Acad. Sci. **103**, 9855 (2006).

[147] M. Chen, M. Schliep, R. D. Willows, Z. L. Cai, B. A. Neilan, and H. Scheer, Science **329**, 1318 (2010).

[148] D. H. Burke, J. E. Hearst, and A. Sidow, Proc. Natl. Acad. Sci. **90**, 7134 (1993).

[149] C. Gisriel, I. Sarrou, B. Ferlez, J. H. Golbeck, K. E. Redding, and R. Fromme, Science **357**, 1021 (2017).

[150] T. Arlt, S. Schmidt, W. Kaiser, C. Lauterwasser, M. Meyer, H. Scheer, and W. Zinth, Proc. Natl. Acad. Sci. **90**, 11757 (1993).

[151] G. H. Schatz, H. Brock, and A. R. Holzwarth, Biophys. J. **54**, 397 (1988).

[152] D. C. Arnett, C. C. Moser, P. L. Dutton, and N. F. Scherer, J. Phys. Chem. B **103**, 2014 (1999).

[153] R. D. J. León-Montiel, I. Kassal, and J. P. Torres, J. Phys. Chem. B **118**, 10588 (2014).

[154] T. Cardona, A. Sedoud, N. Cox, and A. W. Rutherford, Biochim. Biophys. Acta - Bioenerg. **1817**, 26 (2012).

[155] G. Raszewski and T. Renger, J. Am. Chem. Soc. **130**, 4431 (2008).

[156] D. I. Bennett, K. Amarnath, and G. R. Fleming, J. Am. Chem. Soc. **135**, 9164 (2013).

[157] R. M. Pearlstein, Photochem. Photobiol. **35**, 835 (1982).

[158] G. S. Beddard, J. Phys. Chem. B **102**, 10966 (1998).

[159] G. Raszewski, W. Saenger, and T. Renger, Biophys. J. **88**, 986 (2005).

[160] M. E. A. Madjet, F. Müh, and T. Renger, J. Phys. Chem. B **113**, 12603 (2009).

[161] W. Parson and A. Warshel, in *Purple Phototrophic Bacteria*, edited by N. Hunter, F. Daldal, M. C. Thurnauer, and J. T. Beatty (Springer, Rotterdam, 2008) Chap. 9, pp. 355–377.

[162] M. Bixon, J. Jortner, M. E. Michel-Beyerle, A. Ogrodnik, and W. Lersch, Chem. Phys. Lett. **140**, 626 (1987).

[163] W. W. Parson, Z. T. Chu, and A. Warshel, Biophys. J. **74**, 182 (1998).

[164] M. Volk, G. Aumeier, T. Langenbacher, R. Feick, A. Ogrodnik, and M. E. Michel-Beyerle, J. Phys. Chem. B **102**, 735 (2002).

[165] V. I. Novoderezhkin, E. Romero, J. P. Dekker, and R. van Grondelle, Chem. Phys. Chem. **12**, 681 (2011).

[166] C. Creatore, M. A. Parker, S. Emmott, and A. W. Chin, Phys. Rev. Lett. **111**, 1 (2013).

[167] B. T. Phelan, J. Zhang, G. J. Huang, Y. L. Wu, M. Zarea, R. M. Young, and M. R. Wasielewski, J. Am. Chem. Soc. **141**, 12236 (2019).

[168] J. K. Sowa, J. A. Mol, G. A. D. Briggs, and E. M. Gauger, J. Chem. Phys. **149**, 154112 (2018).